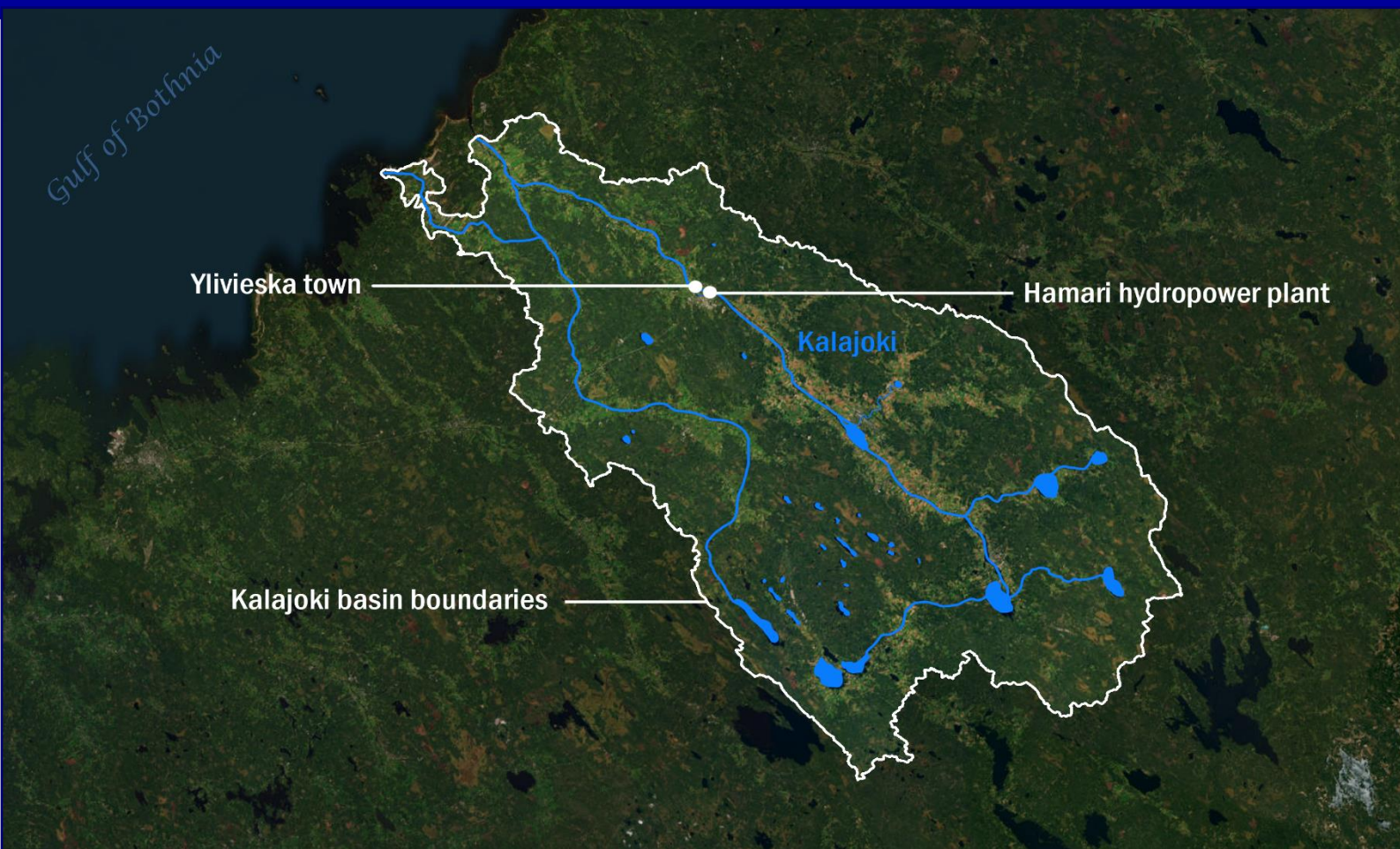


Mitigation of Hydropeaking in a Complex Riverine System: A State-of-the-Art Modelling Approach

A quantitative study with HEC-RAS modelling on hydropeaking by means of a case study in the Kalajoki basin (northern Finland)



Mitigation of Hydropeaking in a Complex Riverine System: A State-of-the-Art Modelling Approach

A quantitative study with HEC-RAS modelling on hydropeaking by means of a case study in the Kalajoki basin (northern Finland)

By

Siirilotta Rosanna Moonen

in partial fulfilment of the requirements for the degree of

Master of Science
in Hydraulic Engineering

at the Delft University of Technology,
to be defended publicly on the 15th of January 2024 at 10:00 AM.

Daily supervisor:	Prof. dr. ir. H. Marttila	TU Delft
Thesis committee:	Dr. ir. D. Wüthrich (Chair), Dr. ir. K. Sloff, Prof. dr. ir. H. Marttila	TU Delft University of Oulu

An electronic version of this thesis is available at <http://repository.tudelft.nl/>.



Preface

The subject of hydropeaking has become increasingly prevalent in recent times. The regulation practice in hydropower generation balances regional markets by rapidly altering ramping rates. The phenomenon is being studied more frequently as the interest in and need for renewable energy sources, like hydropower, is growing. Fossil fuels, known for their unsustainable nature, are being actively replaced on a global scale. However, hydropeaking can have equally detrimental effects on the environment and natural ecosystems. Motivated by these general concerns, my own interest in hydraulic systems and sustainability, and influenced by the missed opportunity to study in Finland when my minor at the University of Aalto (Helsinki) was cancelled due to the COVID-19 pandemic, I chose to dive into the topic for my thesis. This thesis contributes to the finalization of my MSc Hydraulic Engineering at the TU Delft. The research is conducted under the banner of the University of Delft in the Netherlands. However, a substantial portion of it takes place in collaboration with the University of Oulu in Finland.

The combination of my hydraulic engineering background with a specialization in hydraulic structures from the TU Delft and guidance from the Unit of Water, Energy and Environmental engineering at the University of Oulu has enabled me to produce a report that approaches hydropeaking from various angles. As a result, this report serves as a valuable reference for those exploring the subject and its impact on hydrology in hydraulic infrastructural frameworks. Additionally, my experience abroad in Oulu not only enhanced my proficiency in the Finnish language, but also kindled my interest in considering Finland, my mother's birthplace, as a potential destination for future work and living.

Thank you Hannu Marttila, for offering me the subject when I reached out for thesis opportunities. Moreover, for organizing the field trip in May 2023. During the trip, I gained hands-on experience in collecting LSPIV-ACDP-data. I am also grateful to Hannu for providing valuable data and facilitating connections with Scandinavian PhD students and staff at the Finnish institute ELY. My appreciation also goes to my supervisors from the TU Delft, Davide Wüthrich and Kees Sloff. I would also like to acknowledge Zeeshan Tahir Virk, a PhD student at the unit Water, Energy and Environmental Engineering at the University of Oulu, for his insightful suggestions that contributed to my 2D model. Lastly, I am thankful to Faisal Ashraf for his work related to the gathering of logger-data and Juha-Matti Välimäki for his expertise in the processing of LSPIV-data.

*S.R.Moonen
Delft, January 2024*

Abstract

Hydropeaking is a widely applied management practice in the generation of hydropower. When the demand in electricity is high, for example around the time the majority of people comes home from work, the operator of the hydropower plant rapidly increases released discharges to meet this demand. Vice versa, when the demand is low, no or less water is released. The management practice is typically steered by intra-daily differences in electricity prices to achieve maximum economic benefit. However, it is essential to recognize that while the generation of hydropower, among other river regulation practices, offer valuable resources, can also inflict adverse environmental consequences on downstream river segments. River regulation encompasses various human-engineered interventions, including the construction of dams, reservoirs and hydropower plants, channelization and flood risk measures. These practices significantly modify natural river systems. More specifically, hydropeaking introduces high sub-daily variance in downstream reaches of the hydropower plant, which is harmful to the downstream river regime and ecosystems.

The most prominent, known negative impacts due to high flow variations are a direct impact on aquatic biota, for which changes in the thermal regime are regularly co-responsible, and a compromised recreational use of the river corridor. Regarding impacts on aquatic biota, micro-organisms and larger organisms, experience negative effects on growth, survival rates, reproduction and biotic integrity, such as a decline in fish habitat quality. Today, the primary questions regarding hydropeaking are how to balance, mitigate and identify critical flows to minimize these impacts. In Finland, hydropeaking has the highest negative environmental impact of all river regulation practices. Especially for relatively small hydropower plants (under 40 MW). In the Kalajoki basin, located in the northern Ostrobothnia region of Finland, such a high-impact, but relatively small hydropower plant ‘Hamari’ at Ylivieska is currently operating. In previous years, hydropeaking practices have significantly decreased the population of brown trout and recreational usage at Juurikoski, the case study area in the downstream reach of Hamari hydropower plant (HHP). This causes concern for the regional and governmental knowledge institutes. Among Finnish studies, there is a notable scarcity of studies on 2D modelling related to hydropeaking, with most existing studies primarily relying on 1D models. However, challenges arise because accurate modelling of hydropeaking-induced phenomena requires high-quality data on river characteristics and flow regimes. Furthermore, the absence of a universally accepted approach for modelling weirs (including selection weir coefficient), vegetation (addressing roughness), and riverine boulders (considering topography adjustment or roughness) introduces additional complexities.

The main objective is to research the impact of hydropeaking on rapids in a complex riverine structure with hydraulic structures. Additionally, related to the modelling approach, two experimental state-of-the-art calibration methods and their benefits and limitations are investigated. The formulation of operational and morphological mitigation measures to counter such impacts is the secondary objective. Accordingly, the main research question is:

- How does the sub-daily variance introduced by upstream hydropeaking practices affect a complex rapid system situated near weirs downstream of a hydropower plant and how can these impacts be mitigated?

A 2D HEC-RAS model for the downstream region of HHP, the site Juurikoski, provides insight on the different aspects related to this query. Firstly, the impact of hydropeaking on the riverine system is quantified and studied in the original river system. This is labelled as the original scenario and is the first simulation run after

validation of the model. Then, operational and morphological mitigation measures are formulated, which are labelled as scenarios as well. One scenario includes the application of operational limits and two other scenarios implement modifications in the riverine system. These modifications may include a cut-off in the anabranch, a randomization of obstacles (such as stones and vegetation), the lowering of weirs or a division of streams into a rocky part and a fast-flowing part. The performance of the listed scenarios is assessed by the model as well. The results are dependent on the potential and effectiveness (state-of-the-art) methods for calibration, related to data from logger water levels, Acoustic Doppler Current Profiler (ADCP) and Large-Scale Particle Image Velocimetry (LSPIV).

The report provides a modelling approach to tailor mitigation measures according to riverine lay-out, even if the terrain definition is difficult due to limited bathymetry data and increased riverine complexity because of hydraulic structures. Additionally, it assesses the potential of calibration and validation for a 2D hydrodynamical model by state-of-the-art methods. Such as a hot spot analysis comparison based on LSPIV-data and velocity profile comparisons based on ADCP-data. At regional level of the case study, four scenarios are simulated in a 2D hydrodynamical model; one for maximizing economic gain, which is the current situation at Juurikoski, one for benefiting environmental standards by limiting ramping rates and lastly two experimental simulations. The experimental scenarios include morphological adjustments to achieve a compromise between the ecological state of the reach and the economic gain. In conclusion, hydropeaking results in relatively deep water levels and a distinct fast-flowing pattern in a rapid region, despite the presence of vegetation and large riverine boulders. Operational measures seem to be effective, but to what extent remains undefined for medium and high flow discharges. ‘morphological change 2’ shows potential to restore rapid flow and potentially benefit ecology in the downstream reach. This mitigation measure refers to the lowering of weirs, randomization of stone and vegetation placement over the whole reach and strategic placement of stones and vegetation in the southside branch. Both mitigation measures induce a more constant flow in streamwise direction than in the original case.

From a regional practical application perspective, a cut-off of the anabranch as a mitigation measure can be excluded. Adjustments of weir crest heights and the randomization or strategic placement of vegetation and stones may be interesting to further investigate. On a global scale, the results exhibit valuable information to further improve 2D hydrodynamical models, especially in terms of model conditions and calibration methods, but also to further open the discussion on aspects of creativity, effectiveness and practical implications related to hydropeaking mitigation measures.

Key words: river regulation, hydropeaking, environmental impact, calibration, ADCP, LSPIV, Kalajoki, Finland, weir, 2D hydraulic modelling, HEC-RAS, mitigation measures

Content

Preface.....	v
Abstract	vii
List of abbreviations.....	xi
List of symbols.....	xii
1. Introduction	1
1.1. Hydropeaking – A high impact management practice in hydropower generation.....	1
1.2. Problem statement.....	3
1.3. Objective and research questions	5
1.4. Research methodology	6
1.5. Data gathering and analysis	7
1.6. Contents of thesis	7
2. Literature Study.....	8
2.1. Kalajoki (and Juurikoski) river characteristics	8
2.1.1. Geographical attributes	8
2.1.2. Kalajoki – An artificially influenced reach.....	10
2.1.3. Hydrology, climate and climate change.....	11
2.2. Hydropeaking quantification – Impact class determination.....	14
2.3. Riverine equations.....	16
2.3.1. Shallow Water Equations (SWE).....	16
2.3.2. Diffusion Wave Equations (DWE)	16
2.3.3. Comparison between SWE and DWE-sets	16
2.4. Advances in river model calibration	17
2.4.1. The challenge in existing calibration methods.....	17
2.4.2. Experimental calibration with LSPIV and ADCP data – Juurikoski.....	17
3. Materials and methods	18
3.1. Dimensionality and model choice.....	18
3.2. Model input specifications and characteristics	19
3.2.1. Juurikoski shapefiles, discharge data, logger data, ADCP velocity signals and LSPIV images ...	19
3.2.2. Land cover data.....	21
3.2.3. Terrain	22
3.2.4. HEC-RAS Geometry – Computational mesh and lateral structures	23
3.2.5. Boundary conditions, initial conditions and warm up conditions.....	24
3.2.6. Time step determination.....	25
3.2.7. Sensitivity analysis.....	26
3.3. Calibration.....	27
3.3.1. Method 1: Calibration based on depth loggers	27
3.3.2. Experimental Method 2: Calibration with drone based data.....	29
3.3.3. Experimental Method 3: Comparison ADCP and HEC-RAS velocity profiles	31

3.4. Validation.....	34
3.5. Simulation cases.....	35
4. Results.....	38
4.1. Hydropeaking classification HHP.....	38
4.2. Simulation results.....	39
4.2.1. Water levels.....	39
4.2.2. Velocities.....	42
4.2.3. Hydraulic structure analysis.....	44
5. Discussion.....	47
5.1. Mitigation of hydropeaking influence – Juurikoski.....	47
5.1.1. Hydropower operational limits.....	47
5.1.2. Local morphology alteration.....	47
5.1.3. Recommendation hydropeaking mitigation.....	47
5.2. Performance hydrodynamical model and future recommendations – Juurikoski and other cases.....	48
5.2.1. General challenges with data sources.....	48
5.2.1. General challenges model and calibration.....	49
5.2.2. Potential LSPIV and ADCP to calibrate and validate the hydrodynamical model – Juurikoski...	50
5.2.3. Recommendations modelling approach implementation.....	50
6. Conclusions.....	51
6.1. Answers to the research questions.....	51
6.2. Regional and global recommendations.....	53
Bibliography.....	54
Appendix A – Juurikoski ortography.....	60
Appendix B – Discharge HHP.....	64
Appendix C – Weir equations, types and flow regimes.....	65
Appendix D – Juurikoski: Dimensions of hydraulic structures.....	68
Appendix E – LSPIV: Graphical representation of surface velocities near rapids.....	71
Appendix F – ADCP: Velocity profiles for multiple cross sections near rapids.....	72
Appendix G – Model results: Water levels.....	76
Appendix H – Uncertainty and sensitivity analysis data sources.....	79

List of abbreviations

ADCP	Acoustic Doppler Current Profiler
CFL	Courant-Friedrichs-Lewy
CS1	Cross-Section 1
CS2	Cross-Section 2
DEM	Digital Elevation Model
DWE	Diffusion Wave Equations
ELY	Elinkeino-, Liikenne- ja Ympäristökeskus (<i>'centre for economic development, transport and environment'</i>)
HEC-RAS	Hydrologic Engineering Centre – River Analysis System
HHP	Hamari Hydropower Plant
LSPIV	Large-Scale Particle Image Velocimetry
M1	Morphological change 1 scenario
M2	Morphological change 2 scenario
Original	Original scenario
OL	Operational Limits scenario
SWE	Shallow Water Equations
SYKE	Suomen Ympäristökeskus (<i>'Finnish environment institute'</i>)
1D	One Dimensional
2D	Two Dimensional
3D	Three Dimensional

List of symbols

A	Cross sectional area	m^2
C	Courant number	[-]
C_{max}	Maximum Courant number	[-]
C_f	Friction coefficient	[-]
d	Water depth	m
g	Gravitational constant	m/s^2
H	Energy head	m
h	Water level height relative to a reference plane	m
h_{weir}	Weir crest height	m
i	Channel slope	[-]
L_c	Weir crest length	m
n	Manning's roughness coefficient	[-]
Q	Discharge or flow rate	m^3/s
q	Specific discharge	m^2/s
R	Hydraulic radius	m
t	Time	s
u	Flow velocity in streamwise direction	m/s
V_w	Flood wave speed	m/s
v	Flow velocity in transverse direction	m/s
x	Horizontal coordinate in streamwise direction	m
α	Energy coefficient	[-]
ν_t	Turbulent eddy viscosity	m^2/s
ρ	Density of the water	kg/m^3
τ_{sx}	Shear stress in streamwise direction	N/m^2

1. Introduction

1.1. Hydropeaking – A high impact management practice in hydropower generation

In the backdrop of climate change, the need for renewable energy sources such as hydropower is increasing (Jelovica et al., 2022). Hydropower is expected to remain the world's largest source of renewable electricity generation into the 2030s (IEA, 2023). Nevertheless, the river regulation practice of hydropower generation, because of the construction of dams, reservoirs, channelization and flood risk measures, can inflict adverse environmental consequences on downstream river segments (Moreira et al., 2019). The management practice 'hydropeaking' is the process of releasing more water during peak hours of electricity demand and less or no water during low demand during the generation of hydropower. Electricity demands are dependent on people behaviour. For example, people typically come home from work around 17:00 or 18:00. At this time, electricity demand spikes and electricity generation at the hydropower plant follows the demand by rapidly increasing released discharges. Therefore, it is essential during periods of high-energy demand as it balances regional markets (Ashraf et al., 2018). However, hydropeaking is harmful to the downstream river regime and ecosystems (Moreira et al., 2019). Hydropeaking introduces high flow variations downstream of a hydropower plant. Due to these variations, fish habitat conditions (Addo, 2019; Greimel et al., 2018), morphology (Virk, 2022), recreational use (Hauer et al., 2017, Virk, 2022) and fluvial processes (Virk, 2022) of river segments are deteriorated. In 2022, Jelovica et al. stated that "the need to balance, mitigate and identify critical flows to minimize the impact of hydropeaking is inevitable".

Issues related to hydropeaking practices are global; major players like Brazil (Figueiredo et al., 2021), America (Déry et al., 2021), Canada (Déry et al., 2021), China (Roney, 2021) experience the same issue, but also countries in Europe such as Spain (Batalla et al., 2021), Italy (Zolezzi et al., 2023), Switzerland (Meile et al., 2011; Tonolla et al., 2017) and Scandinavian countries (Ashraf et al., 2018) are mentioned in recent years. Furthermore, the EU currently funds hydropower research projects that demonstrate the potential of technology and aim to reduce its environmental impact, in context of improving existing plants and their sustainable performance (EC, 2023). In Finland, the Nordic Investment Bank finances hydropower plant upgrades and the construction of a small-scale plant in Finland (NIB, 2020). However, most existing hydropower plants are still categorized under "high impact" due to hydropeaking (Ashraf et al., 2020). Next to banking institutions, energy companies also strive toward an environmental approach regarding hydropower. Fortum, one of the large energy company in Finland, owns or co-owns 33 hydropower plants (total capacity 1.55 GW) (2021) and yearly reports on the actions taken to promote biodiversity and reduce climate or environmental impact due to hydropeaking. Despite these efforts, little is known about the effectiveness of the corresponding mitigation measures due to riverine complexity. Luke, the Natural Resources Institute Finland, in collaboration with other governmental and knowledge institutions such as 'Elinkeino-, Liikenne- ja Ympäristökeskus' (ELY) and the University of Oulu, has also been assessing and valuing ecosystem services in previous years to manage hydropower systems (SYKE, n.d.).

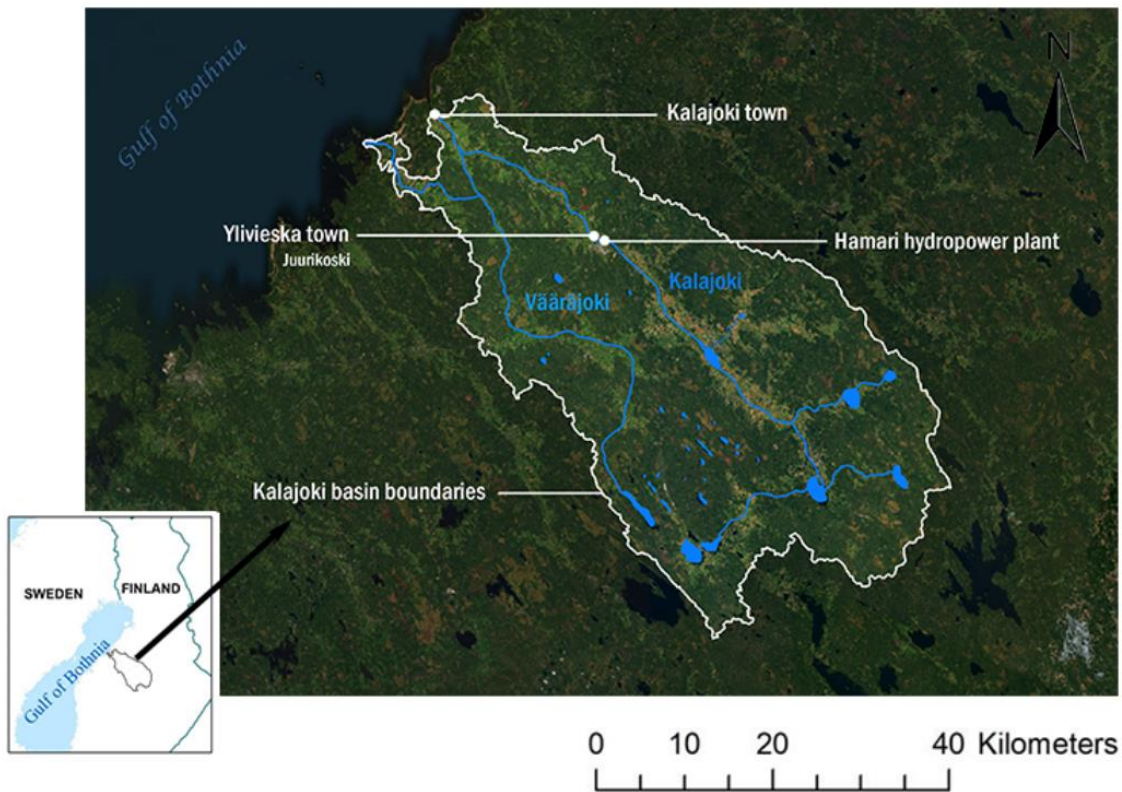


Figure 1: Kalajoki basin with the case study area Ylivieska and Hamari hydropower plant

In the river Kalajoki, running through the town of Ylivieska, located in the northern Ostrobothnia region of Finland, a high-impact, relatively small (2.5 MW) hydropower plant is currently operating. Figure 1 illustrates the Kalajoki basin and the location of the case study area, the site Juurikoski in Ylivieska. The main features of the case study are the relatively flat topography including heavily vegetated and rocky pool-like areas between subsequent weirs, the spatially and in time varying flow regime and the ecological component, namely the aquatic ecosystems for trout. The last feature has been recently studied on a local scale by Addo (2019) and the regional ELY-centre (K. Aronsuu, personal communication, May 2023). In previous years, hydropeaking practices at the Hamari Hydropower Plant (HHP) have significantly decreased the population of brown trout at Juurikoski (Addo, 2019). This causes concern for the regional ELY-centre (K. Aronsuu, personal communication, May 2023), since they have a partial responsibility to manage waterways and ecosystems in Finland. However, the environmental impact of the small hydropower plant (2.5 MW) on downstream rapids could be limited if the right mitigation measures are implemented. Nevertheless, for complex riverine systems with weirs or other hydraulic structures, existing modelling approaches related to hydropeaking are deemed insufficient, particularly in the context of Juurikoski in Finland. Among Finnish literary works, there is a notable scarcity of studies on 2D modelling related to hydropeaking. Most existing studies primarily rely on 1D models. However, the challenges arise because accurate modelling of hydropeaking-induced phenomena necessitates high-quality data on river characteristics and flow regimes. Furthermore, the absence of a universally accepted approach for modelling river elements introduces additional challenges. This includes the selection weir coefficient, plus how to address roughness or topography related to vegetation or riverine boulders. It's important to mention that impact of ice disturbance in combination with power generation influence in different seasons is not included in this thesis. Nevertheless, snow melt and associated high sudden discharges is still a dominating factor related to annual floodings in

boreal rivers (Aronsoo & Wennman, 2012). At Ylivieska and many other cold climate regions, “ice disturbance” refers to disruptions of the flow cause by the presence and movement of ice. More specifically, the potential hazard of the formation of ice jams or dams increases the risk of localized (upstream) flooding during winter or early spring. When temperatures rise during early or late spring, the rapid melting and release of discharges can cause localized flooding downstream. Slush ice on the other hand can cause local issues. At Ylivieska, slush ice was a major problem in the past (K. Aronsoo, personal communication, August 2023). As a closing remark, Figure 2 portrays a rapid at Juurikoski. The image clearly illustrates the complexity of the landscape. It features vegetation, large riverine rocks and other discontinuities in terrain. Notably absent from the landscape pictures of Juurikoski are the multiple submerged weirs scattered throughout the reach. These hydraulic structures add another layer of complexity to the prediction of hydrological river behaviour.



Figure 2: A rapid at Juurikoski during very low discharges due to hydropeaking practices

1.2. Problem statement

Kalajoki basin is submissive to large sub-daily flow fluctuations due to hydropeaking practices in regulated river reaches. The case study area, Juurikoski, experiences deterioration of natural rapids and their ecosystems. The impact of hydropeaking on this complex rapid system, concluding multiple weirs, has not been fully quantified or qualitatively described thus far. Ultimately, the effectiveness of operational and morphological mitigation measures are moderately understood. Currently, a 2D method approach to accurately capture sub-daily flow variations in a complex system (for the case study: vegetation, large riverine boulders, relatively flat slope, subsequent pool-like areas between subsequent weirs) is not universally defined. A 2D model for Juurikoski is non-existent. However, a reference 1D model set-up by Addo (2019) is mentioned in literature. 2D and 3D models in the context of hydropeaking exist, but are not widely published in scientific literature, especially not in Finland, although the corresponding issues are widely present. Related to literature, hydropeaking is mentioned more frequently in recent years. In Table 1, a list of the existing and relevant body of literature is displayed.

Table 1: Body Of Literature

Thematic Area	Key Contributors
Hydropeaking in Nordic Rivers	(Ashraf et al., 2018; Jelovica et al., 2023, Virk, 2022)
Modelling Approach on Hydropeaking	(Addo, 2019; Jelovica et al., 2023; Virk, 2022)
Hydraulic Structures: Impact to the Flow	(Ali, 2013; Harms, 2021)
1D or 2D Modelling with HEC-RAS	(Addo, 2019; Costabile et al., 2020; Shrestha et al., 2020; Shustikove et al., 2019)
Hydropeaking Environmental Impact	(Addo, 2019; Moreira et al., 2019; Person, 2013; Saltveit et al., 2001; Valentin et al., 1996)
Mitigation Measures Hydropeaking Impacts	(Charmasson & Zinke, 2011; Greimel et al., 2018; Hayes et al., 2022; Moreira et al., 2019)

According to Table 1, there is substantial literature available about environmental impact and modelling approaches related to hydropeaking. Even so, not all modelling approaches are comprehensive or efficient, as they heavily depend on the predefined objective of the research. Furthermore, even though the flow at hydraulic structures is relatively well understood (Ali, 2013; Harms, 2021), literature on flow behaviour near hydraulic structures in rapidly altering flow regimes due to hydropeaking is almost non-existent. The exploration of hydraulic structures or other morphological alterations as a solution to negative environmental impacts due to hydropeaking is often absent or lacks clarification. In particular ELY, the governmental organisation for economic development, transport and environment in Finland, is interested in similar solutions. Since the personal communication in May 2023 with K. Aronsuu, an experienced researcher at the ELY-centre located in Oulu, I am aware that ELY is interested in practical applications for the restoration of naturally occurring rapids at Juurikoski in particular. Nevertheless, they are currently lacking knowledge on multiple fronts; cost effectiveness of mitigation options, how interventions on rapid systems influence meltwater dangers and what regulations could be implemented to benefit both power generation practices and trout (migration) behaviour. This report only addresses the last point, namely the implementation of regulation or morphological mitigation measures to decrease sub-daily variance impacts.

1.3. Objective and research questions

The main objective is to investigate the impact of hydropeaking on rapids in a complex riverine system with subsequent weirs. The availability of ADCP and LSPIV velocities lends to research two different experimental calibration approaches. The reason why such calibrations could be beneficial is to improve reliability of the model and an increased accuracy related to quantifications of localized flow patterns induced by sub-daily flow variations at key locations near weirs and rapids. This could be valuable information regarding the formulation of mitigation measures to counter hydropeaking impacts, which is the secondary objective. Accordingly, the main research question and sub questions are:

- How does the sub-daily variance introduced by upstream hydropeaking practices affect a complex rapid system situated near weirs downstream of a hydropower plant and how can these impacts be mitigated?
 - a. What defines a good modelling approach with the aim to improve reliability of the model to define appropriate mitigation measures?
 - Can the model be calibrated by LSPIV drone-based surface velocities and is this calibration method beneficial?
 - Are ADCP measurements accurate enough to relatively measure very low and high flows?
 - Is ADCP-data relevant for calibration of the model and is it beneficial to locally alter the roughness of the channel bed based on a comparison analysis between measured and modelled value during this process?
 - b. In a hydrodynamical context, how is hydropeaking at the HHP influencing the main rapids of the Juurikoski site?
 - c. How do the model outcomes differ when considering modified river hydrology or morphology compared to the original riverine system?
 - d. What are the characteristics of efficient mitigation measures to counter environmental impacts?

1.4. Research methodology

Figure 3 schematically depicts all phases and feedback relations of the scientific research methodology. It includes the analysis of literature, the construction of the problem statement and objective, the modelling approach, data specifications, the synthesis, evaluation and analysis of a 2D hydraulic model and ultimately, the processing of outcomes for a scientific understanding of a complex hydraulic rapid system. The literature review covers all aspects of the phenomenon hydropeaking in the context of the Kalajoki basin. Related to synthesis of the hydraulic model, the modelling approach and set-up is a direct result of the fusion of the literature study and data collection, processing and analysis. An important aspect of the modelling approach is the evaluation by means of calibration and validation, which relies on data from water depth loggers, an Acoustic Doppler Current Profiler (ADCP) and drone- based Large-Scale Particle Image Velocimetry (LSPIV). After satisfactory calibration and validation, four scenarios are simulated. In the scenarios, hydrological or morphological changes to the river or structures are introduced. The outcomes from the simulations are variables such as water levels, velocities and shear stress. The results are statistically and graphically processed to be qualitatively and quantitatively assessed. Finally, the findings are discussed, besides the formulation of conclusive remarks and recommendations for readers and future research.

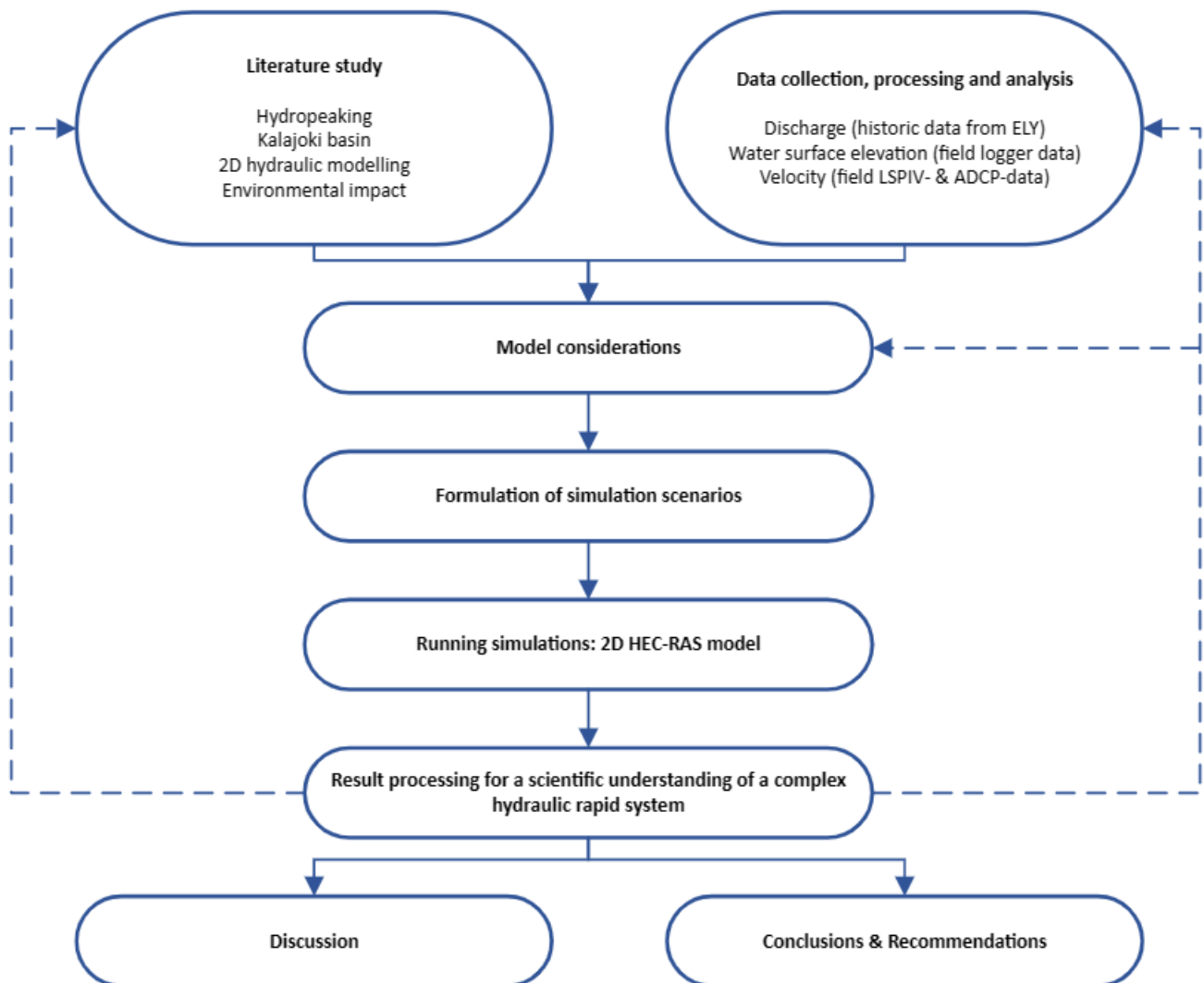


Figure 3: Research methodology

1.5. Data gathering and analysis

In 2020, researchers at the University of Oulu carried out the latest flow measurement campaign on the site of the case study dates. During this campaign, hourly discharges at the base of the HHP from the hydropower company, water depth time series at 6 different logger locations and point clouds describing the terrain with the Global Positioning System (GPS) were retrieved. The results are primary recent, qualified and verified datasets. Prior to model implementation, abnormalities and erroneous data are filtered out. Additionally, an uncertainty analysis and a sensitivity analysis for selected data sources are executed. Notably, files containing water levels could serve for calibration and validation.

Next to discharge and water depths, flow velocities were recorded by two different state-of-the-art methods. A remote floating device with installed ADCP can be steered along the cross sectional span between banks. However, there must be no obstacles or too shallow depth for the remote floating device to be able to move along the desired path. As a result, velocity profiles and a visualization of estimated terrain are retrieved along the whole cross-section it covers. Alternatively, LSPIV-data is gathered by a drone that was remotely steered to fly over the rapids, taking 10 second video clips to provide a complete imagery for the rapids, i.e. upstream, at the location and downstream.

Regarding the 2D hydrodynamical model itself, missing data or values, for example Manning coefficients to describe terrain characteristics, are based on local characteristics of the river bed, such as grain size, the presence of larger elements such as riverine boulders and vegetation. Empirical values for the Manning coefficients are listed in the HEC-RAS 2D Manual, but the actual value is tuned during the hydraulic calibration.

For obvious ethical reasons, gathering of data has been executed by an unbiased party, namely the University of Oulu. Unbiased analysis and reporting is equally important for this report. Maximizing economic profit at the powerplant while improving the environmental conditions are equally important aspects during the case study. The research is not carried out in name of the operating companies and stakeholders at HHP, but they can consult this thesis report for advice.

1.6. Contents of thesis

Chapter 2 contains the literature study, where the geographical and hydrological characteristics of Kalajoki basin, Kalajoki river and case study site Juurikoski are stated. Additionally, a hydropeaking method to classify Nordic rivers is included in this chapter, as well as relevant riverine equations to quantify flow (alterations). The riverine equations are especially relevant to understand the fundamental basis of hydraulic modelling software like HEC-RAS. The last subchapter contains information about existing calibration approaches and experimental methods. Chapter 3 relates to the synthesis, entailing calibration and validation methods, and the evaluation of the hydraulic model. Two experimental methods for calibration are based on state-of-the-art methods related to ADCP- and drone based LSPIV-data. At the end of Chapter 3, four simulation cases are defined, in order simulate hydrological and morphological changes to the river and hydraulic structures. The corresponding results are processed and analyzed in Chapter 4. Finally, Chapter 5 contains the discussion and recommendations, regionally as well as globally. Finally, Chapter 6 states the lessons learned and conclusions from this Master's thesis report.

2. Literature Study

The literature study is initiated by a descriptive study on the Kalajoki basin geographics and other attributes. It also involves a throughout description of the hydrological character of the basin and case study area. In the final two subchapters, a chapter about relevant riverine equations and existing (state-of-the-art) calibration methods are stated, which relate to the modelling approach in the next chapter.

2.1. Kalajoki (and Juurikoski) river characteristics

2.1.1. Geographical attributes

Figure 4 illustrates the Kalajoki basin, located in northern Ostrobothnia (Finland). Its main river, Kalajoki, stretches in total around 110 kilometers from its source at the Hautaperä reservoir to its mouth at the Gulf of Bothnia (Aronsoo & Wennman, 2012). At *Tyngän Kylä* (Tynkä), the tributary Vääräjoki feeds into the Kalajoki, approximately 11 km upstream from the mouth. The town of Ylievieska is located 40 km upstream from the source. A few hundred meters above Ylievieska, the HHP is located, also shown in Figure 4.

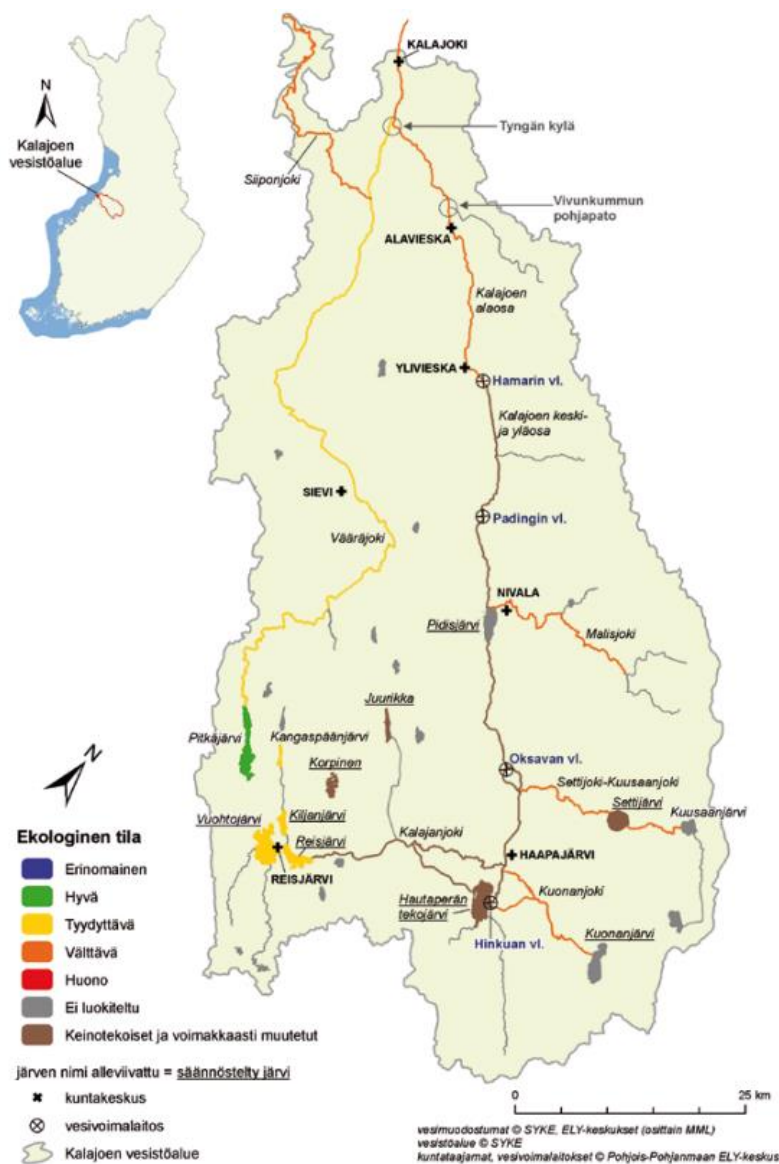


Figure 4: Kalajoki basin with hydropower plants, (artificial) lakes and tributaries. From *Vesirakentamisen ja säännöstelyn sekä niihin liittyvien kompensatiotoimenpiteiden vaikutukset Kalajoen kala, nahkiais- ja rapukantoihin* (Elinvoimaa Alueelle 5, p. 5), by K. Aronsoo & K. Wennman, 2012, ELY. Copyright 2012 by ELY. Note that the figure is somewhat distorted and is only used for illustration purposes.

Kalajoki basin represents a low land river system with 100 m elevation (total slope 0.001) from headwaters to its river mouth. Additionally, the mean discharge is $29 \text{ m}^3\text{s}^{-1}$, with a minimum of $4.1 \text{ m}^3\text{s}^{-1}$ and a maximum of $246 \text{ m}^3\text{s}^{-1}$ (Addo, 2019). The catchment area is approximately 4260 km^2 and changes in precipitation rates influence the hydrology of Kalajoki basin greatly, since the leakage percent is only 1.8% (Aronsoo & Wennman, 2012). During periods of high flow, it carries a significant load of suspended solids, and under normal flow conditions, it exhibits elevated concentrations of metals, as noted by Addo (2019). Moreover, it possesses a humic quality and maintains consistently low pH-values, which renders it suitable for irrigation (Aronsoo & Wennman, 2012). As an indirect result, the land predominantly serves agricultural purposes, cultivating grains, potatoes and providing pasture for grazing cattle (Aronsoo & Wennman, 2012). In summary, Table 2 lists the different elements of Kalajoki basin and their purpose or relevance. During a field trip in August along Kalajoki, the river use, land use and river bed were visually inspected. It is worth noting that the most prominent river in the basin has no real navigational purpose, except for some small recreational boats. Nevertheless, it is an important catalysator for agricultural land use on the banks. At Juurikoski, the riverbed composition of the channel is mainly a combination of gravel and sand, while more downstream, the river mouth is primarily sandy.

Table 2: Elements and Their Relevance in the Lower Basin of Kalajoki

Element	Purpose/Relevance
Navigational waterways	Passageways for small boats
Navigational waterways	Possibilities for rowing, kayaking and water sports
Water quality	Good and safe fishing (salmon, brown trout, lamprey, pike)
Water quality	Possibility for recreational swimming
Water quality, flooding precautions	Agricultural value of the banks (grain, potatoes, meat and milk)
Flooding precautions (banks, weirs)	Economical valuable assets (buildings, industry terrain)

Juurikoski is located in the centre of Ylivieska and spans approximately 550 meters. It has coordinates at $71^{\circ}08'35''$ N latitude and $25^{\circ}47'35''$ E longitude. Figure 5 schematizes the locations of several weirs, rapids and two small islands. Main rapid areas are located at weirs 3, 4 and 5. Moreover, each letter (A,B,C) corresponds to a rapid and corresponding weir opening. On the aerial photograph, the southside banks harbour a channel that diverts a relatively small fraction of the stream towards a flour mill. Since the mill is no longer operational, the same amount of incoming water is released at the downstream end of this side channel.



Figure 5: Schematization of hydraulic structures at Juurikoski.

Typical for Juurikoski is that on top and at backward facing step of each weir, a sub-rapid can be observed (see Figure A.1 in Appendix A). Beware that long crested weirs are assumed to have a hydrostatic water depth. However, in this case, big riverine rocks are present near the structures, which introduce curved streamlines and vortices to the flow.

2.1.2. Kalajoki – An artificially influenced reach

The weirs at Juurikoski were implemented to regulate flow during periods of rapid snowmelt, and to reduce peak flows, often from hydropeaking practices. Other flood protection measures, such as embankments or dredging works, also occurred frequently in previous years. To simplify how Kalajoki is artificially influenced throughout the years, the basin is subdivided in a lower basin, a middle basin and an upper basin. The lower basin stretches about 45 km. It is relatively unmodified compared to the middle and especially upper basin, respectively 45-60 km and 60-110 km from the source. However, the lower basin is partly embanked, dredged and the flow is short-term regulated (Aronsoo & Wennman, 2012). The hydropower plants in the middle and upper basin, build 40 to 50 years ago, create complications for the lower reach of the basin. Historic interventions among the whole river stated by Aronsoo and Wennman (2012) provide clarifications on the past and current riverine lay-outs. Appendix A shows the evolution of the rapids of Juurikoski during the time of several interventions.

The first large-scale Kalajoki regulation project (1903-1910) had the sole purpose of flood protection. In the years after this, embankments were constructed and natural as well as artificial reservoirs were implemented in the upper basin. Hautaperä (see Figure 4), a far upstream artificial lake, had the biggest impact on regulation.

Oksava and Hinkua, both hydropower plants downstream of Hautaperä, were built in the few years after that. Consequently, dredging became essential for maintenance. In the 80s, excavations, straightening measures and embankments at the middle part spanning over 50 km were carried out. HHP, just above the city centre of Ylivieska, was built and commissioned in 1984. From the 90s onward, fish migration structures and ponds were introduced. Around this time, the lower basin lies under continuous work to provide safety against flooding. During the 2000s, there was a greater emphasis on the restoration of rapids and fish habitats. In 2002-2003, two foundation dams were built in the lower part near the city Alavieska. In 2004-2005, a project to excavate the river at the Juurikoski site and level the bed with bottom dams was executed to improve the landscape and promote flood protection. Several hectares of natural rapids were lost by this intervention (Aronsuu & Wennman, 2012).

Since the implementation of hydropower plants Hamari, Padinki, Oksava and Hinkua, the lower basin has experienced significant disturbances primarily due to hydropeaking. This influence surpasses the impacts of any other intervention in the river reach. However, there are positive aspects to this artificial influence on the Kalajoki reach, extending beyond the generation of sustainable electricity. During the summer of 2012, the national news broadcaster YLE reported on instances of flooding in northern Ostrobothnia, which included the Kalajoki region. Damage linked to Kalajoki river however was reasonably modest in comparison to rivers located north of Kalajoki, such as Siikajoki and Oulujoki. Plausible explanations for this could be attributed to the continuous development efforts that the Kalajoki basin has undergone in previous decades.

2.1.3. Hydrology, climate and climate change

By definition of the Köppen Geiger climate classification, the climate is considered boreal and sub-arctic (Virk, 2022). This means that the winter months are coldest and the summer months the most warm, leaving the mean annual temperature around 0 degrees Celsius. Additionally, snowfall occurs usually from October till early May (leading to large amounts of meltwater in April) with a mean snow depth of 60-80 cm (Virk, 2022). The annual average precipitation is 500 mm/year, with the largest percentage of rainfall occurring in summertime (Addo, 2019). According to climate change projections, both the mean temperature and precipitation may increase (Ashraf et al., 2018). Snow accumulation has already declined in previous years (Virk, 2022). Premature spring peak flooding and increased spring and winter runoff are dictating recent natural flow regimes (Ashraf et al., 2018), but hard to distinguish for Kalajoki due to artificial influence. Since there is no indisputable significant trend yet regarding discharges at Kalajoki, climate changes are treated as projections, not actual scenarios in this report. Climate change may become more relevant for future studies about hydropower management practices.

Yearly data about the hydrological conditions of Finnish rivers are open-sourced by SYKE. Kalajoki is considered relatively small for national standards. Consequently, data about Kalajoki is provided by two hydropower stations. Malisjoki is the most upstream gauging station, whereas Niskakoski is the most downstream gauging station. From data between 1971 and 2017, the maximum discharge reached a value of $47 \text{ m}^3\text{s}^{-1}$ and $0.03 \text{ m}^3\text{s}^{-1}$ as a minimum at Malisjoki. The maximum discharge to have occurred at Niskakoski was $427 \text{ m}^3\text{s}^{-1}$, with a minimum of $1.2 \text{ m}^3\text{s}^{-1}$. The order of magnitude of discharges at Maliskoski with respect to the discharges at Niskakoski is plausible, since (small) tributaries join downstream of Maliskoski. Therefore, runoff from the catchment area becomes respectively bigger. The small leakage and snowmelt storage capacity also contribute to a larger amount of run-off. Figure 6 shows a blue and a red flow hydrograph, both from 2022, which correspond analogically to Malisjoki and Niskakoski.

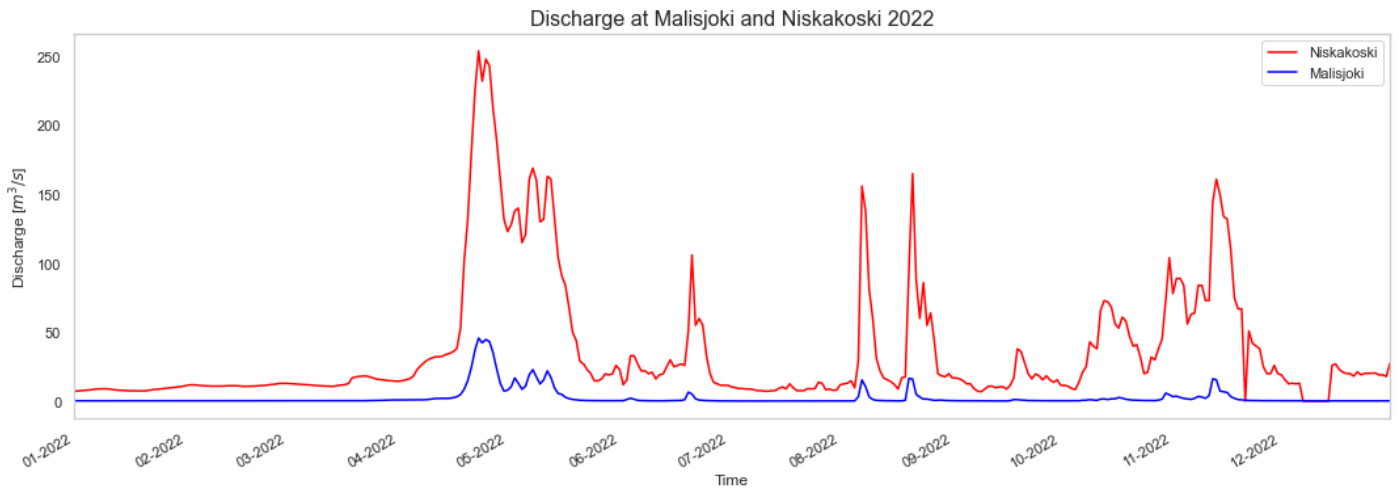


Figure 6: Discharge time series: Malisjoki versus Niskakoski in 2022

The highest discharges typically occur during springtime due to the contribution of meltwater in sub-arctic rivers (Addo, 2019). Derived from Figure 6, the measurement of the upper discharge was conducted at the end of April, whereas minimum discharges occur in August, which aligns with the previously mentioned trend. Note that these gauging stations are located relatively far away from hydropower plants and that the timeline is on a monthly scale. Thus, the influence due to hydropeaking is hard to derive from these hydrographs.

Figures 7,8 and 9 show yearly hydrographs from 2018, 2022 and 2023. They also illustrate an average hydrograph over a timespan of 25 years. From the figures can be deduced that in comparison with previous years, short-term flow alterations were respectively larger during summertime than in 2018 for both Malisjoki and Niskakoski (SYKE, 2023). The same data shows that maximum discharges are overall higher and minimum discharge overall lower in recent years than in previous decennia. A possible interpretation might be an increase of hydropeaking practices, but might also be climate change or another unknown factor.

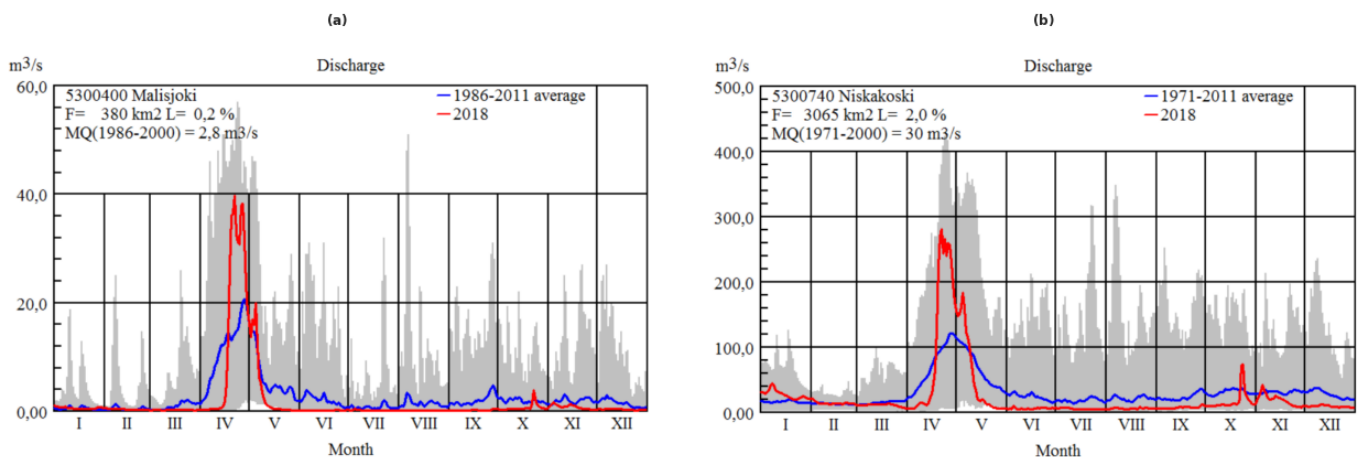


Figure 7: Discharge time series: At Malisjoki (a) and Niskakoski (b) in 2018. From *Current hydrological information (in Finnish)*, 2023, SYKE.

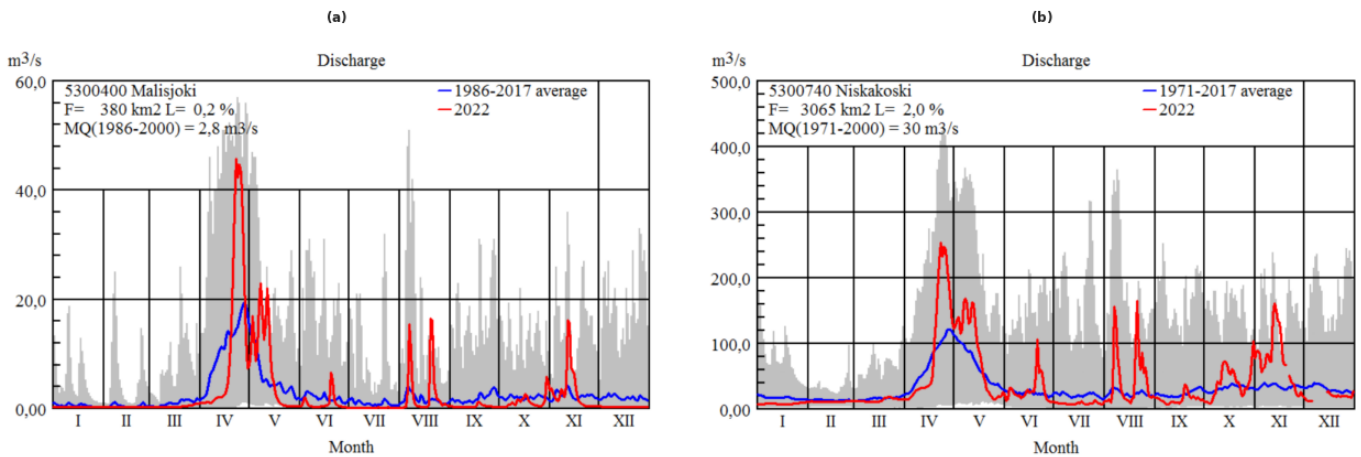


Figure 8: Discharge time series: At Malisjoki (a) and Niskakoski (b) in 2022. From *Current hydrological information (in Finnish)*, 2023, SYKE.

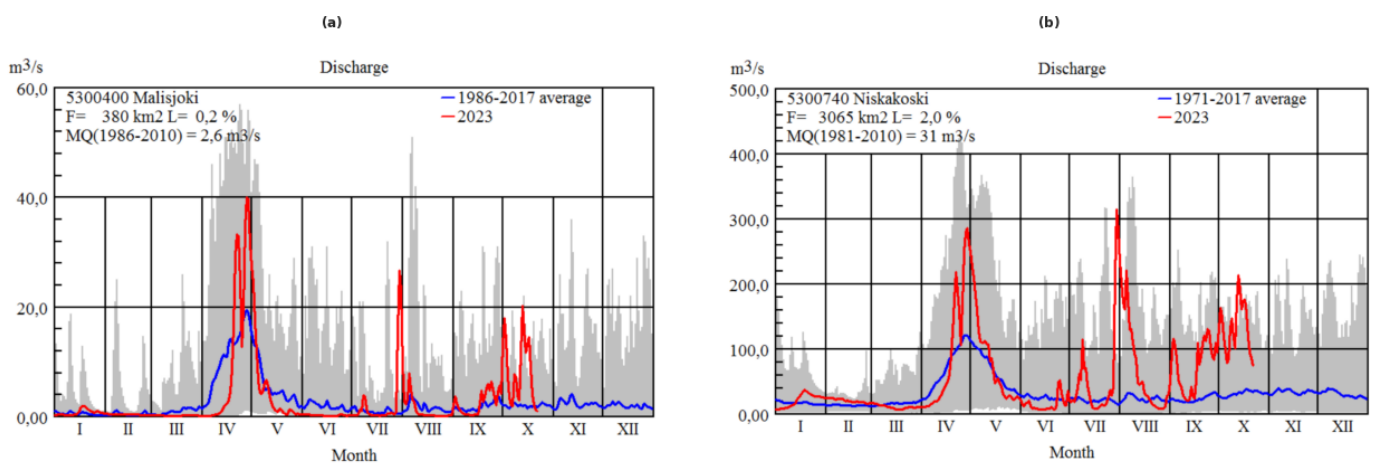


Figure 9: Discharge time series: At Malisjoki (a) and Niskakoski (b) in 2023. From *Current hydrological information (in Finnish)*, 2023, SYKE.

At the HHP above Juurikoski, ramping rates for the relatively small turbine vary between $2.5 \text{ m}^3/\text{s}$ and $8 \text{ m}^3/\text{s}$. In Padinki, a gauging station upstream, these rates vary from $0 \text{ m}^3/\text{s}$ to $15 \text{ m}^3/\text{s}$ (K. Aronsuu, personal communication, June 2023). This causes an incompatibility issue between flow in upstream and downstream reaches. For the implementation or modification of hydraulic structures to counter this incompatibility, the city of Ylivieska can give a permit. This is in contrast to operational measures, where the power company has to provide permission. ELY is the advisory and researching entity between the two parties. According to K. Aronsuu (personal communication, June 2023), political decisions regarding the aesthetic characteristics of the site influenced and most likely prevented the restoration of rapids in previous years. However, a more natural river flow regime at Juurikoski could not only be beneficial for the site itself, but also for river reaches in the lower basin.

2.2. Hydropeaking quantification – Impact class determination

Figure 10, by Ashraf et al. (2018) outlines the impact classification of unregulated and regulated gauging stations in Norway, Sweden and Finland. In Finland, the percentage of ‘high impact’ plants is substantially higher than for rivers in the other two Nordic countries. This is because Finland has relatively small head elevations, especially in comparison to Norway. Run-of-river hydropower plants constructed on rivers with small elevation head experience overall higher hydropeaking impacts than others.

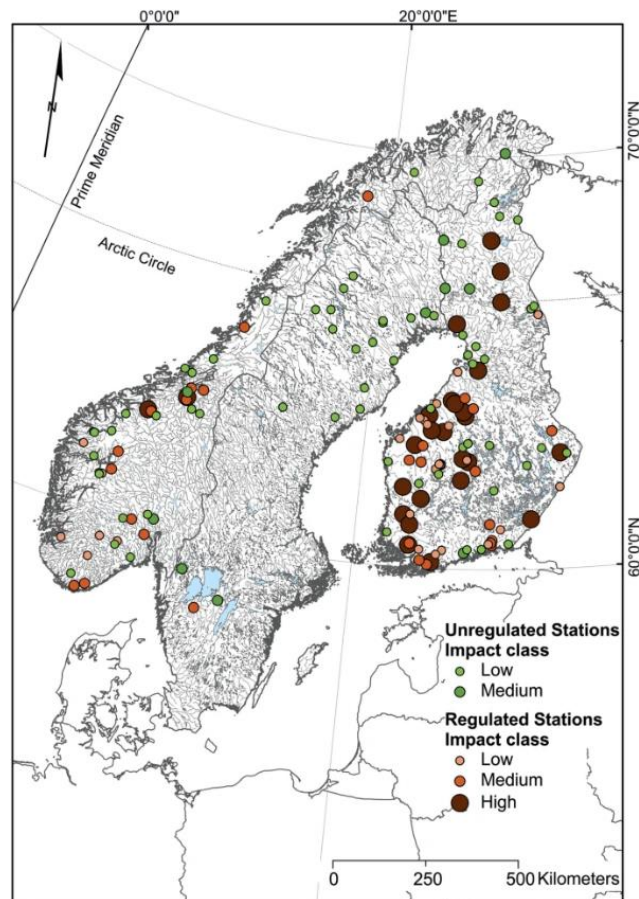


Figure 10: Classification of unregulated and regulate stations dependent on impact in Nordic countries. Ashraf et al., 2018.

Hydropeaking in sub-arctic rivers has increased significantly in the past years. The main driving force being seasonal variation, taking into account aspects like meltwater and variations in power consumption. Additionally, research analysis showed hydropeaking values to be higher in summer months, when power production is generally lower than in winter months. Since the plants in Finland are overall reasonable small, the phenomenon hydropeaking has the biggest environmental impact of all aspects involving hydropower plants. This is observed in natural flow regimes, sediment transport and water temperatures.

There exist multiple methods to quantify hydropeaking trends. Hydropeaking indicators provide an easy classification of data series according to literature. A simple method was proposed by Meile et al. (2011), most likely further developed by Carolli et al. (2015). The method implements coefficients based on time series of river discharge. Another method by Le Coarer (2007) applies ‘hydrosignatures’ for ecological modelling. These quantitative metrics essentially quantify hydraulic diversity by a representation in the depth-velocity plane. Ten years later, Le Coarer (2017) linked the assessment of hydropeaking flow alterations for various

scales of rivers to hydraulic signatures. In conclusion, the method by Meile et al. (2011) is the most straightforward. Note however that the description of hydropeaking indicators by Carolli et al. (2015) is applied in the following formulas. According to Carolli et al. (2015) the first indicator HP1, a dimensionless measure of magnitude of hydropeaking, is defined by:

$$HP1_i = \frac{Q_{max,i} - Q_{min,i}}{Q_{mean,i}}, \quad i \in [1, 365] \quad (1)$$

$$HP1 = median(HP1_i) \quad (2)$$

i denotes the day of the year, Q_{max} is the maximum discharge value, Q_{min} is the minimum discharge and Q_{mean} is the normalized mean value. The second indicator HP2 [$m^3s^{-1}h^{-1}$] measures the temporal rate of discharge changes. It is based on a probabilistic approach, utilizing the 90th percentile of the discretized time derivative of the instantaneous stream-flow series:

$$(HP2_k)_i = \frac{\Delta Q_k}{\Delta t_k} = \left(\frac{Q_k - Q_{k-1}}{t_k - t_{k-1}} \right)_i, \quad i \in [1, 365] \quad (3)$$

$$HP2_i = P_{90} | (HP2_k)_i | \quad (4)$$

$$HP2 = median(HP2_i) \quad (5)$$

Q_k denotes each available discharge datum. The interval for k is $1 \leq k \leq 24$ regarding data sampled every 60 minutes. HP1-indicators are related to long-term hourly peaking magnitudes, while HP2-indicators are related to ramping. Figure 11 represents a scatterplot of Nordic hydropower plants and their impact classification, depending on both HP1 and HP2.

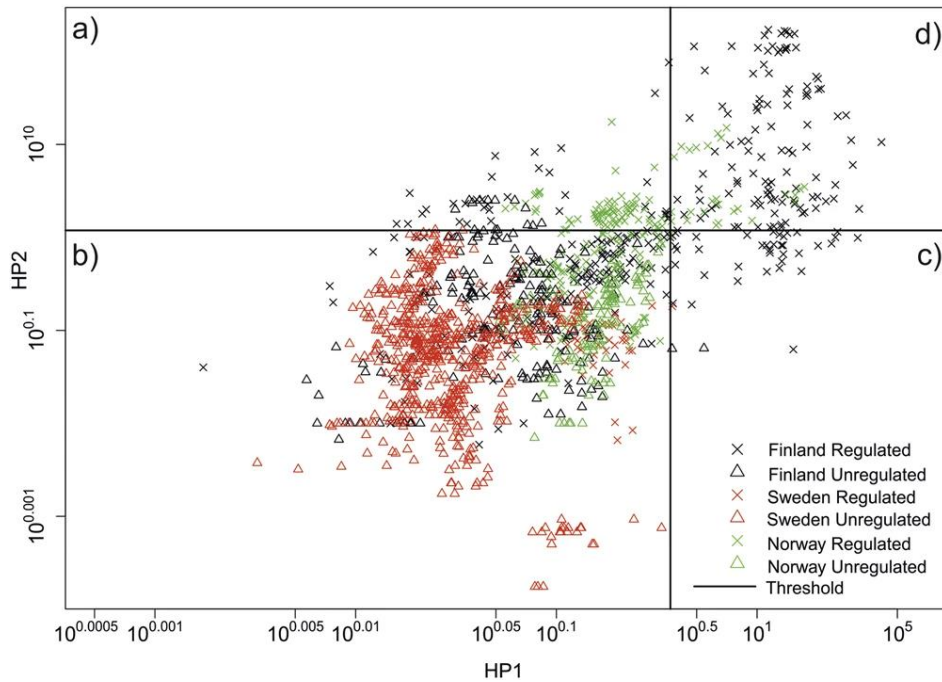


Figure 11: Classification hydropeaking impact. Four parts of the graph identified as three different hydropeaking impact class are: (b) low impact, (a,c) medium impact, and (d) high impact. Ashraf et al., 2018.

2.3. Riverine equations

2.3.1. Shallow Water Equations (SWE)

Formula 6 and 7 show the Shallow Water Equations (SWE). The SWE contain both mass conservation and full SWE-momentum equations (Mario et al., 2022). The full SWE-momentum equations account for gravity, friction, hydrostatic pressure, acceleration (local and convective), turbulence, the Coriolis effect and even wind forces, if applicable. The 2D SWE are formulated below, u and v being the generalized velocity components in x and y - direction:

$$\frac{Du}{dt} - fv = -g \frac{\partial H}{\partial x} + v_t \nabla^2 u - c_f u + \frac{\tau_{sx}}{\rho h} \quad (6)$$

$$\frac{Dv}{dt} - fu = -g \frac{\partial H}{\partial y} + v_t \nabla^2 v - c_f v + \frac{\tau_{sy}}{\rho h} \quad (7)$$

Cartesian coordinates are at the base of these equations, considering only the components of rotation aligned with the local normal. This is a fairly standard approximation of a spherical planet, i.e. Earth, denoted by the f plane. f is equal to $2\Omega \sin\theta$ where Ω is the frequency of the Earth's rotation and θ is the latitude. At mid-latitude, this value is approximately $1 \times 10^{-4} \text{ 1/s}$.

2.3.2. Diffusion Wave Equations (DWE)

The Diffusion Wave Equations (DWE), referring to Formula 8 and 9, contain the mass conservation and diffusion form momentum equations (Dawson & Mirabito, 2008). The diffusion form momentum equations only account for gravity, friction and hydrostatic pressure. The 2D diffusion wave form of momentum equations is:

$$g \frac{\partial H}{\partial x} = -c_f u \quad (8)$$

$$g \frac{\partial H}{\partial y} = -c_f v \quad (9)$$

The terms $\frac{\partial H}{\partial x}$ and $\frac{\partial H}{\partial y}$ are partial derivatives. They indicate changes in pressure differential force. The right sided term in Formulas 8 and 9, consist of the coefficient due to friction times velocity, either in streamwise or lateral direction.

2.3.3. Comparison between SWE and DWE-sets

According to the 2D HEC-RAS user's manual (USACE Hydrologic Engineering Center, 2023), DWE are more forgiving numerically than SWE. Additionally, DWE can handle larger computational time and is practical for fast routing of floods. For the case study however, the SWE-set proves to be more accurate than the DWE. As argumentation, the system has a very flat slope, let's assume less than 0.0002, so gravity and friction are not dominant. Furthermore, for detailed velocities and water levels near hydraulic structures, SWE displays slightly more information. The flow in such areas is known to have transitions from subcritical flow to supercritical flow (and vice versa) and spatial variations along the river channel, so the SWE-set is preferred.

2.4. Advances in river model calibration

2.4.1. The challenge in existing calibration methods

Nowadays, there are many different software packages available to model rivers in the 1D, 2D and 3D-plane. Moreover, there are different calibration approaches for hydraulic river models. Kuanestani et al. (2022) listed the most recent papers together with the dimensionality of modelling software, name of the software, discharge range for calibration and calibration approach. Their summary gives insight in the current methods applied related to modelling and calibration, but also challenges to overcome. Kuanestani et al (2022) stated that “given these changes in hydrometeorological conditions, the question arises whether it is possible to set up a hydraulic model that simulates both high, intermediate and low flows in rivers accurately”. By “these changes”, they refer to global climate changes which affect river processes. Additionally, a conventional calibration typically relies on water levels to alter main channel roughness. 2D software, such as LISFLOOD-FP, 1D-2D MIKEFLOOD and Delft3D Flexible Mesh suite are typically calibrated on this principle. Concluding, there is limited literature available on other calibration methods, which could potentially contribute to a robust model to simulate both high, intermediate and low flows accurately.

2.4.2. Experimental calibration with LSPIV and ADCP data – Juurikoski

In literature, the source of measured data for calibration varies per study. For example, Bomers et al. (2019) created a 2D HEC-RAS model, based on relatively up-to-date measured data retrieved by Rijkswaterstaat. However, the method of data gathering and its benefits, are not often thoroughly discussed. Data gathering with LSPIV or ADCP measurement tools, can provide high density and localized site information. This type of data is often applied for various purposes, but usually not for calibration. Therefore, a calibration method based on LSPIV- or ADCP-would be considered state-of-the-art. LSPIV captures surface water velocities using imagery, offering fine-scale details to refine the model. ADCP allows for precise measurement at various depths, enhancing the accuracy of the model. Concluding, these methods offer a data-rich approach, which contributes to contemporary hydraulic modelling practices.

The paper by Guillén (2017) discusses the use of LSPIV-velocities in the assessment of urban flash flood vulnerability. But even more interestingly, it shows the potential of LSPIV for calibration. Channel and floodplain roughness not only has a relationship with water levels, but velocities as well. The model approach by Guillén (2017) contains a 1D HEC-RAS model set-up. However, the case study requires a 2D model. Therefore, an experimental method by a hot spot analysis in ArcGIS is proposed. A hot spot analysis requires two almost identical raster maps that can be placed on top of each other. Since 2D HEC-RAS is able to reproduce raster velocity maps from a top view perspective with velocity components in x- and y-direction and LSPIV can be processed to achieve a similar layer, a layering of both raster maps is possible. If hot spot analyses are performed separately for each layer, a hot spot comparison analysis can show similarity between flow regions. This method is labelled as experimental ‘calibration method 2’.

Calibration of 2D or 3D hydro- or morpho dynamic models usually rely on a considerable amount of (3D) ADCP recordings (Geurrero et al. 2013; Parsapour-Moghaddam et al. 2018). The recording visualizations are typically compared to models in the x-, y- plane, but not in the x-, z- plane. Especially in context of hydropeaking, a comparison of velocity profiles could be a valuable resource to localize hydropeaking impacts. Looking back on the paper by Guillén (2017), control sections can be applied to calibrate the n-roughness coefficient. The method involves the distribution of ADCP cross-sectional data sections, then the calculation of section velocities. Accordingly, HEC-RAS cross-sections are subdivided and n-roughness coefficients are calibrated per specified region according to a comparison analysis between measured and modelled section velocities. This is considered experimental ‘calibration method 3’.

3. Materials and methods

In this chapter, the data types, 2D hydrodynamical modelling approach and simulation scenarios are defined. Model calibration and validation are crucial steps to ensure reliability and accuracy of a predictive numerical model. Three calibration methods, two based on state-of-the-art methods, will be discussed, while the conventional method 1 based on logger data is applied to ensure quality during the generation of simulation results.

3.1. Dimensionality and model choice

In hydraulic modelling practices, the first modelling dilemma often relates to the dimensionality of the model (Z. Virk, personal communication, May 2023). 1D and 2D models run quickly in comparison to 3D models. For 1D-modelling, river parameters have no variations along the cross-section. A 2D-modelling approach offers more insight in a case with significant lateral flows, lateral hydraulic structures such as weirs and braided systems. An advantage of 2D-modelling is that computational cells do not need to be flat bottomed, since cell faces and edges do not have to be straight with a single elevation value. Morphological changes to the river bed are typically simulated in 3D, since sediment volumes are relevant. Delft3D FM is an example of capable software for computations related to morphological processes, additional to complex hydrodynamic and sediment transport in 2D and 3D. Combined modelling is advisable in areas that require a higher level of hydrodynamic fidelity to perform unsteady flow analysis. An example would be a case study with one distinct channel and floodplains. Concluding, the riverine features to be studied and accordingly the end goal, in this case the modelling and mapping of (localized) riverine flow behaviour, determines the dimensionality.

2D HEC-RAS models are usually applied for flood risk analysis in basins, e.g. rainfall-runoff simulations and flood plain inundation simulations. However, the software is convenient in other fields, including fish habitat simulations, sediment transport modelling, vulnerability mapping etc. An additional great benefit of this software is that streamwise and lateral flow can be accurately represented. Around hydraulic structures, on irregular terrain or even floodplains. Other 2D-modelling options would be MIKE21, LISFLOOD and state-of-the-art models (Costabile et al., 2020; Shrestha et al., 2020; Shustikova et al., 2019). However, for these software options, the computational intensity is lowest for 2D modelling in HEC-RAS. Moreover, the software is free and widely used in practice, hence its popularity in hydraulic engineering. The riverine system of the case study at Juurikoski is somewhat braided with diverging and converging streams around inland islands. Both streamwise and lateral flow are significant in the system. Moreover, the goal is to simulate hydrological changes and to analyse flow near hydraulic structures.

Concluding, 2D-dimensionality agrees with the availability of LSPIV-data and aim to define mitigation measures, for which depth-averaged flow information in the x-, y-plane suffices to get an initial idea. HEC-RAS is recommended since it is widely known outside the Netherlands, making the report fit for comparison studies in Finland. Also because of the user-friendly interface to model 1D and 2D-flow, lateral structures and specify localized roughness parameters. For the case study in particular, in Finnish literature, a 2D HEC-RAS model results could be interesting to compare with existing 1D model results for Juurikoski. Delft3D FM is also a good option, but for convenience and because of the relatively straightforward, smaller-scale river layout compared to highly complex and typically large-scale coastal and estuarine applications, 2D HEC-RAS is most likely sufficient.

3.2. Model input specifications and characteristics

HEC-RAS solves the Saint-Venant Equations in order to simulate a river system. Before these computations, the model has to be properly set up. Figure 12 outlines every aspect of the modelling method applied. The type of data source, input processing, input layers and other elements, computational methods, output variables and output processing are the main categories in the schematization. Most of the boxes are further elaborated in the next sections.

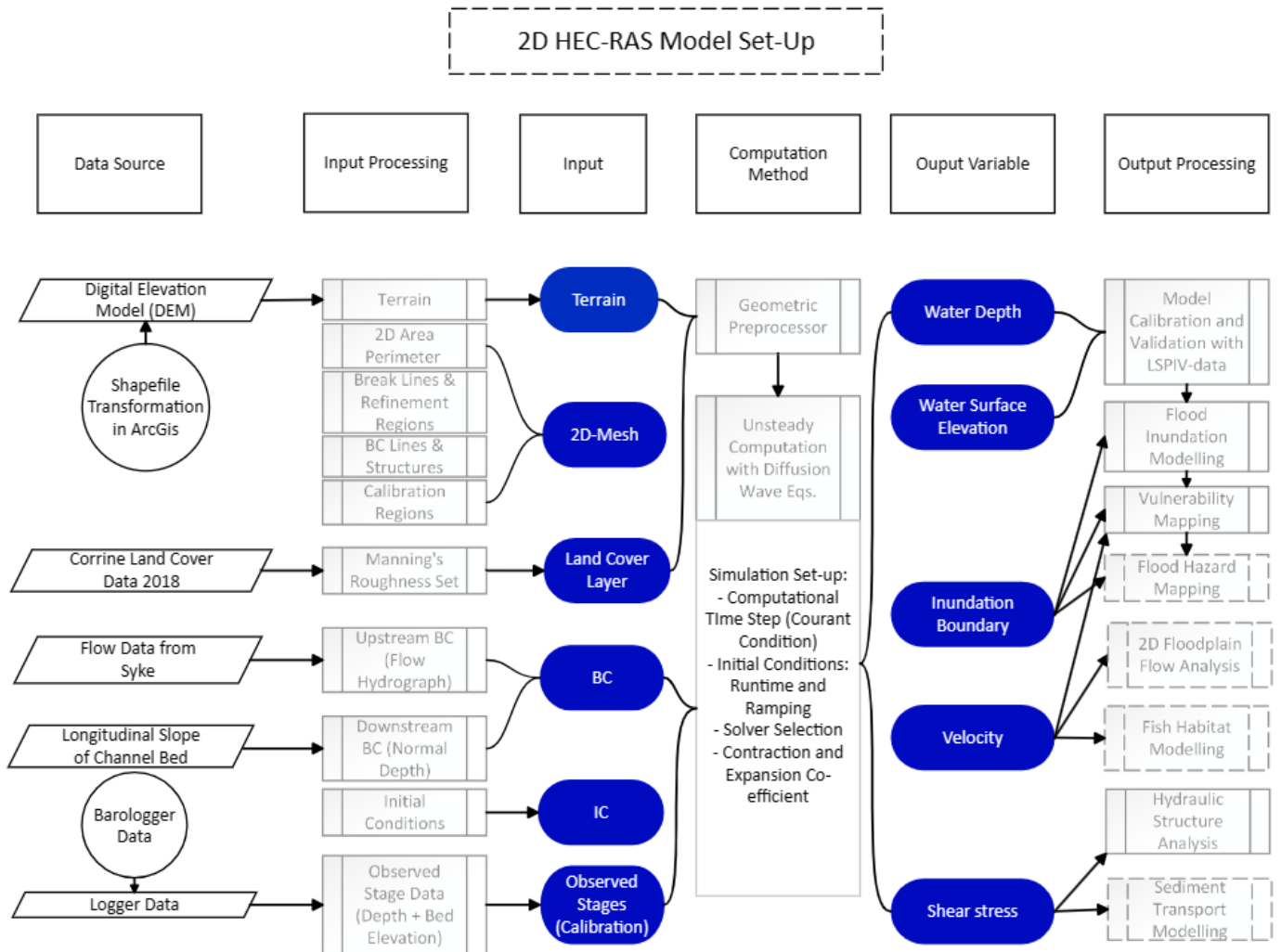


Figure 12: 2D HEC-RAS model set-up

A 2D model computes parameters such as discharge, velocity, water levels and shear stress. For the outputs to be as realistic as possible, significant contributors are the resolution of the terrain model and overall terrain geometry. Moreover, the resolution and level of accuracy of flow data influences the quality and reliability of the model outcomes greatly. In this subchapter, all relevant input for the 2D hydraulic model will be further discussed.

3.2.1. Juurikoski shapefiles, discharge data, logger data, ADCP velocity signals and LSPIV images

The data specifications are listed by the type of data implemented in the model. ELY provided discharge data from the base of HHP, while a research team from the University of Oulu provided GPS based point cloud data, water level time series on six locations, ADCP- along multiple cross sections and drone based LSPIV-data across the site:

- **GPS Point Cloud Data (for Terrain)**

The available depth-sounding survey data for Juurikoski is a point cloud based on 3D Cartesian coordinates. The point clouds are imported in ArcGIS and transformed with a linear interpolation method into a DEM (Digital Elevation Model) to model terrain layers. Additionally, missing local grid cells are acquired from the Finnish national database (Paituli, 2023). Finally, the Juurikoski terrain site is created by merging multiple TIN-files.

- **Discharge Data**

Hourly discharge series on the 24th of June 2020 at the base of HHP are made available by ELY.

- **Logger Data**

Observed water levels are useful for calibration and validation. Solinst water pressure loggers were installed on the site. Figure 13 indicates the placement of loggers 1 through 6, which measure the pressure exerted by the water column above the sensor. The hydrostatic pressure equation, relating pressure to fluid depth and density, allows the determination of water levels. Consequently, water levels can be determined. Loggers 2, 3, 4, 5 and 6 lie within the area of interest. Logger 1, while not explicitly covered in this report, is examined for alignment with values downstream.

- **ADCP Cross-Sectional Data**

The ADCP datafiles displays information about the velocity of water at various depths across a specific transect of the river. The cross sectional datafile that matches the low flow conditions between 11:00-17:00 on the 24th of June 2020, labelled from here on as CS1, is chosen as a reference for comparison with a model profile line on the same cross section.

- **LSPIV Data (Processing)**

The LSPIV-files contain 10 second video clips, consisting of 300 frames per second. The frames and corresponding averaged point data are subjected to image co-registration, data analysis, postprocessing and georeferencing. The most important objective during these procedures is to portray velocities in x- and y-direction accurately for various areas and to filter out false velocity values. Firstly, video clip frames are aligned, or co-registered, with the first frame to minimize error cause by drone movement. Secondly, by applying MATLAB's PIVlab-extension package, the results are frame-by-frame u and v velocity components in image-coordinates. The data is now to be filtered for additional false velocity values, occurring mainly in areas with no flowing waters or waves caused by wind. Finally, a transformation to world coordinates is performed with an affine transformation method based on known points in the image area.

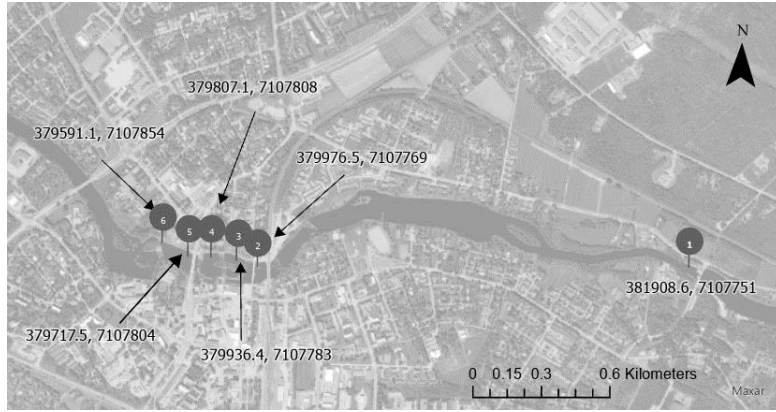


Figure 13: Logger locations expressed in Cartesian coordinates

The released discharges from HHP introduce an unsteady flow at Juurikoski. In Figure 14, the hourly discharges are represented by a hydrograph. This hydrograph describes the upstream model boundary. The flow variation is less than $0.1 \text{ m}^3 \text{ s}^{-1}$, observed on all hours. An exception occurs on 14:00-15:00, when the big turbine was turned on. Additionally, a delay of 10 minutes in the change in water level below the plant is observed from data (see Appendix B). A few minutes before 15:00, a peak of approximately $12 \text{ m}^3 \text{ s}^{-1}$ can be observed. The peak rapidly decreases to $1 \text{ m}^3 \text{ s}^{-1}$ around 16:30, before the discharge spikes again. This second peak remains for a longer period between 19:00-22:00.

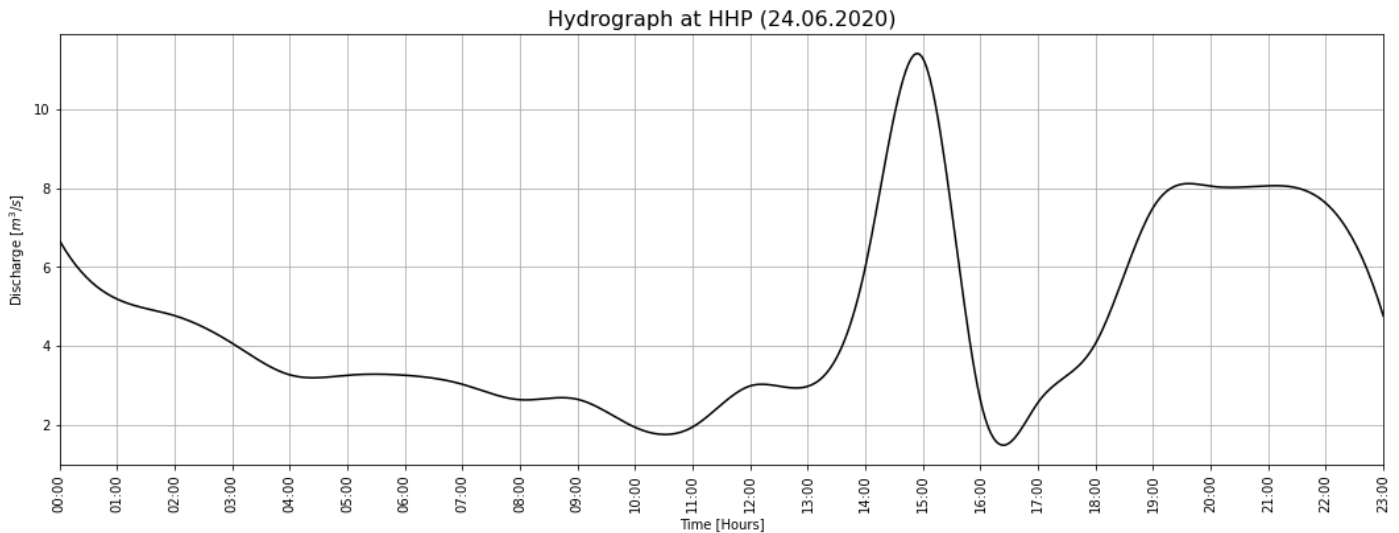


Figure 14: Hydrograph - Ramping practices at HHP

Solely a 24 hours flow dataset is not sufficient to simulate the river flow, since flow needs time to establish steady conditions as well as to approximate the equilibrium water depth. Consequently, a base flow, i.e. 48 hours prior to hydropeaking practices, is applied, on top of which a peak flow is defined, i.e. 24 hours of hydropeaking practices.

3.2.2. Land cover data

For an open channel and steady uniform flow, widely applied is Manning's equation. In empirical Formula 10, n is defined as Manning's roughness coefficient. It represents the roughness or friction applied to the flow by the channel (Bengtson, 2017).

$$Q = \left(\frac{1.00}{n}\right) AR^{\frac{2}{3}}\sqrt{i} \quad (10)$$

In Formula 10, Q is the discharge, n the Manning’s roughness coefficient, A the cross-sectional area of the flow, R the hydraulic radius and i the hydraulic gradient. Applying Manning’s roughness coefficients as calibration parameters to represent the channel bed (or floodplain) resistance is a common practice in numerical modelling based on Saint-Venant equations. Furthermore, an unsteady flow analysis can be performed by such a model, even if Manning’s equation is developed for steady flow.

The model land cover layer contains specified n-values and permeability percentages. These values are attained from the open sourced database of SYKE. Table 3 shows an overview of typical values per land use type, based on the Corrine Land Cover 2018 dataset. A high Manning’s coefficient or number results in a lower flow conveyance. Similarly, a low Manning’s number indicates less resistance to the flow. For concrete infrastructure, such as weir structures and river beds, the soil is assumed to have zero porosity. The riverine rocks on top of the weir need to be accounted for by assigning higher roughness coefficients. Typically, river gravel diameters vary between 75 mm and 150 mm (Voorendt, 2022), but aerial photographs show that they can be much larger.

Table 3: Manning’s n Values and Percentage Imperviousness for Land Cover Types

	Manning’s Values	Percent Impervious
Infrastructure	0.06 – 0.2	100
River Bed	0.025 – 0.05	100
Vegetation	0.07 - 0.16	50
Riverine rocks	0.07 - 0.16	50
Weir	0.07 - 0.16	100

The Corrine Land Cover 2018 datafile can be imported as a shapefile in HEC-RAS. However, the smallest area distinguished is 25 ha, since the spatial set is generated on a national scale. A smaller shapefile ArcGIS software is created to interchange with this shapefile. Finally, every ‘patch’ or polygon of the smaller shapefile, gets its value assigned from Table 3.

3.2.3. Terrain

Before the merging process of TIN-files, the Juurikoski point cloud is linearly interpolated to get a full Digital Elevation Model (DEM). The accuracy and quality of the resulting surface depends on the point density, the pixel size and the interpolation technique applied (Virk, 2022). The point density of 0.5 *points/m²* indicates a rather sparse point cloud. The pixel size relates to the spatial resolution of the point cloud. It describes the terrain elevation and is chosen according to the amount of average point spacing. Note that a large value will result in loss of accuracy and a small value results in an increased computational time. After five iterations, a pixel size of 3m x 3m (i.e. value of elevation will not change within 9 *m²*) shows to be sufficient to produce a relatively smooth continuous surface and enough detail to produce realistic topographic attributes. This can be checked by zooming in and zooming out. A streamwise profile cut over the reach shows the flat sloping character of 0.001 for the river. Also, lateral profile cuts can be analysed. A pixel size of 3m x 3m shows realistic elevations of the banks with respect to the bed level.

3.2.4. HEC-RAS Geometry – Computational mesh and lateral structures

HEC-RAS creates a computational mesh over the terrain layer file to limit the total amount of hydrodynamic computations during simulations. Figure 15 includes the computational mesh, which has a grid size of 3 m. A grid cell size of 3 m by 3 m (after 2 iterations) proves to be sufficient. By this choice, river processes such as confluence and expansion near rapids, which have a width of 3 m, or lateral momentum exchange due to patches representing vegetation and large boulders, are captured. Thus, a larger grid cell size does not capture flow dynamics on the right scale. The biodiverse riparian edges and floodplains extend approximately 100 m from the banks of the river, so the 2D-perimeter extends beyond this width. The mesh can be further refined for branching and confluences near in-stream islands.

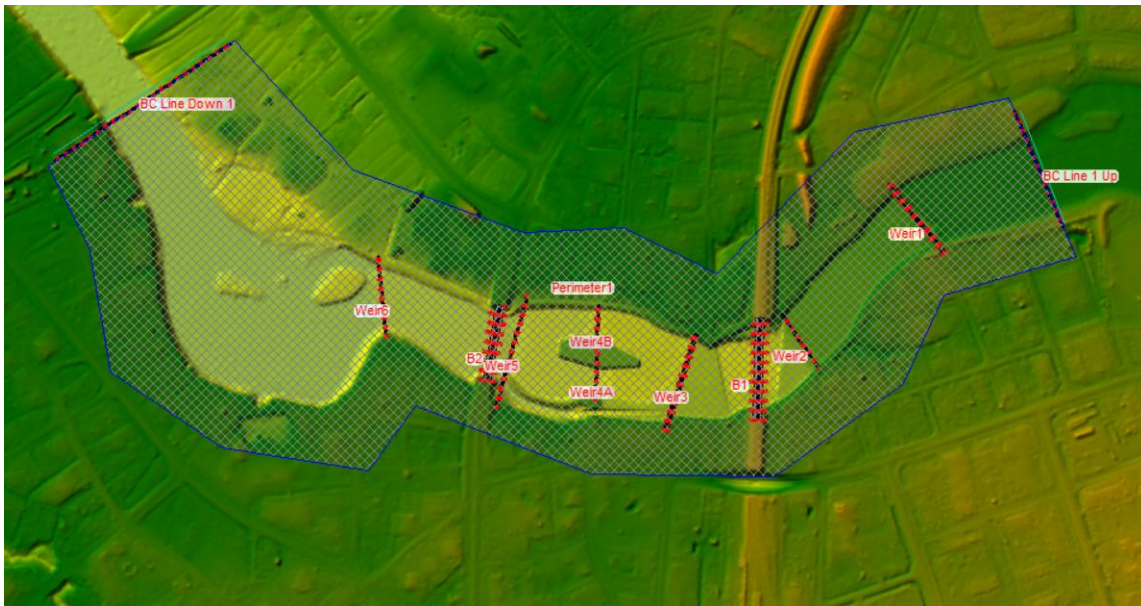


Figure 15: Geometry of the computational mesh and hydraulic structures in HEC-RAS

The location of hydraulic structures in the reach are presented in Figure 15. In Figure 16, the lateral geometries of the broad crested weirs are presented. As shown in Appendix C, weirs at Juurikoski fall under the ‘long crested’ weir type. Addo (2019) stated widths and lengths for weir 3, 4A, 4B and 5 for Juurikoski in his Master’s thesis. No specific weir crest height information was retrieved from the available data, therefore assumptions about the weir crest, but also about missing weir width and weir lengths are made. Appendix D provides an overview of weir (and bridge) dimensions. The weir design in HEC-RAS heavily relies on the terrain. Consequently, the reference points of the spillway must lie above the terrain, to cancel out numerical errors during computational runs. For culvert-like hydraulic structure modelling, HEC-RAS is limited in a way that structures are considered constant in shape, flow rate and bottom slope. A dimensionless “weir coefficient” of 1.66 in SI Units is specified and represents the discharge capacity. This value is based on iterative results, to assure a reasonable amount of resistance to the flow. Note that this coefficient is lower than for inline structures such as culverts.

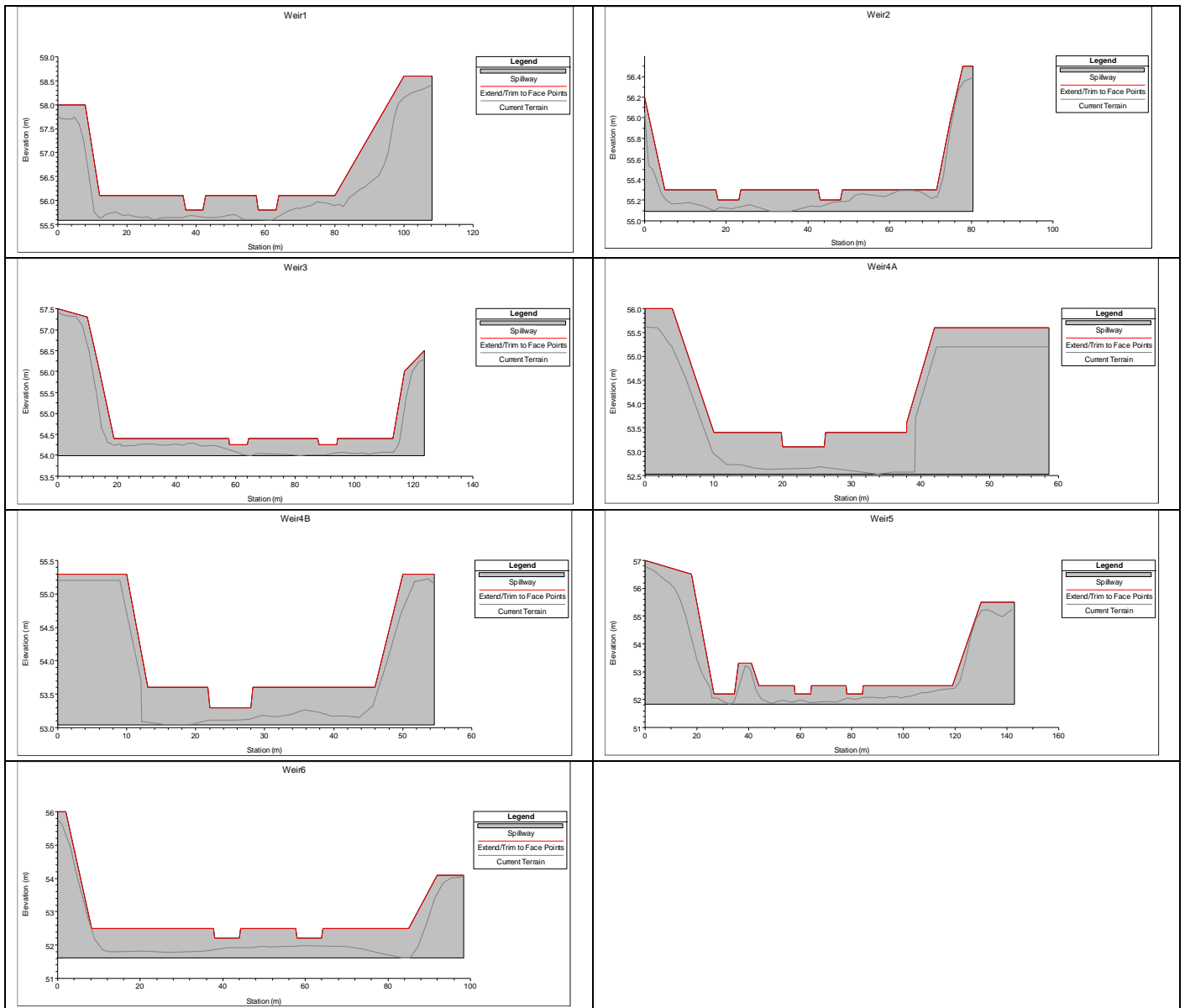


Figure 16: Geometry of lateral structures in HEC-RAS

3.2.5. Boundary conditions, initial conditions and warm up conditions

The boundary conditions are either part of the riverine morphology, such as the bed level or channel geometry, or flow discharge input. The upstream boundary is the sub-daily discharge time series at HHP and the downstream boundary is the equilibrium or normal depth at the downstream end of the study area. The river has an initial state before the simulation of hydropeaking of HHP occurs. Initial base flow conditions of 48 hours prior to the 24 hours ramping event, in this case hydropeaking on the 24th of June 2020, are defined based on sub-daily discharge data from the ELY database. Thus, the upstream boundary condition is a hydrograph, containing a discharge time series of 72 hours. The downstream boundary is the friction slope, in this case 0.001. The principle of the backwater curve holds, since the reach is submissive to subcritical conditions. However, backwater effects will be minimal, since the topography is very flat sloping.

Warm up conditions can be set for unsteady analysis in which the boundary conditions are repeated for the warm up period. The model starts with the initial conditions (initial base flow 48 a priori the day of hydropeaking practices) and holds all of the boundary conditions (the upstream hydrograph and downstream

slope) constant, based on their value at the beginning of the simulation, and then runs a series of arbitrary time steps, let's say 1000, with the constant inflow. This allows the model to establish water surface elevations and flows that are consistent with the unsteady flow equations applied, especially important when lateral structures are present to exclude transitional flows.

3.2.6. Time step determination

For the HEC-RAS software to solve the SWE (Eulerian-Lagrangian Method) for unsteady flow data, a time step must be specified. A time step is chosen based on the balance the accuracy and computational efficiency of simulation runs. The parameter contributes heavily to numerical stability, especially in unsteady flow conditions, i.e. rapidly altering flow. According to the Courant-Friedrichs-Lewy (CFL) conditions, this time step can be estimated by:

$$C = \frac{(V_w \Delta T)}{\Delta X} \leq 1.0 \text{ (with a max } C = 3.0) \quad (11)$$

$$\Delta T \leq \frac{(\Delta X)}{V} \text{ (with } C = 1.0) \quad (12)$$

$$\Delta T \leq \frac{5}{0.25} \quad (13)$$

$$\Delta T \leq 20 \text{ sec} \quad (14)$$

Where C is the Courant Number, V_w is the flood wave velocity, ΔT is the time step, ΔX the distance of the travelling flood wave. If the modelled flood wave event changes gradually with time and space, larger time steps can be used. Hence, the Courant Number can be set until a maximum value of 3. In the hydropeaking case however, changes in flow due to sub-hourly discharge variation occur relatively fast with respect to time and space, so a time step close to a Courant number of 1, and therefore a smaller time step, might be feasible. The speed of the travelling flood wave can be approximated by Formulas 15 and 16. In theory, the horizontal direction related to the travelling flood wave speed is also relevant for the time step determination.

$$V_w = \frac{\Delta Q_{av}}{\Delta A_{av}} \quad (15)$$

$$V_w = \bar{u} + \sqrt{g\bar{h}} \quad (16)$$

In Formula 15, ΔQ_{av} is the difference in discharge over the time step and ΔA_{av} the difference in cross sectional area over the time step. Another way to achieve the speed of the travelling flood wave, is the expression in Formula 16, with \bar{u} the average speed of the flow and $\sqrt{g\bar{h}}$ the celerity of a small-amplitude wave in an open channel flow. In the latter term, g is the gravitational constant and h the average water level. The implicit finite volume solution algorithm allows large computational time steps during a simulation. The latest version of the model software applies an adaptive timestep setting, so that the maximum and minimum courant numbers are automatically adjusted by a factor. It is therefore able to estimate an appropriate time step from the iterative process. The time step is another significant parameter since it determines per cell how much water can accumulate during that time step. If this value is too short, the water accumulation per cell will not be filled till its maximum capacity and prematurely jump to the next calculation step. Concluding, a time step of 20 seconds is chosen in combination with the SWE. This time step suffices, since water accumulation per cell

occurs gradually until maximum water levels are reached and the input hydrograph is in the order of hours. Meaning that smaller time steps are not relevant in prospect with the report's focus.

3.2.7. Sensitivity analysis

An unsteady flow analysis is run, because flow variations are rapidly accelerating throughout the reach due to hydropeaking practices. If numerical parameters are not well chosen, the model may fail to converge to a solution or produce unrealistic results, typically paired with time-consuming simulations. Hence, the utilization of a hydrodynamical model is paired with uncertainties. Various parameters are chosen based on literature and known modelling practices argued in previous subchapters. Table 4 refers to the chosen parameters as 'Selected'. A base scenario is run with the selected parameters. Also, minimum and maximum values (see Table 4) for a certain parameter are applied to the model, while the other parameters stay identical to the default model run. This leads to 8 different sensitivity model runs.

Table 4: Parameters for the selected and experimental values during the sensitivity analysis

	Selected	Min	Max	Unit
Δx	3	1	5	m
Δt	20	10	20	s
Theta	0.8	0.6	1	[-]
Theta Warmup	0.8	0.6	1	[-]
Warm Up Conditions	$1e^3$	0	$1e^6$	[-]

The grid cell size and time step dominate the hydrodynamic model calculations, as seen in the computational log time. Other adjustable parameters are theta and theta warmup. Theta is an implicit factor. It is applied to weigh spatial derivatives between the current and previously solved solutions and ranges from 0.6 to 1.0 according to literature. The value 0.6 tends to provide more numerical accuracy, while 1.0 provides a better numerical stability. 0.8 is a compromise. Theta warmup is applied during the warm up periods for unsteady flow simulation. Warm up conditions cancel out transient flows if the warm up period is long enough. For 1000 steps, this is the case.

The runtime, the volume accounting error and the quality of results varies slightly for each sensitivity run. All values in Table 4 converge to a stable solution, even if the runtime varies significantly, especially for minimum grid cell size and time step. Thus, the 2D HEC-RAS model is rather robust. The selected grid cell size suffices to capture hydrodynamical behaviour in rapid systems which are in the order of a few meters, with rapid spillway widths of approximately 3 meters. Furthermore, the selected time step suffices to capture dynamic flow behaviour with respect to hourly varying discharges.

3.3. Calibration

Model calibration and validation are crucial steps to ensure reliability and accuracy of a predictive numerical model. Conventional calibration is typically based on fine-tuning the roughness of the channel bed and floodplains (Method 1). Furthermore, the availability of ADCP and LSPIV velocities lends to research two different experimental calibration approaches (Method 2 and Method 3). After validation, a variety of events can be simulated in the model.

3.3.1. Method 1: Calibration based on depth loggers

The coefficient of determination (see Formula 17 and 18) provides information about the goodness of fit of a model, in this case in the context of hydrodynamic models using implicit finite volume solutions. In general, an R-squared approaching zero yields to an insufficient fit and an R-squared towards one to a sufficient fit. 0.65 and 0.95 is assumed to be a valid interval, based on the objective of the model, which is to get a reasonable first estimation of flow behaviour. A lower threshold of 0.65 could be interpreted in a sense that at least 65% of the variation in the dependent (modelled) variable values is accounted for by the independent (observed) variable values.

$$R^2 = 1 - \frac{\text{sum squared regression}}{\text{total sum of squares}} \quad (17)$$

$$R^2 = 1 - \frac{\sum_i (y_i - \hat{y}_i)^2}{\sum_i (y_i - \bar{y})^2} \quad (18)$$

Let's assume a variable y , in this case the water level at a specified logger location. y_i is the observed y -value, \hat{y}_i the predicted y -value and \bar{y} the mean of all values. The residual for each observation is the difference between predicted values of y and observed values of y . The *sum squared regression* is the sum of the residuals squared, while the *total sum of squares* is the sum of the distance the observed values are away from the mean squared.

The main calibration parameter in the Manning's roughness coefficient, with unit $s/m^{1/3}$. It is the only physical parameter than can be tuned by iterative steps. The initial values depend on local characteristics of the river bed, such as grain size, presence of larger elements (riverine boulders) and vegetation. Then, per refinement region, the land cover dataset is fine-tuned according to empirical limits 0.01-0.2 in literature, such as the HEC-RAS 2D manual.

Table 5: Final Manning's Roughness Coefficient

	Manning's Value	Percent Impervious
Infrastructure	0.12	100
River Bed	0.05	100
Vegetation	0.08	50
Large riverine boulders	0.10	50
Weir	0.10	100

Table 5 lists the chosen Manning's Roughness Coefficients per land cover or terrain element. The Manning's values are kept constant for each cell they are assigned to during the simulation. Manning's values near logger 4 are fine-tuned higher than the chosen values, to slightly decrease the rapidly accelerating flow and increase water level elevations at loggers 2 and 3. An important note on Manning's equation is that high water levels

or high discharges lower the resistance to the flow. This means that both the flow depth and the roughness are in direct relation with resistance to the flow. Especially for unsteady flow conditions this phenomenon has a large impact, since relatively fast varying flow depth alters resistance to the flow.

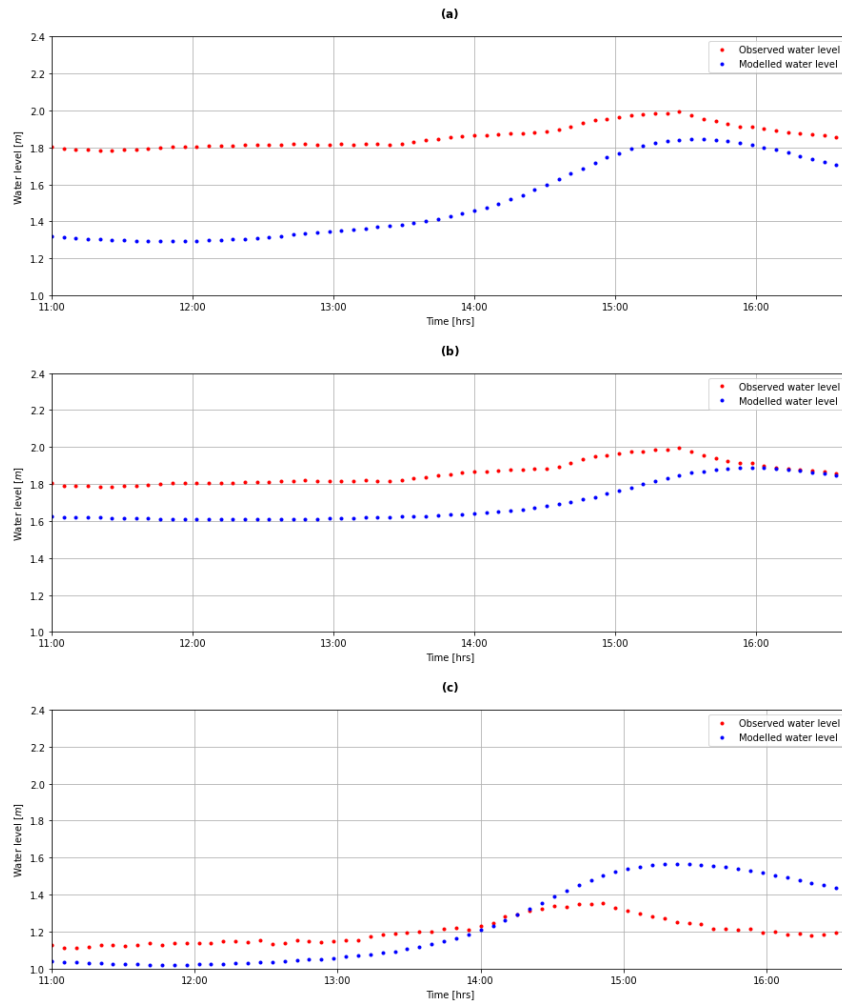


Figure 17: Observed and modelled water levels versus time for logger position 3 (a), logger position 5 (b) and logger position 6 (c) during low flow conditions

Figure 17 illustrates the development of water levels for loggers 3, 5 and 6 over an hourly time series during low flow conditions. A successfully calibrated model should produce a relatively similar peak magnitude, peak lag and initial water level in comparison with the observed data. For logger 3, the peaks align, but there is a mismatch of approximately 0.45 m between initial water levels. Probably due to a mismatch in terrain or Manning’s value downstream and upstream of the location of the logger. Another important observation is that the peak flood waves for loggers 5 and 6 arrive approximately 30 minutes late with respect to the observed peak water level. A possible explanation for this is that the loggers are positioned at the most downstream end, which creates a time lag due to the larger distance from the plant. Additionally, there is some uncertainty related to the accuracy of bathymetric information and exact flow conditions at the logger position. Thus, there can be significant microtopographic or localized flow impact to the logger depth.

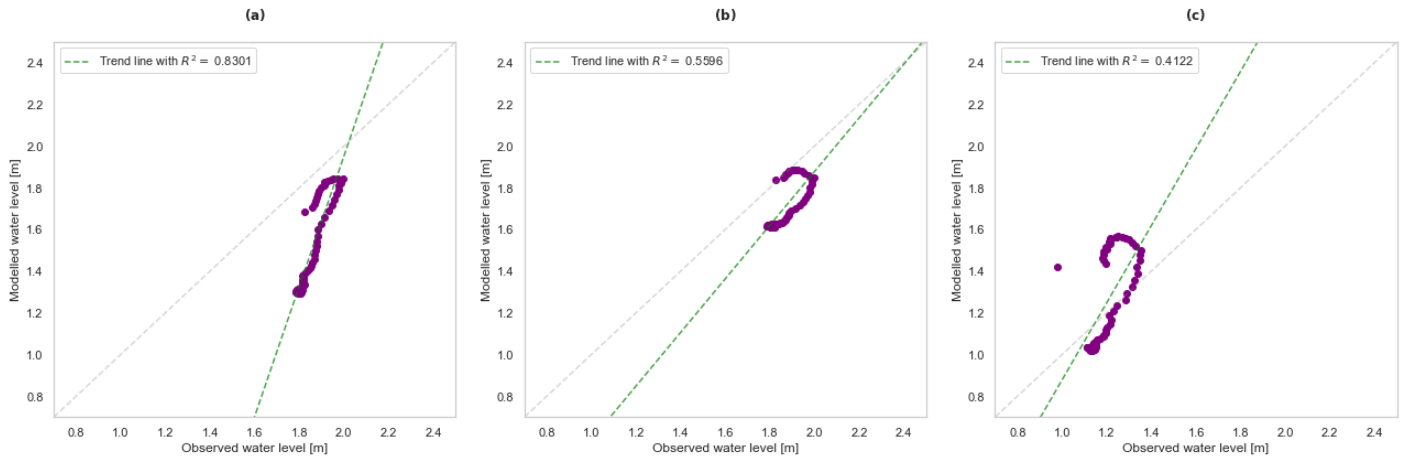


Figure 18: Scatterplots of observed and modelled water levels per R-squared for logger position 3 (a), logger position 5 (b) and logger position 6 (c) for low flow conditions

In Figure 18, scatterplots show that most values lie relatively close to each other. In case of a perfectly calibrated model, the slope of regression line should be around 1:1 (see grey dashed line). The trend lines varies from this ratio to some extent. Moreover, the R-squared values are out of the defined, plausible range for logger 5 and 6, probably due to the mismatch in the arrival time of the peak flood waves. However, more iterative simulation runs with different roughness values, which stay constant during simulation computation time, do not converge to a better solution.

The model suggests that more roughness is needed at low flows, most probably due to the presence of rocks. The water levels are not strongly influenced by the downstream water level boundary, since the terrain is very flat. However, the impact of weirs (and chosen weir coefficients) can locally alter water levels, but this is examined in Chapter 4. Note that warm up conditions, in this case 100 steps, assure that the model contains no initial transient flows, rather a fully developed flow. So by default, calibration inaccuracies are not linked to transient flow situations.

3.3.2. Experimental Method 2: Calibration with drone based data

To calibrate the model based on LSPIV-data, a hot spot analysis comparison between velocity result layers is applied to define the similarity values for different rapid regions. Based on these values, refined regions can be specified to include more detail in the map. Appendix E provides graphical representation of surface velocities for a few rapids, based on LSPIV-data. Figure 19 illustrates, from top to bottom, the plotted LSPIV-data, the velocity result layer from HEC-RAS at approximately the same time stamp (16:20:00) and the hot spot analysis similarity result layer.

The raster map containing velocity magnitudes from HEC-RAS can be directly exported and imported in ArcGIS. However, the LSPIV-data requires some preprocessing to achieve a comparable raster map. Initially, the point cloud data is converted from point to raster format, applying a cell grid size similar to the one related to HEC-RAS velocity result layer. Subsequently, a comparison between both optimized hot spot result layers is performed to achieve the bottom image in Figure 19. Similarity values are subdivided into intervals, with low values indicating dissimilarity and high values relative adequacy in feature values. Strongly associated results tend to 1. More than 50% of the raster area has a similarity value above 0.6 and more than 30% above 0.8. The similarity value can be interpreted as a fuzzy probability that any pair of corresponding features have

the same significance level category. Particularly, around upstream rapids, values exhibit higher similarity values compared to flow areas along the upper banks and the most downstream rapid.

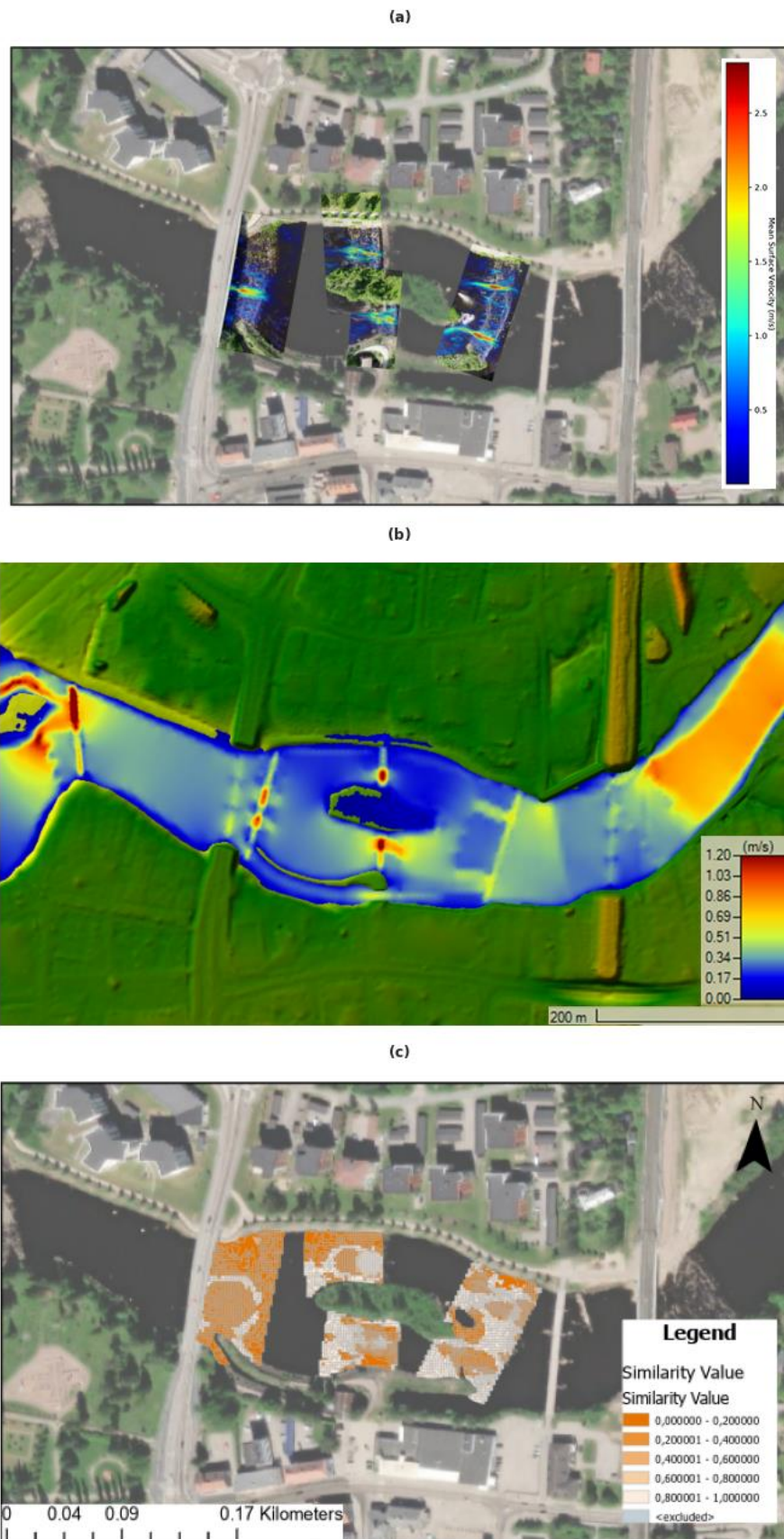


Figure 19: Hot spot analysis comparison (c) between plotted post processed LSPIV-data (a) and HEC-RAS velocity result layer (b)

3.3.3. Experimental Method 3: Comparison ADCP and HEC-RAS velocity profiles

Figure 20 demonstrates dynamical ADCP-measurements taken across two banks before the second bridge during a field study on the 24th of June, referred to as CS1. Appendix F summarizes terrain and cross-sectional velocity profiles from multiple ADCP-recordings. The objective of the measurements is to capture rapid characteristics during hydropeaking practices. Mean speed values between 0.8 m/s and 1.0 m/s in rapid area 5 were observed almost simultaneously with high discharge values around 8 m³/s and 11 m³/s around 01:18 AM. Between the time interval of 13:00 and 14:00, the released discharges at HHP climbed towards a peak of 11.29 m³/s. Thus, hydropeaking practices are clearly visible in the recordings.

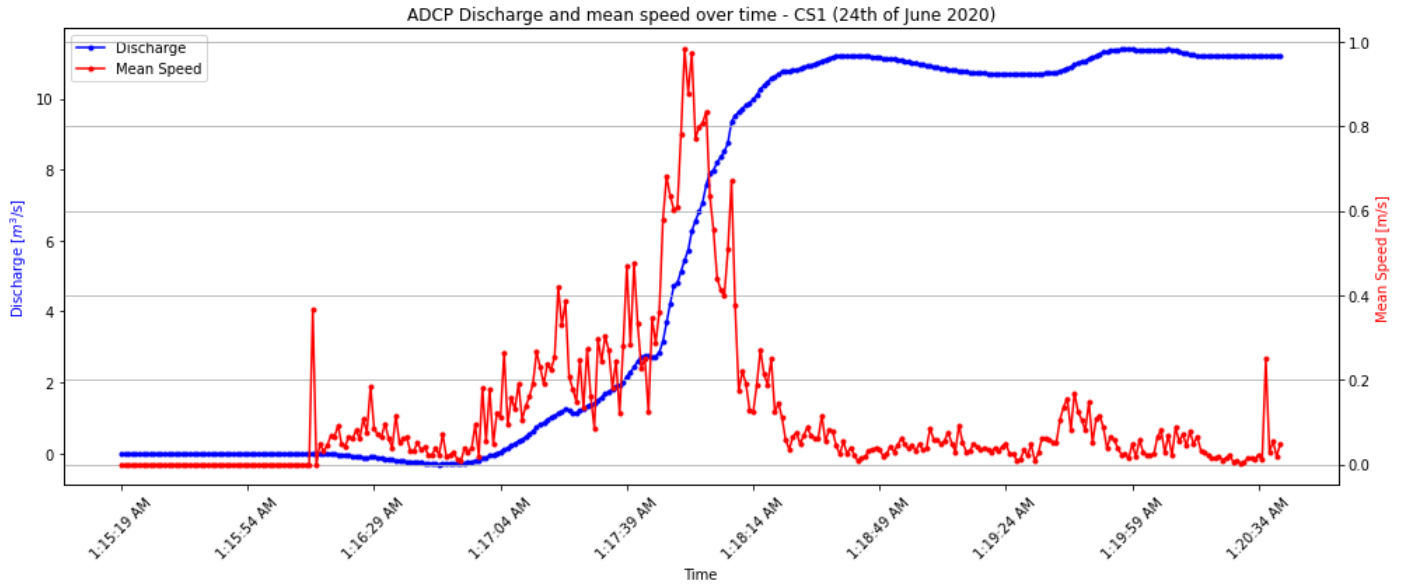


Figure 20: ADCP results for cross-section CS1 on the 24th of June 2020

The flow is defined based on measured data as follows; slow flow < 0.02 m/s, rapid flow > 0.35 m/s and in between a normal flow prevails. The values are based on the 10th and 90th percentile of a cross-sectional sample dataset, which exhibits similar values to other cross-sectional samples. Hence the term ‘rapid’, which refers to these rapid flows in localized areas. The Froude number (*Fr*) is defined in Formula 19. *Fr* < 1 holds for every defined flow category, so a subcritical flow condition for the majority of the reach is safe to assume. A subcritical flow implies a gradual varying flow and hydraulic jumps.

$$Fr = \frac{v}{\sqrt{gh}} \quad (19)$$

Figure 21 includes a 3D visualization of the mean speeds of two cross-sections CS1 and CS2 covered by ADCP in a spatial reference frame. The ADCP cross-sectional datafile before the second bridge is defined as ‘Cross-Section 1’, shortened by CS1 (see Appendix F, Figure F.3), and behind the second bridge as ‘Cross-Section 2’, analogically CS2 (see Appendix F, Figure F.5). On track 30, the location of the rapid, maximum velocities hover just below 1 m/s. Mean speeds have a mean of 0.115 m/s and a standard deviation of 0.176 corresponding to CS1, and 0.265 m/s and 0.172 m/s according to CS2. Velocity profiles are significantly pronounced for a rather deep rapid system 5, associated with CS1. The mean speeds are significantly higher on the exact location of the narrow weir opening. Figure 22 displays HEC-RAS profile lines 4 and 6 corresponding to CS1 and CS2. Notice that the cut in the terrain divides the main channel from the side channel. The figure shows that there is little to no similarity with the ADCP-recordings in Appendix F.

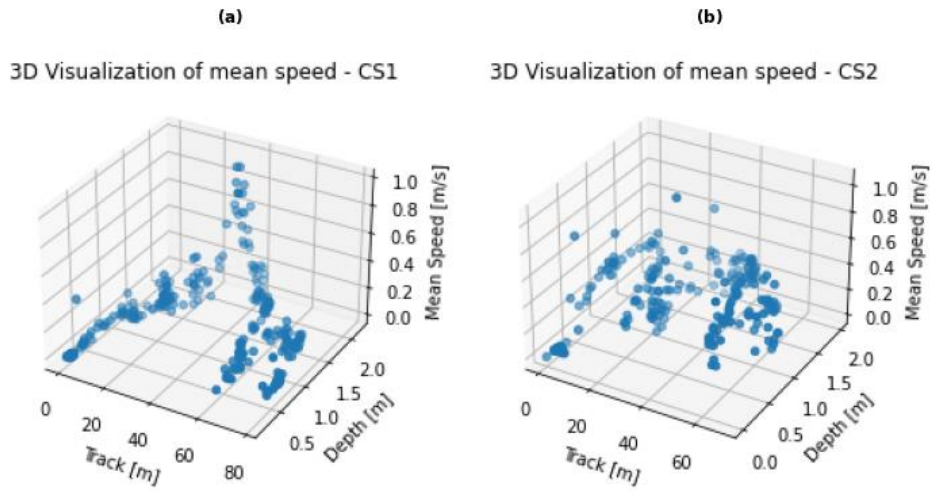


Figure 21: Spatial variation of mean speed for ADCP cross-sections CS1 (a) and CS2 (b)

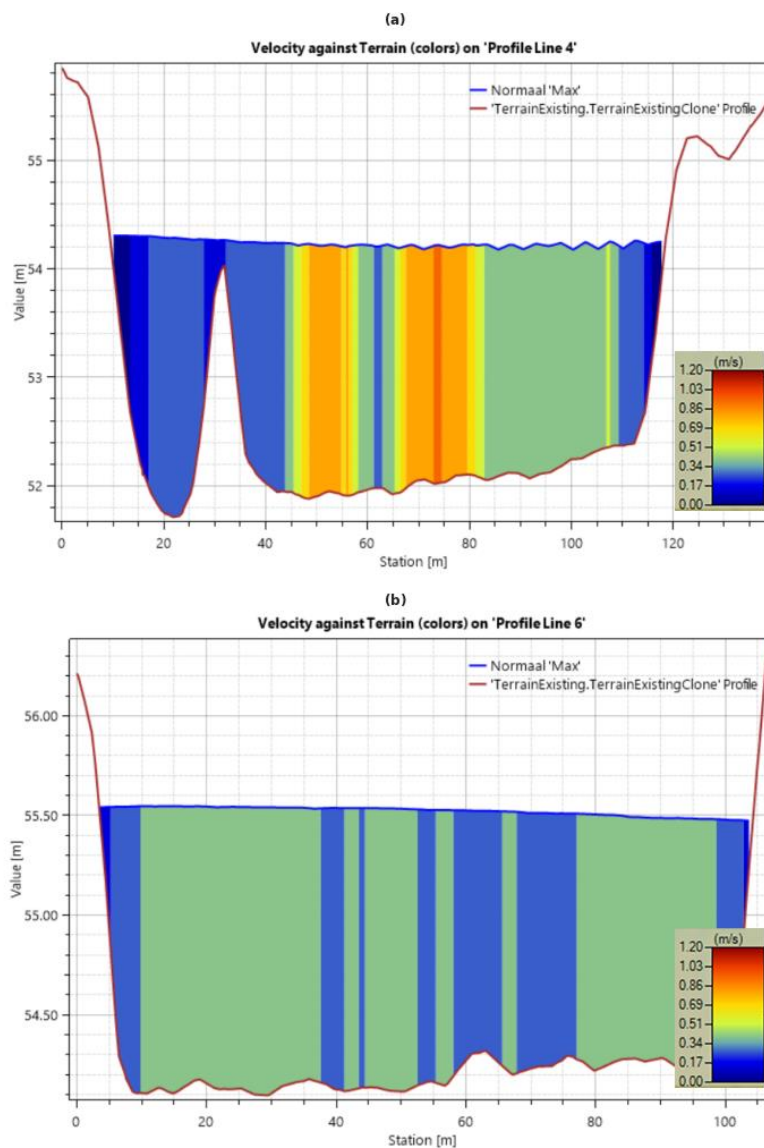


Figure 22: HEC-RAS results - Velocity against terrain on Profile Line 4 and 6 aligning with CS1 (a) and CS2 (b)

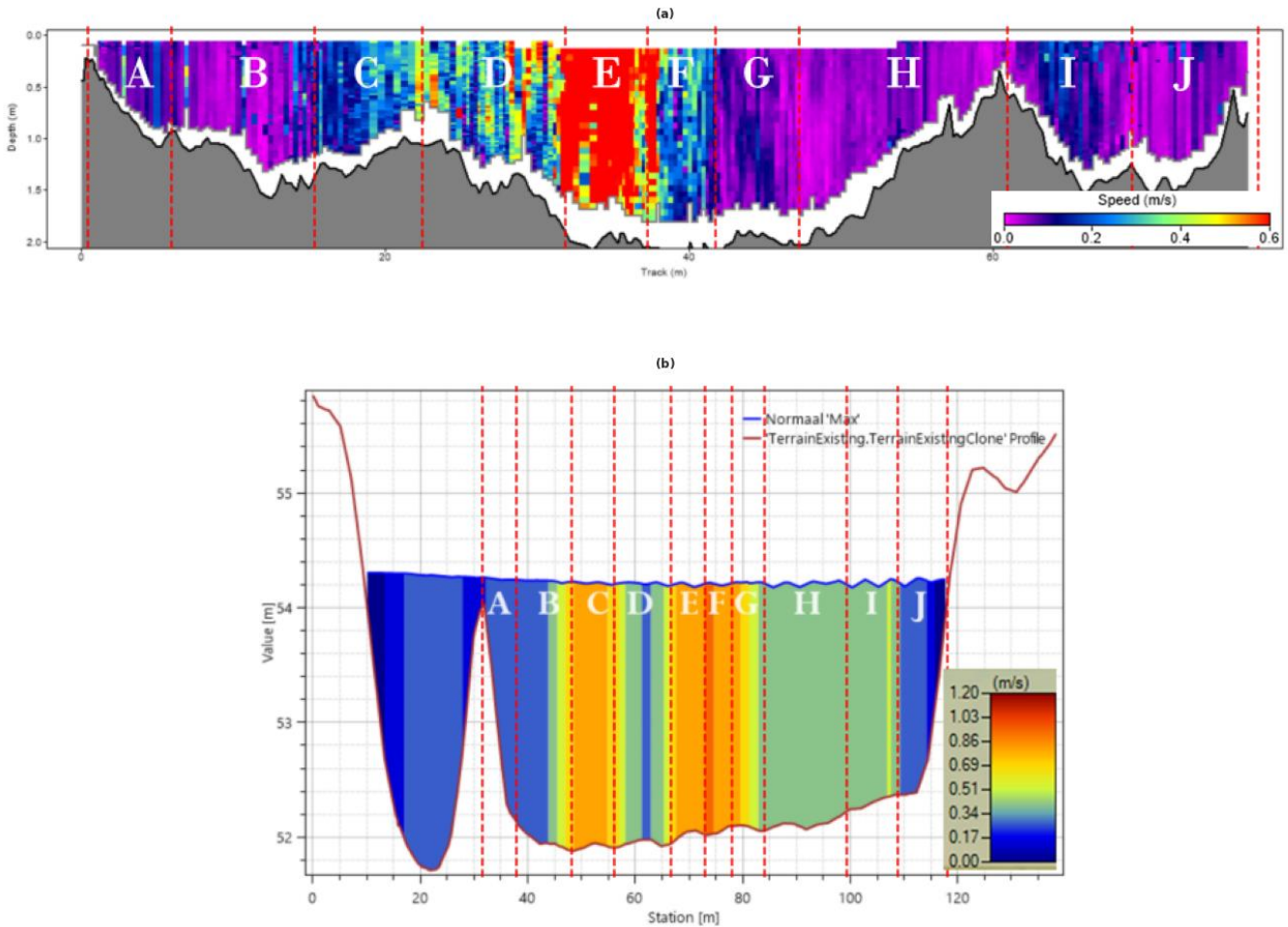


Figure 23: Velocity profiles against terrain in RiverSurveyor based on ADCP cross sectional (area behind the first bridge) image (a) and velocity against terrain on a profile line (behind the first bridge) in HEC-RAS (b)

Rapid regions in HEC-RAS are iteratively fine-tuned according to the identified rapid regions from ADCP to improve calibration. However, a comparison between cross-sectional data from ADCP and HEC-RAS is not straightforward. Figure 23 and Table 6 subdivides the cross-section 1 into ten control sections (A,B,C,D,E,F,G,H,I,J). Note that section E describes the location of the rapid. For every section, the section velocity is determined for measured and modelled data. Section velocities are sampled velocities, so that depth-averaged values of the flow recorded along the specific track location within the interval are retrieved. Following, in a pairwise manner the mean and mean value error are calculated for each section.

Table 6: Section velocities for measured and modelled simulation results

	A	B	C	D	E	F	G	H	I	J
$V_{ADCP,i}$ [m/s]	0.08	0.07	0.22	0.31	0.70	0.17	0.06	0.04	0.08	0.04
$V_{HR,i}$ [m/s]	0.17	0.35	0.63	0.31	0.83	0.87	0.53	0.35	0.36	0.11

Next, a comparative analysis between section velocities based on Table 6 suggests a discrepancy between modelled and observed velocities, with the model consistently overestimating the flow speed. Especially near the banks. The MSE (Mean Squared Error) and MAE (Mean Absolute Error) of approximately 0.12 and 0.27 are directly linked to discrepancy between measured and modelled values. The Root Mean Squared Error (RMSE) of 0.34 indicates a relatively large spread of errors, contributes to previous statement. Fine tuning of

Manning’s values during iterative runs can align low flow and rapid flow areas according to measured data. This could improve the reliability of the model. As a result of fine-tuning, the statistical parameters should converge to lower values if better modelled values are achieved in HEC-RAS. Concluding however, it is unbeneficial to calibrate the model based on ADCP-data due to relatively unrealistic bathymetry along the profile lines. Moreover, fine tuning refinement regions is time intensive work.

3.4. Validation

Water level time series from logger 2 and 4 are randomly chosen and applied for validation. Logger data is not available for artificial high flow and artificial medium flow situations. Consequently, the validation is based on low flow conditions, ensuring that model outcomes are reliable during low flow conditions, but not necessarily during medium and high flow discharges. Figure 24 illustrates the development of water levels for loggers 2 and 4 over an hourly time series during low flow conditions. Initial observed water levels are around 1.7 for logger 2 and 1.65 for logger 4, while the modelled outcomes show values around 1.6 for logger 2 and 1.7 for logger 4. The peak magnitudes of observed water levels and modelled water levels are relatively close to each other for logger 4, despite being larger than 0.5 m for logger 2. The latter is possibly due to a rapidly accelerating flow in upstream regions. However, there is practically no time lag for logger 2, while logger 4 does experience a time lag of 20 minutes in the modelled water levels.

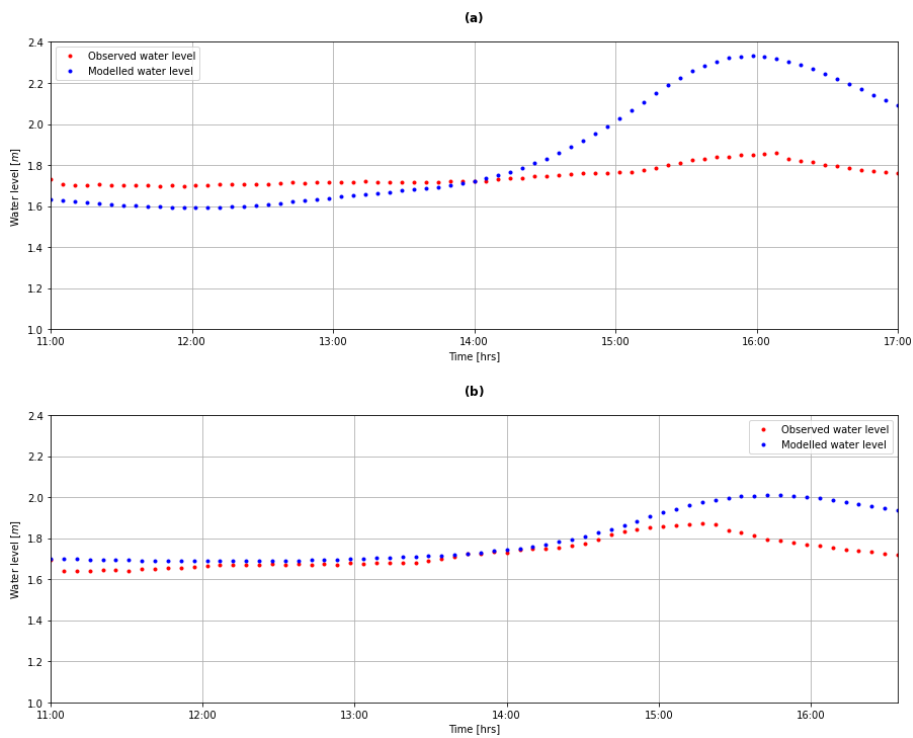


Figure 24: Observed and modelled water levels versus time for logger position 2 (a) and logger position 4 (b) during low flow conditions

Derived from Figure 25, most values lie relatively close to each other in the scatterplots and are slightly positively correlated. Despite this observation, the trend lines are too steep. Nevertheless, R-squared values 0.6663 for logger 4 and 0.9478 for logger 2 lie within the predefined range of 0.65 and 0.95. Thus, even if the model is not calibrated perfectly, the validation is assumed to be sufficient to serve the purpose of the model. Namely, to make an analysis of (local) flow behaviour and a study the effectiveness of potential mitigation

measures. However, the recommendations should be verified by an improved model in future studies for practical implementation.

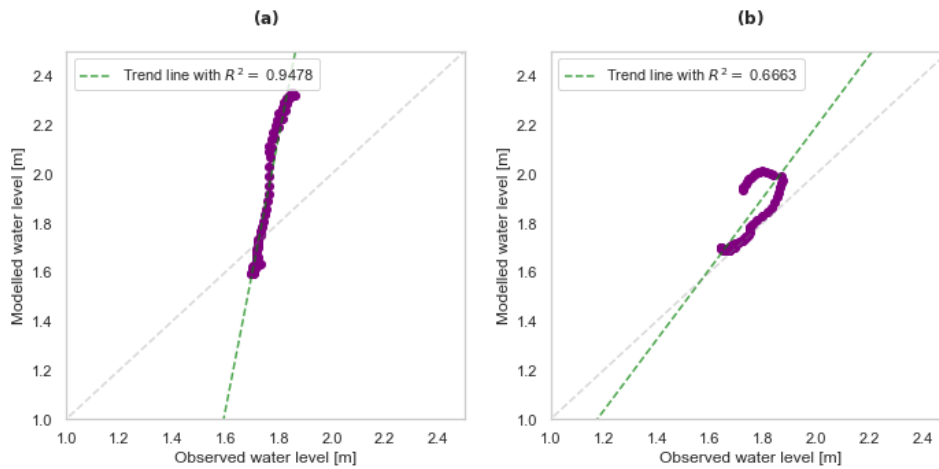


Figure 25: Scatterplots of observed and modelled water levels per R-squared for logger position 2 (a) and logger position 4 (b) for low flow conditions

3.5. Simulation cases

In this subchapter, hypothetical scenarios with potential mitigation measures for hydropеaking impacts are set up. These scenarios can be simulated to introduce variations on the original flow scenario. Figure 26 gives a solution tree, with on top the main aim of the case study, namely the restoration of rapids at Juurikoski. This means that ideally, a constant flow is present over the whole reach and rapids do not experience severe low (or high) water levels, and neither slow or too rapidly accelerating flows. Operational measures can be described by an alteration of thresholds regarding the released discharge range at the hydropower plant. On the other hand, morphological measures are described by a change in the river structure, such as a branch cut-off, or changes related to structural elements such as boulders, vegetation and weirs.

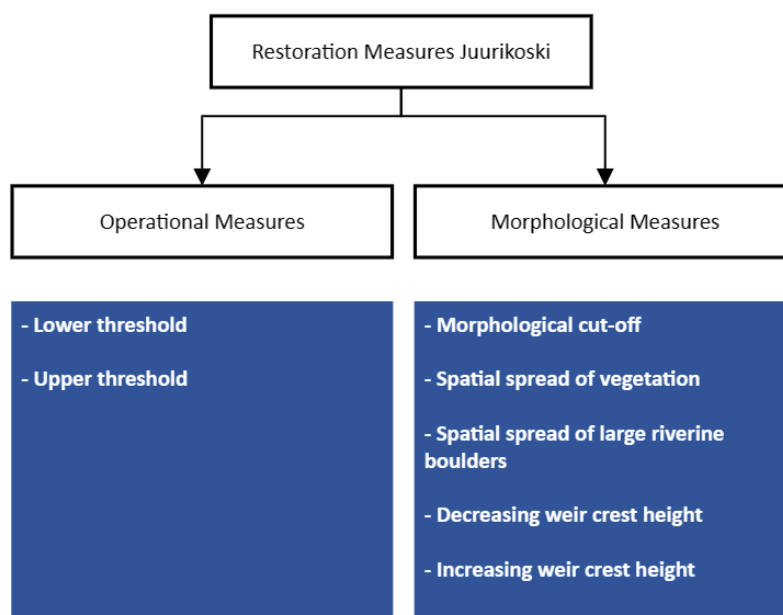


Figure 26: Solution Tree Restoration Measures Juurikoski

Figure 27 further refines the scenarios, based on the potential disadvantages and potential benefits. Operational limits can only limit hydropeaking impacts by some extent, which is yet unknown. Furthermore, an agreement must be reached with the hydropower plant operator to implement such measures. Moreover, morphological change 1 refers to the transformation of the anabranch to one stream. Due to decreased cross-sectional area at the location of the intervention, flooding may occur upstream. Due to the same reason, flow conveyance, or rather flow speed, is expected to increase to some extent based on the discharge formula ($Q = A \cdot u$).

Operational Limits (OL)		Morphological Change 1 (M1)		Morphological Change 2 (M2)	
Limited improvement (-)	Benefits environment (+)	Large impact in landscape (-)	Benefits environment (+)	Removal of weirs (-)	Benefits environment (+)
Agreement with operator required (-)	Respects site aesthetics (+)	Hard implementation (-)	Increases flow conveyance (+)	Implementation of an upstream controlling weir (-)	Respects site aesthetics (+)
	Easy implementation (+)	Potential flooding upstream (-)	No operational changes (+)		Easy implementation (+)
					Building with nature (+)
					No operational changes(+)

Figure 27: Mitigation options – cons and pros

Based on Figure 26 and 27, four scenarios are defined in Figure 28, in order to simulate different hydrological and morphological conditions at Juurikoski. The first riverine system (a) corresponds to the original scenario oriented toward economic gain. The operational limit scenario (b) prioritizes the wellbeing of the environment, since fish are known to thrive within certain discharge limitations according to their species. The third (c) and the fourth (d) riverine system are experimental scenarios to verify whether a compromise between optimal economic and optimal ecological conditions can be reached simultaneously.



Figure 28: Three distinct riverine systems to simulate four scenarios: Original scenario ‘Original’ (corresponding to a), operational limits scenario ‘OL’ (corresponding to a), morphological change 1 scenario ‘M1’ (corresponding to b) and morphological change 2 scenario ‘M2’ (corresponding to c)

The original scenario is labelled ‘Original’, the operational limits scenario as ‘OL’, the morphological change 1 scenario as ‘M1’ and the morphological change 2 scenario as ‘M2’. ‘Original’ applies upstream boundary discharge conditions during the 24th of June 2020, when hydropeaking was observed. ‘OL’ contains a lower limit of $2 \text{ m}^3/\text{s}$ and an upper limit of $8 \text{ m}^3/\text{s}$, defined in collaboration with ELY. ‘M1’ contains an alteration of a diverging stream to a continuous stream and the lowering of weir crest heights by a maximum of 0.2 m if possible. The reasoning behind this is to provide more flow stability, potentially valuable in the context of fish migration and habitat. Scenario ‘M2’ is based on a suggestion by ELY to split central Juurikoski in two separate parts. One part contains the southside of the innermost island. This side has a deep pool and minimal flow bypassing. The other part, the northern part, has a more rapidly constant flowing riverine branch and smaller fluctuations. The removal of the downstream weirs, enhancement of the reach with natural river pebble stones on the southside and an upstream weir are subjects to this river system. Preferably a controlling weir, but defined in scenario ‘M2’ as a static weir. The reasoning behind the characteristics of ‘M2’ is to restore the previously natural occurring rapids.

4. Results

In this chapter, the hydropeaking classification of HHP (see description of classification in Chapter 2.2) is determined. Additionally, simulation results are analytically processed and visualized. Appendix G summarizes result layers related to water level, velocity and shear stress. Finally, a subchapter involving stage and flow hydrographs related to the weirs are presented as well.

4.1. Hydropeaking classification HHP

In Figure 29, the indicators are plotted versus the available continuous time series on the 24th of June 2020 at the base of HHP, provided by ELY.

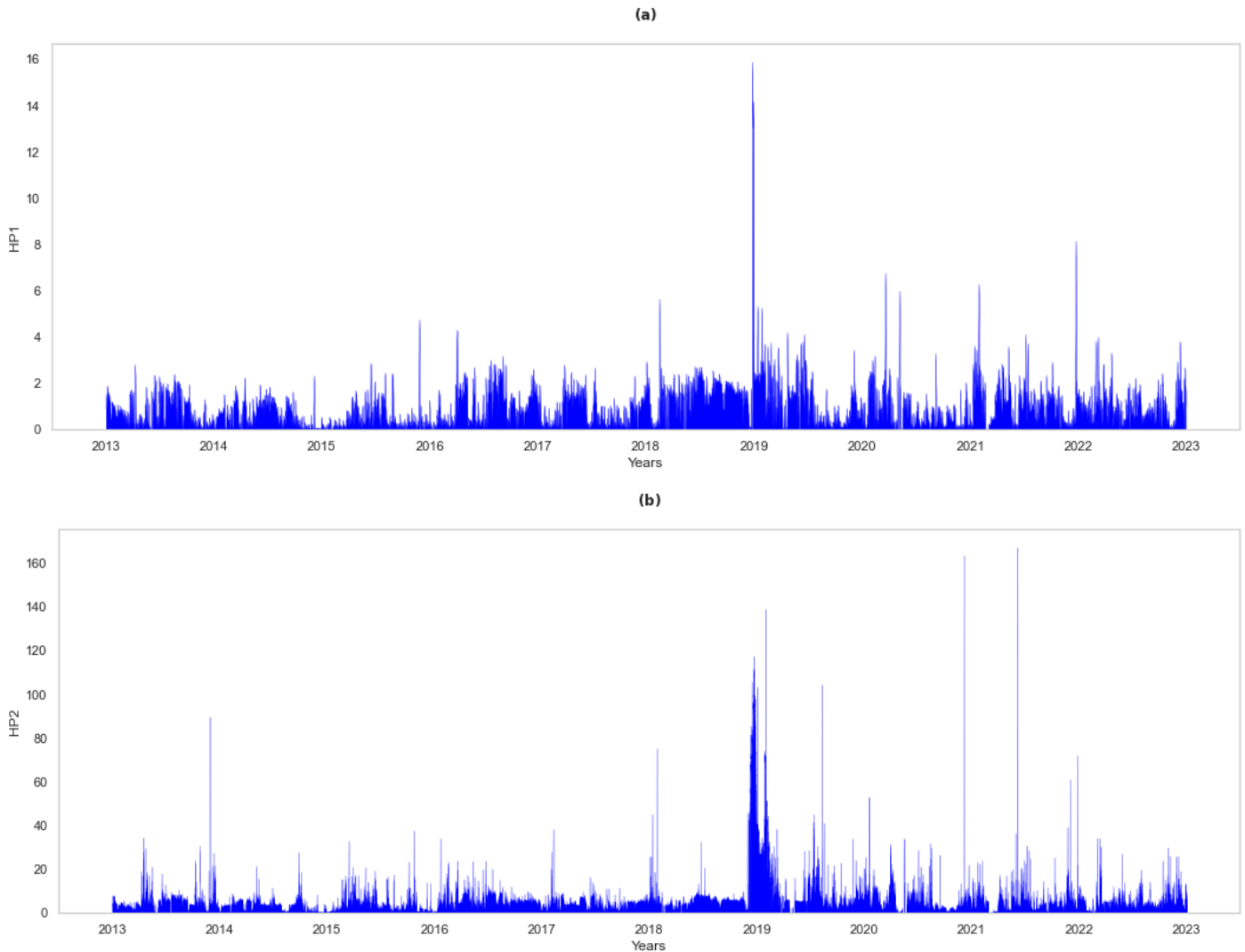


Figure 29: HP1 (a) and HP2 (b) indicators against daily data

According to the graphs, the highest indicators occur in most recent years. Moreover, HP1, the median of individual HP1-indicators, over the whole time series is approximately 0.77. For HP2, this value is somewhat lower, namely 0.3. Carolli et al. (2015) calculated thresholds from 292 ‘unpeaked’ datasets using a non-parametric method. After identification of these thresholds, three different classes of hydropeaking pressure can be distinguished. Dependent on values HP1 and HP2, which lie below or above such thresholds, station outliers in hydropeaking magnitude or temporal rate of discharge variations compared to the unpeaked group can be pinpointed.

However, for HHP, only an indication of hydropeaking impact class is sufficient to prove the hypothesis of large hydropeaking impact. Based on Figure 11 from the literature study, the hydropeaking impact at the HHP station is classified as medium impact. This confirms the beliefs K. Aronsuu from ELY (personal communication, May 2023) that hydropeaking has significant impact on Juurikoski. It is crucial to highlight that natural peaking trends vary significantly during seasons. To indicate a trend without neutralizing the natural distortion in the flow signal would be unsubstantiated, so a clear conclusion remains undisclosed. Undisturbed flow data should be included in the flow hydrograph analyses besides the artificially varying flow, but is non-existent in the case of HPP.

4.2. Simulation results

By experimentation with the different configurations for Juurikoski, insightful data about various variables can be retrieved and analysed. The main variables discussed are the water level and velocity. Statistical characteristics of modelled outcomes are utilized to visualize the extent of the impact of operational and site modifications in the context of hydropeaking.

4.2.1. Water levels

Figure 30 contains three subplots with water levels per logger location. The reference datum is assumed to be zero. The first subplot represents water levels during low flow conditions, the second subplot during medium flow conditions and the third subplot during high flow conditions.

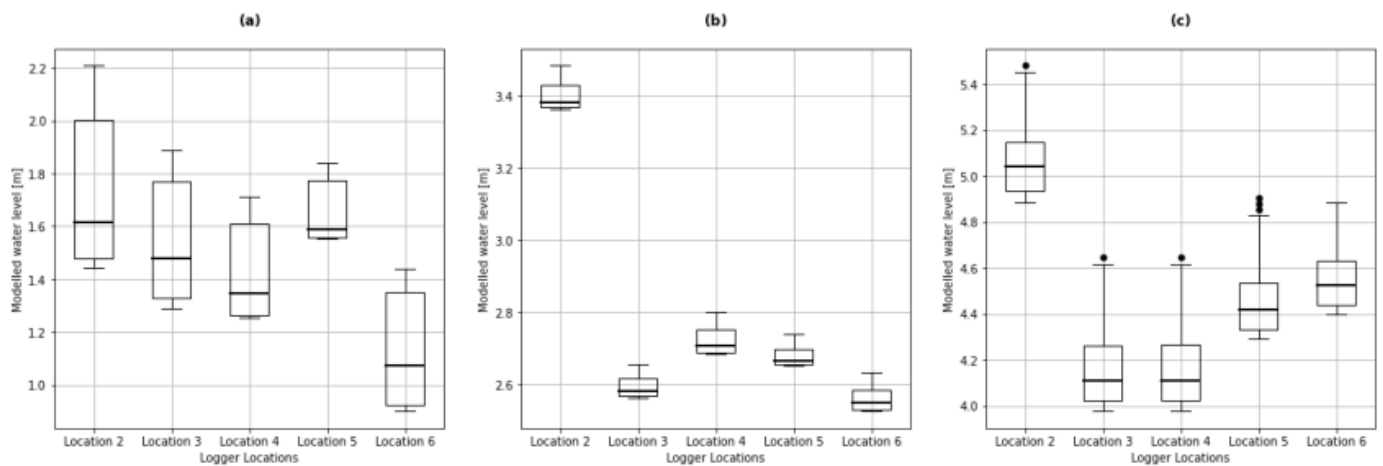


Figure 30: Boxplots for modelled water levels per logger location for the original scenario during low (a), medium (b) and high (c) flow conditions

Released discharges between $2 \text{ m}^3/\text{s}$ and $11 \text{ m}^3/\text{s}$ defined as low flow conditions, align with the time interval between 11:00 and 17:30 on the 24th of June 2020. The extent of the boxplots indicates fluctuations of water levels due to the peaking cycle. During this time interval, real discharge data was recorded at the base of HHP, when hydropeaking occurred. During a similar time interval, for medium flow conditions recorded on the 16th, 17th and 18th of March 2020, discharges lie between $15 \text{ m}^3/\text{s}$ and $40 \text{ m}^3/\text{s}$. For high flow conditions recorded on the 2nd, 3rd and 4th of January 2020, discharges are between $32.605 \text{ m}^3/\text{s}$ to $123.934 \text{ m}^3/\text{s}$. Note that $123.934 \text{ m}^3/\text{s}$ is an outlier regarding hourly data on a yearly basis. The model is calibrated for low flow conditions. Consequently, the reliability of the model predictions for medium and high flow conditions is relatively low. This is evident from the significant discrepancy between the predictions for medium and high flow conditions at logger location 2. Additionally, hydropeaking is not pronounced for medium flow conditions, as indicated by the size of the boxes and length of the whiskers. Furthermore, water level fluctuations for low flow conditions depend on the distance with respect to the HHP. Modelled outcomes at

logger locations close to the HHP show a more pronounced water level fluctuation pattern than further downstream. Only logger 6 shows a deviation to this trend. The water level is overall lower on this location, possibly due to diversion of water volumes to the bigger stream and its location, namely a narrow stream between the upper banks and a small island-like patch of terrain.

Figure 31 presents boxplots per logger location based on water level outcomes per scenario. According to Appendix G, for logger location 4 located in the middle of the Juurikoski span, water level means are approximately 1.43 m, 1.40 m, 1.20 m and 1.28 m for scenario ‘Original’, ‘OL’, ‘M1’ and ‘M2’. Generally, the standard deviations hover around 0.2. The initial graph represents the results of the original low flow condition simulation, with a minimum around 0.90 m and maximum value of 2.21 m for downstream and upstream logger positions. The second graph gives a similar visualization, but the minimum value is 1.06 m and maximum value 2.03 m, analogically for the downstream and upstream logger positions. This indicates that operational limits influence the extension of fluctuations in water level significantly. Less water level fluctuations, or rather a water level variation within strict limits, is typically favourable for fish habitat and migration. In the third graph (c), the introduction of morphological change 1 results in a wider range of water level values compared to the original riverine system. Minimum values and maximum are rather scattered along the site; on logger location 3 a minimum of 0.56 is observed and on logger location 6 a maximum of 1.69. Conversely, the fourth graph, corresponding to morphological change 2, exhibits outcomes very similar to those of the original configuration, with a minimum of 0.91 on logger location 6 and a maximum of 2.04 on logger location 2.

To give a more quantitative description of the modelled water level data, a smooth estimation of the underlying probability density function is applied. Figure 32 represents four kernel density plots for modelled water levels per scenario during low flow conditions. A kernel density plot displays the distribution of modelled values in a nonparametric probability manner by applying a continuous curve. Mathematically, the kernel density estimate (with scaled version of the kernel) at a point is given by Formula 20:

$$\hat{f}(x, h) = \frac{1}{nh} \sum_{i=1}^n K\left(\frac{x-x_i}{h}\right) \quad (20)$$

A smooth scale kernel function is centred at each data point and then the average is determined. A common kernel is the Gaussian kernel, see Formula 21:

$$K(u) = \frac{1}{\sqrt{2\pi}} \exp\left(-\frac{u^2}{2}\right) \quad (21)$$

In the Formula 20 and 21, n is the number of data points, h is the bandwidth (Silverman’s rule of thumb for a first estimation) and K is the kernel function. The bandwidth is chosen as h = 0.2 to provide a smooth curve. A values of 0.1 gives a rather edgy visualisation instead of a smooth curve and higher values than 0.2 oversimplify data.

Notable for each scenario and dataset is that generally the data can be summarized by a kernel density function by two clusters, i.e. they have two modes. These modes likely correspond to the hydropeaking cycles. On logger location 4, in the middle of the Juurikoski span, the central tendency of the plots lies close the water level means. The peak densities are typically configured around 1.5 m. The highest density is for scenario ‘OL’, which is 7 around a water level of 1.6 m. To shortly summarize, based on Figures 31 and 32, solely ‘OL’ and ‘M2’ diminish the sub-variance in daily water level. The morphological intervention related to ‘morphological change 1’-scenario doesn’t seem to improve the reach in an ecological or recreational sense, despite its intention to simplify a complex riverine system.

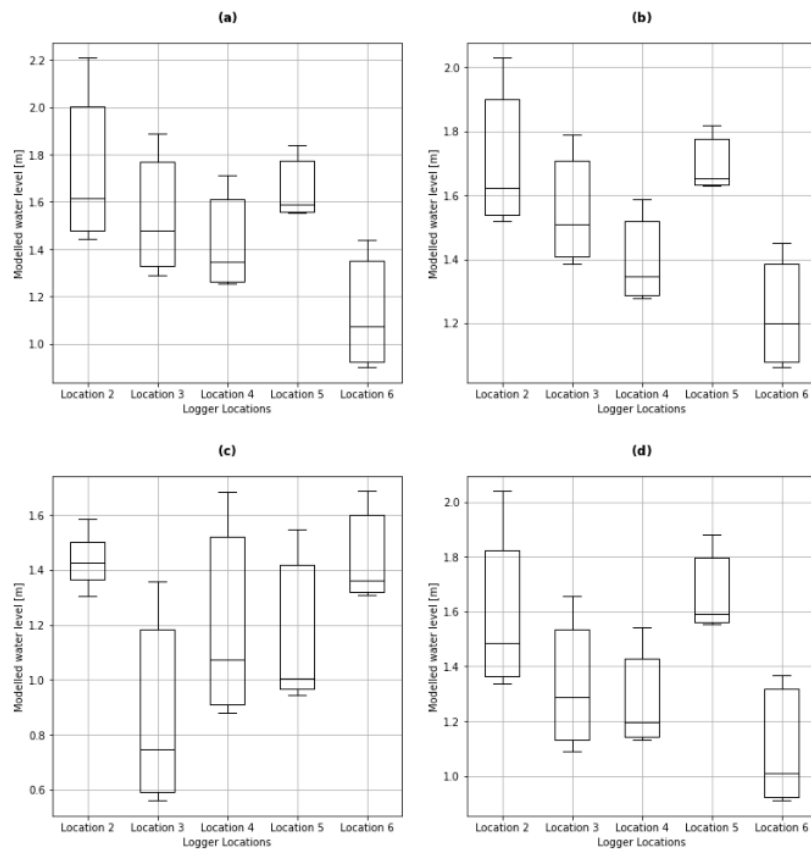


Figure 31: Boxplots for modelled water levels per logger location for four simulation scenarios during low flow conditions: Original scenario ‘Original’ (a), operational limits scenario ‘OL’ (b), morphological change 1 scenario ‘M1’ (c) and morphological change 2 scenario ‘M2’ (d)

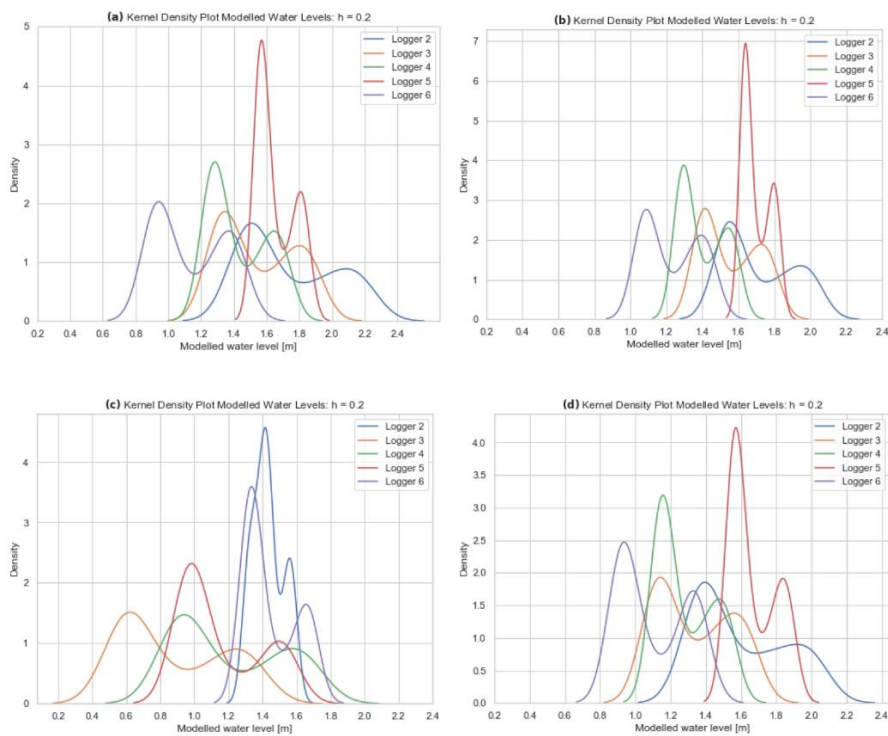


Figure 32: Kernel density plots for modelled water levels per logger location for four simulation scenarios during low flow conditions: Original scenario ‘Original’ (a), operational limits scenario ‘OL’ (b), morphological change 1 scenario ‘M1’ (c) and morphological change 2 scenario ‘M2’ (d)

4.2.2. Velocities

Figure 33 illustrates the depth averaged velocities along the site for the distinct simulation cases. The rapids, are typically described by red spots on the maps. They are located at the weir locations and narrow openings in the riverine system. There are some dark blue spots with extremely low values (<0.01 m/s) across the banks, which can be ignored for all scenarios, except 'M1', since in this scenario they occur because of discontinuities in the terrain.

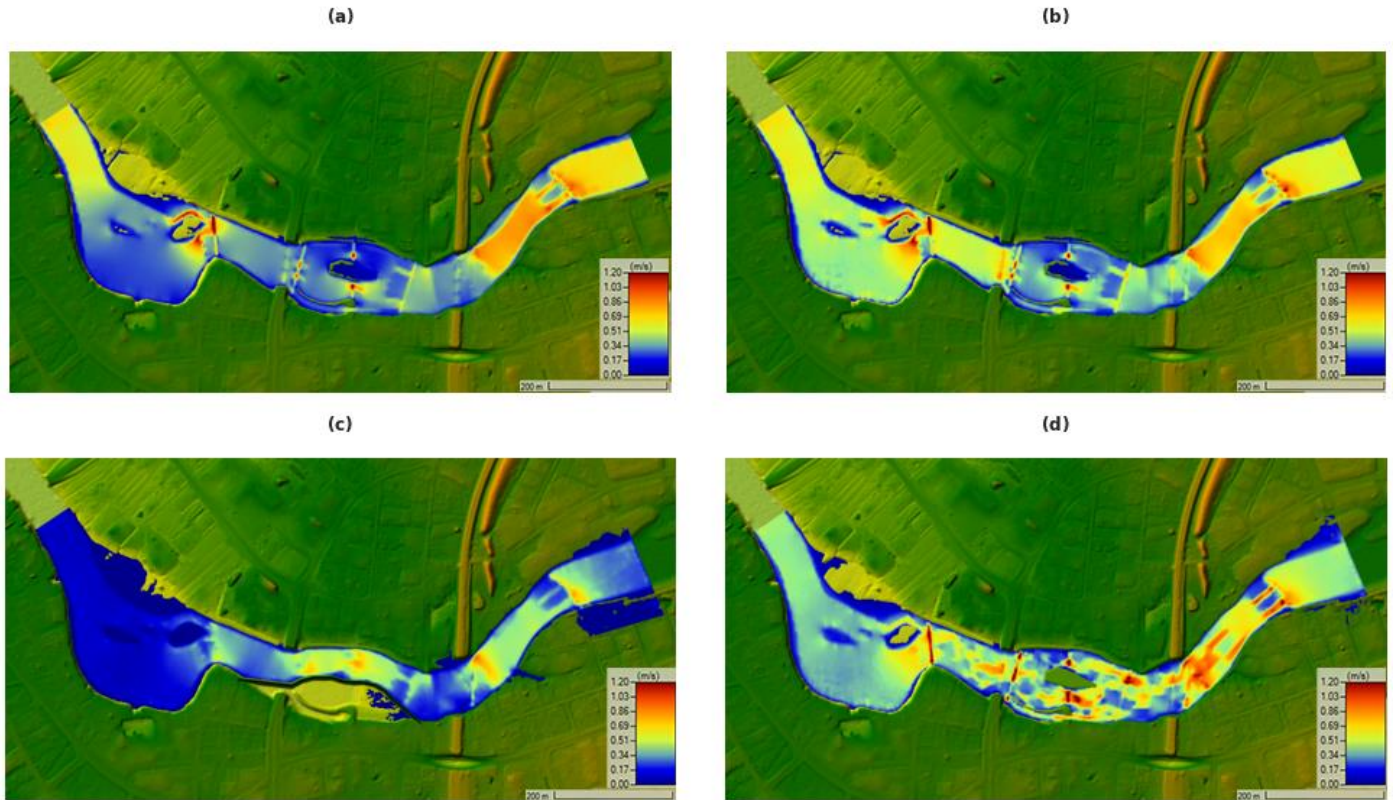


Figure 33: Depth-averaged velocity maps from model result layers during low flow conditions: Original scenario (a), operational limits scenario (b), morphological change 1 scenario (c) and morphological change 2 scenario (d)

Morphological changes, such as topographic steering, drastically alter flow regimes. 'M1', the case with one continuous stream, gives rise to undesired responses like flooding of the river banks. Even though rapids and corresponding bottlenecks are hardly present, for practical application there would be additional mitigation measures needed to avoid the flooding of banks. 'M2' shows large flow-variation in lateral direction. This indicates turbulent pattern with vortices, induced by lateral momentum exchange. Nevertheless, it maintains a constant overall streamwise pattern with respect to the other scenarios. The red spots in the case of 'M2' are due to sudden discontinuities in terrain, rather than hydraulic structures and bottlenecks in the flow. Moreover, scenario 'OL' seems have a similar pattern in the sense that the extent to which the velocities along the river stream fluctuate is way smaller than the original situation. From a fish habitat modelling perspective, a naturally varying, but rather constant river flow along the whole reach, is much more preferable than occasional rapids and large variation between the sequential areas in streamwise direction along the river.

The velocity statistics correspond more or less with observed values from ADCP-datafiles analysed in RiverSurveyor. The simulation results in HEC-RAS vary mostly from 0 m/s to 0.2 m/s, while in RiverSurveyor most values lie between 0 m/s and 0.1 m/s on general river parts and between 0.4 m/s - 0.9 m/s on rapid locations. The HEC-RAS software seems to be limited in reproducing high velocities in the rapid regions.

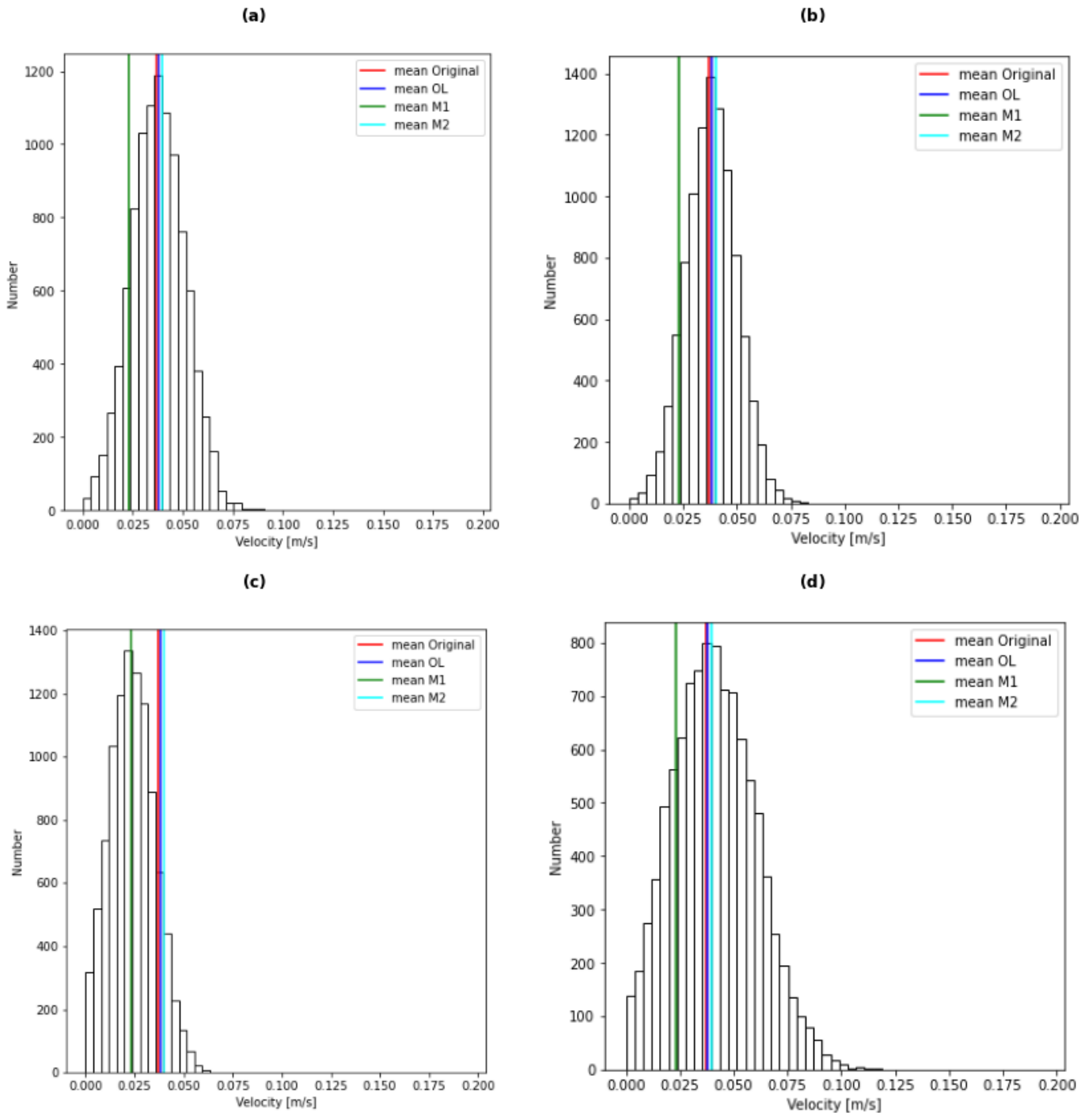


Figure 34: Histograms with depth-averaged velocities from model result layers during low flow conditions: Original scenario (a), operational limits scenario (b), morphological change 1 scenario (c) and morphological change 2 scenario (d)

Figure 34 shows four theoretical histograms generated based on an assumed normal distribution. This distribution is described by the minimum, maximum, mean and standard deviation of all velocity values from the numerical solution per modelled scenario. Note that the histograms corresponding to ‘M1’ is slightly positively skewed, while ‘M2’ is significantly positively skewed. The aim is to make an assessment of potential outliers and therefore analyse if HEC-RAS produces a realistic velocity distribution for rapid changes in discharges, where outliers are typically present. For the skewed histogram relating to ‘M2’ (see Figure 34, subplot d), the maximum value of 0.194 m/s from the numerical simulation is most likely an outlier.

Furthermore, for all histograms, values between 0.15 m/s and 0.2 m/s are absent, despite the presence of such values in the model. Concluding, HEC-RAS performs reasonable or rather gives a realistic flow description regarding high velocities or theoretical outliers.

Table 7 summarizes velocity statistics for each case. The mean for case ‘OL’ is 0.038 m/s, with a slightly lower standard deviation of 0.017 and a maximum of 0.094 m/s. This supports the claim that there is less variation in velocities for a case with operational limits, but does not support the overall lower speed of the flow. Also note that case ‘M2’ reaches the highest maximum velocities, occurring rather randomly during the full simulation times series, over the whole reach. In contrast to scenario ‘M1’, which has the lowest mean and a short range of velocity values. Note that the definition of rapid regions is typically characterized by the presence of velocities above the 90th percentile value. Note that during hydropeaking, for the rapid at CS1, velocities lie above 0.2 according to ADCP-data, while the numerical solution from HEC-RAS gives a maximum value of 0.108 m/s for the original scenario.

Table 7: Velocity Statistics per Case

	Mean [m/s]	Standard Deviation [-]	Maximum [m/s]	10th percentile value [m/s]	90th percentile value [m/s]
Original	0.037	0.019	0.108	0.009	0.038
OL	0.038	0.017	0.094	0.020	0.055
M1	0.023	0.017	0.083	0.022	0.054
M2	0.040	0.030	0.194	0.0164	0.067

4.2.3. Hydraulic structure analysis

4.2.3.1. Shear stress – Spatial analysis

Figure 35 visualizes shear stresses in all four scenarios. Since focus of the study remains in hydrology, the erosive and accretive behaviour of the riverbed, as well as dune or ripple formation, introduced by shear lies out of the scope. Nevertheless, it is important to note the considerable impact of hydraulic structures in the reach. Shear stresses near weirs are considerably, in the order of 100, higher, than elsewhere along the stream. According to the shear stress formula, shear stress is proportional to the square of flow velocity. As the flow accelerates near a weir structure, shear stress tends to increase. The shear stress in an open channel flow is also dependent on the Manning’s roughness coefficient, the hydraulic radius and the slope of the channel. Notice also that along the banks, shear stresses are relatively low. In summary, the mappings imply that the current hydraulic structures impose a large amount of resistance to the flow, in the original scenario, but also the ‘OL’ and ‘M1’-scenario.

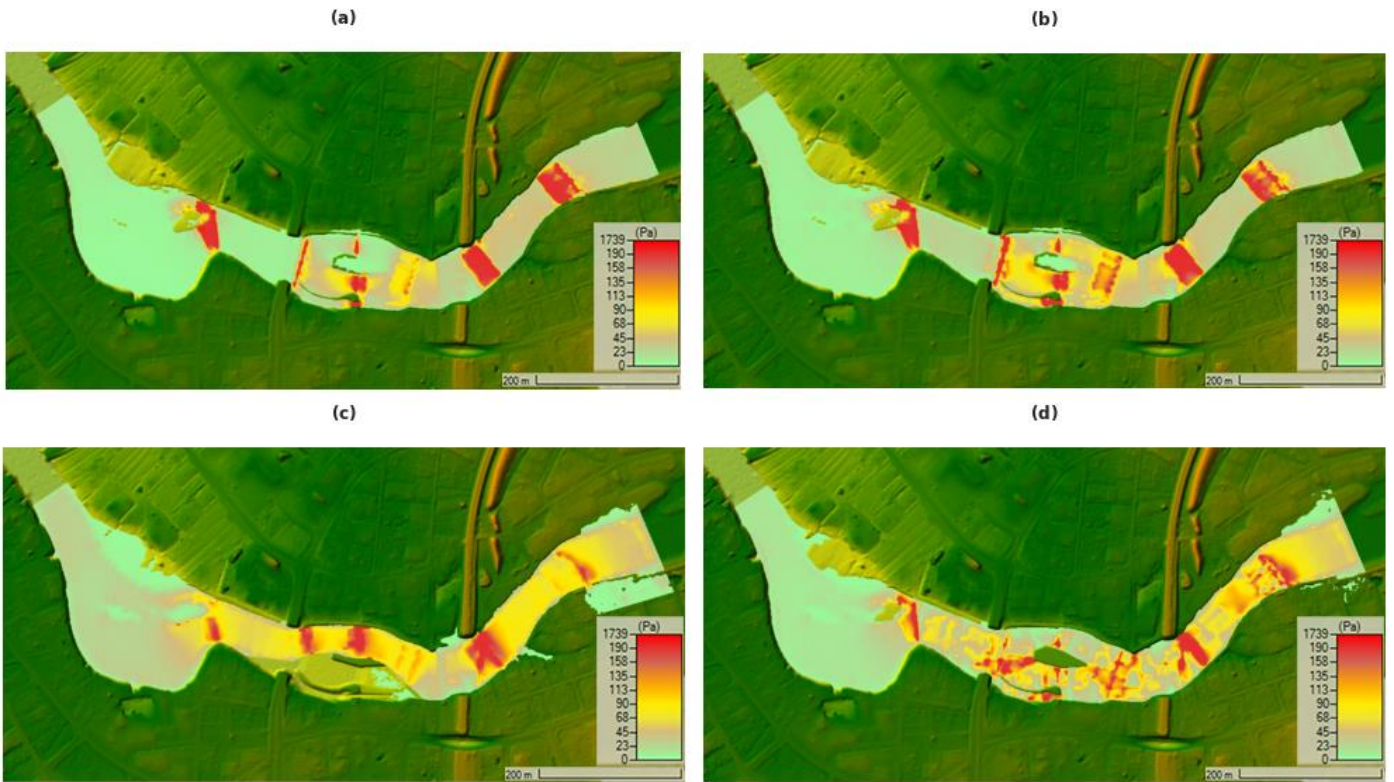


Figure 35: Shear stress maps from model result layers during low flow conditions: Original scenario (a), operational limits scenario (b), morphological change 1 scenario (c) and morphological change 2 scenario (d)

4.2.3.2. Stage and flow hydrograph at weirs

Figure 36 illustrates the headwater, tailwater and weir flow for weir 3, 4A, 4B and 5 during low flow conditions in the original scenario. In general, the difference between head water and tail water gets larger if the weir crest height is significant too. Generally, at peak moments of hydropeaking practices, the weir flow spikes. This means that during a short pulse a considerable amount of water conveys downstream.

For Weir 3, the weir flow over the whole time series is almost equal to the hydrograph at the headwater and tailwater. So it seems that weir 3 has little impact on the flow conditions with respect to the others, according to the stage and flow hydrograph. Weir 4 shows the largest difference between the peak of the weir flow and head water, suggesting that a large part of the water retained behind it overflows at the moment of hydropeaking. Based on this individual weir flow behaviour, recommendations are to lower weir 4B or increase the weir coefficient and to increase the crest height or decrease the weir coefficient of weir 3, for the purpose of dividing flow conveyance and resistance equally over the subsequent weirs in the context of rapidly changing temporal discharges. Not that changes to the weir coefficient and weir crest are not interchangeable. In practice, lowering the weir coefficient affects the flow resistance and consequently overflow levels. On the other hand, an increased crest height influences both the retaining capacity and overflow levels.

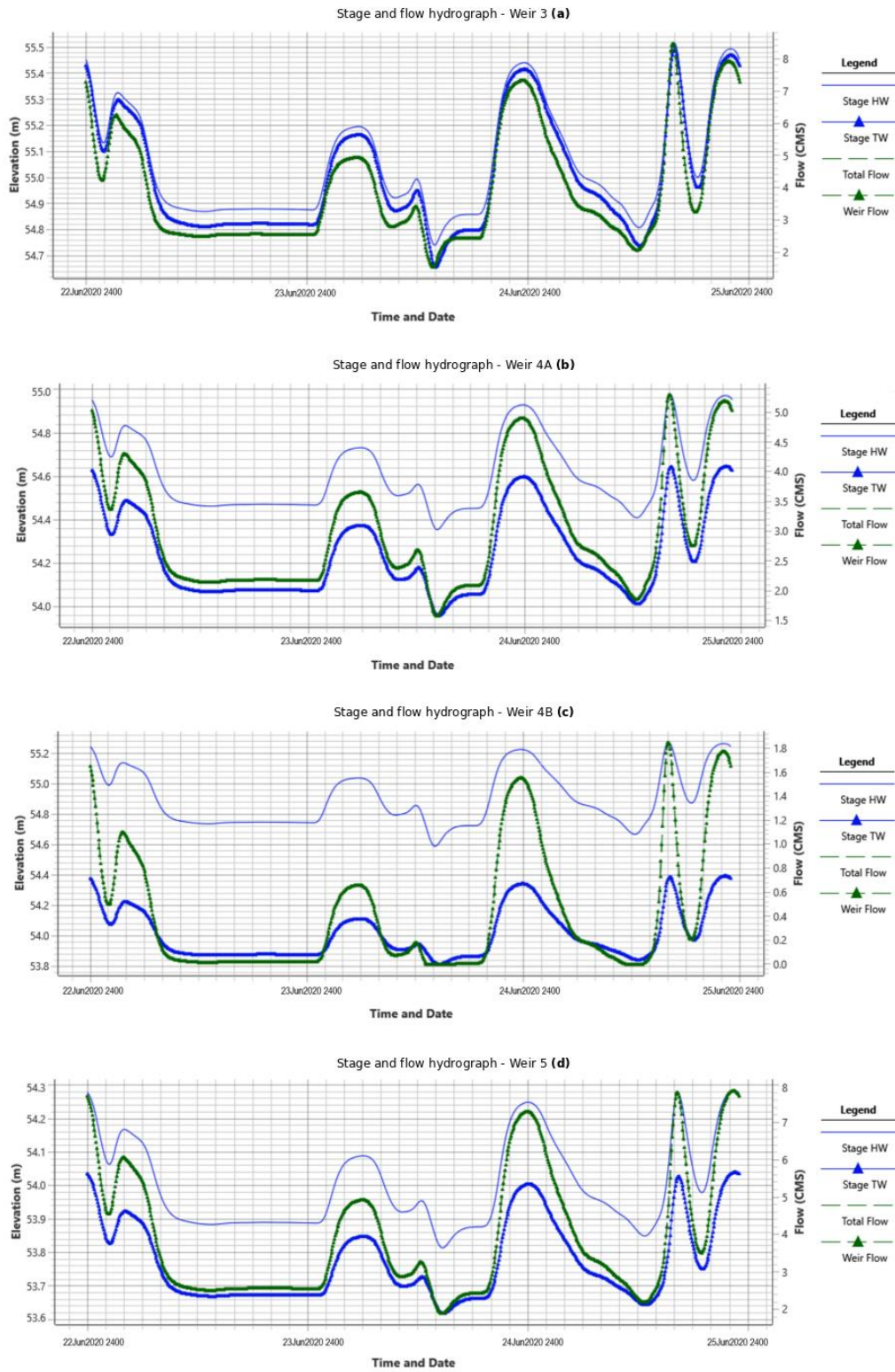


Figure 36: Stage and flow hydrograph during low flow conditions in the original scenario: Weir 3 (a), weir 4A (b), weir 4B (c) and weir 5 (d)

5. Discussion

Data limitations have impacts on results, therefore the proposed mitigation measures must be viewed in context of associated uncertainties. Inherent uncertainties can arise from various sources; the measurement instrument precision, data sampling frequencies, model simplifications, boundary conditions and data processing techniques. In the first subchapter, an uncertainty analysis and discussion is subdivided by the different scenarios, from which local recommendations for Juurikoski are deduced. In the second subchapter, the performance of the hydrodynamical model and potential of calibration methods are discussed. Global model implementation recommendations are stated in the final subchapter.

5.1. Mitigation of hydropeaking influence – Juurikoski

5.1.1. Hydropower operational limits

The increased lower threshold and decreased upper threshold in the operational range of the hydropower plant, is only slightly visible in results downstream. Model results must be fairly accurate to correctly translate discharge changes upstream, to water level and velocity variation downstream. Especially near rapids, which require an even higher accuracy to describe these detailed areas.

Moreover, operational limits seem to decrease rapid flows to some extent, but their level of efficiency has to be proven for medium and high flow conditions as well. Unfortunately, a measured water level time series in January 2020 during high flow or March 2020 during medium flow conditions is non-existent. Furthermore, the method of calibration is very influential on flow outcomes, especially in the context of rapidly changing flow conditions. Calibration method 1, based on water levels, is in fact more suitable for flood risk or inundation boundary analyses. The purpose of the model however is to accurately represent velocities, to make a clear statement about hydropeaking impact on rapids, in comparison with normal (more or less steady with minor presence of vegetation and large riverine boulders) flow areas. Consequently, an optimal model would have been calibrated mainly based on a combination of method 2 and 3, relying on velocities from ADCP and LSPIV, and perhaps validated with logger data. However, since local velocities are highly dependent on the bathymetry and computational capacity of the HEC-RAS, this is not feasible.

5.1.2. Local morphology alteration

The ‘M1’-scenario involves a transformation of an anabranch to a one way stream. This morphological change may be oversimplified in the model by the definition of a wall, with a terrain height similar to that of the banks. Another point is that calibration of the model is mainly based on the land cover dataset. In the ‘M2’-simulation, a non-uniform spread of vegetation and rocks along the river bed is assumed. However, if land cover use changes due to morphological rearrangements, some of Manning’s values may have to change as well. This compromises the accuracy of calibration.

5.1.3. Recommendation hydropeaking mitigation

Related to hydropeaking impact mitigation, the operational limits scenario is relatively easy in terms of practical application. Of course, only if the stakeholders, the local and regional authorities and the hydropower plant, reach a collaboration agreement. The ‘M1’-scenario drastically impacts landscape, while no improvement is suggested based on results. Even more concerning is the amount of increase in resistance to the flow. Consequently, flood protection would have to be implemented. Concluding, ‘M1’-scenario can be excluded from a practical point of view. The ‘M2’-scenario has potential, but will have to be applied in phases to decrease complexity of the proposed solution. First a set of construction works involving (large) riverine

stones and vegetation can be accomplished. Afterwards perhaps a more structurally impactful change to the submerged weirs. In between phases, a drone could fly over the reach to collect LSPIV-data to assess impacts of each phase.

5.2. Performance hydrodynamical model and future recommendations – Juurikoski and other cases

5.2.1. General challenges with data sources

An uncertainty quantification and sensitivity analysis is performed for the mean speed variable for both ADCP- and LSPIV datasets. Note that by mean speed, for the ADCP-datasets each mean speed at a point in the y-,z-plane is meant, while in the LSPIV-sets to the surface velocities in the x-, y-plane is referred to.

For the M9 profiler, up to three frequencies are applied: 3MHz, 1 MHz and 0.5 MHz. ADCPs are typically designed to capture normal to high flow velocities. An universal capability would be in the order of 0.01 m/s. Besides the device configuration and calibration, the Signal-to-Noise-Ratio (SNR) dictates how accurate measurements are. Figure 37 illustrates the SNR-values at 3 dB for CS1. The choice of SNR-settings is a trade-off between capturing low-velocity flows and maintaining qualitative data. The individual SNR-values in transects depend highly on the depth per measurement, but an overall relatively high SNR is achieved at 3 dB (see Appendix H, Figures H.1 and H.2).

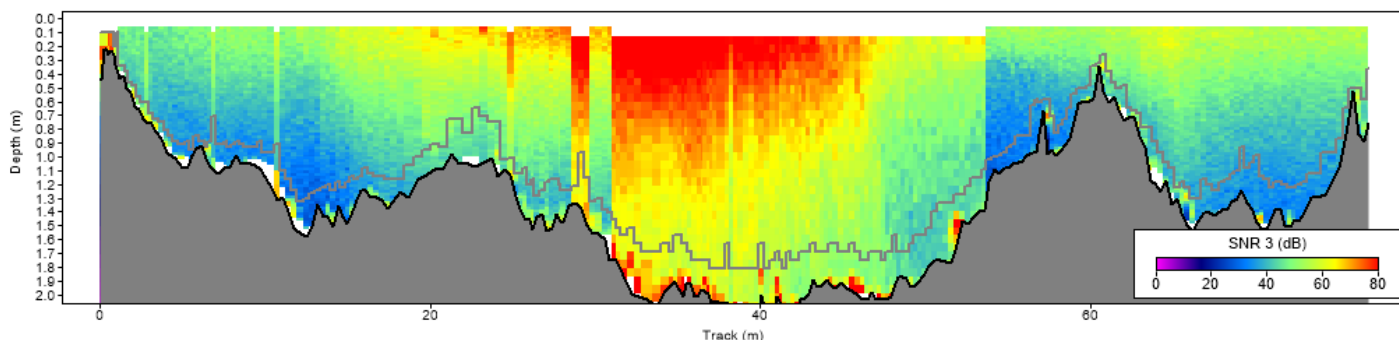


Figure 37: Cross-sectional SNR-values at 3 dB (ADCP-file CS1)

Around this value, the weak signals at low flow speeds along with noise are filtered out. Notice the SNR-values along the cross-sections are rather low at low flow speed regions and near the bottom, but are rather strong in rapids, the main areas of interest in this report. Additionally, the minimum detectable velocity according to the samples is 0.001 m/s. Table H.1 in Appendix H, shows that the normalized measure of variability are higher for ADCP-data than for LSPIV-data. Thus, ADCP-data has a relatively higher variability. Related to the sensitivity analysis, the mean speed can be analysed relative to the depth, number of pings and number of cells. Figures H.3 and Figure H.4 display sensitivity curves for each parameter. According to these sensitivity curves, the depth is of major importance regarding uncertainty with respect to the velocity variable.

The LSPIV-frames and corresponding averaged point data are subjected to image co-registration, data analysis, postprocessing and georeferencing. Consequently, various sources of uncertainty are present. Moreover, during comparison with other velocity export files, velocity magnitudes and angles may not match with a certain window. E.g. the LSPIV window is 16x16 pixels or 44 cm x 44 cm, while the window in HEC-RAS is unknown. In Table H.1 of Appendix H, an uncertainty quantification related to the velocities is presented, where fairly large standard deviations are observed. A sensitivity analysis is also given in Figures H.5 and H.6 based on the x-pixel and y-pixel parameter. The x-pixel shows various values of the uncertainty

measure, while the y-pixel gives a constant zero value. Thus, the y-pixel is considered irrelevant to assess the uncertainty.

To improve the quality of data and therefore reduce uncertainties in future measurements, the depth parameter and the importance of the x-pixels must be accounted for in some way. These parameters are the most impactful during sensitivity analysis. However, measuring flow in unsteady conditions makes it challenging to control such parameters. Finally, it is best to stay within certain ranges according to the sensitivity analysis while the measurements are recorded. For instance, between a number of cells above 30 and below 60 for ADCP.

5.2.1. General challenges model and calibration

During conventional calibration method 1, the modelled peak is too high for downstream reaches, possibly due to too quickly accelerating water volumes. If Manning's number is increased for the upstream reaches to reduce this peak, more resistance to the flow is created, but a mismatch between upstream and downstream loggers becomes more pronounced. Additionally, the interpretation of the R-squared value is defined rather broadly in literature. Nevertheless, in regression analysis evaluation the coefficient of determination R-squared is more informative than other statistical values such as the mean squared error among others (Chicco et al., 2021). Another important aspect is the distribution between data to calibrate and to validate the flow. Since there are only a few hours of flow data available from loggers downstream of HHP, the time series must be divided in some way. A cross-validation, "a statistical method of evaluating and comparing learning algorithms by dividing data into two segments: one used to learn or train a model and the other used to validate the model" according to Refaeilzadeh et al. (2009) for instance, is not recommended due to complexity of the procedure. Dieterle (2003) mentioned in his ph. D. thesis that the larger the calibration data set the better the model and the larger the validation data set the better the estimation of the predictivity. In accordance with this statement, the logger data is randomly divided. This means that loggers 3, 5 and 6 serve for calibration and loggers 2 and 4 serve for validation.

Besides the calibration procedure, the computation settings can drastically influence outcomes as well. The physical meaning behind the computational time step is the filling up of cells during a certain time interval and could be abruptly halted if not chosen long enough. Similarly, a long computational time step leads to a choked flow pattern instead of a continuously moving river flow. Another important aspect that heavily influences calibration accuracy and model outcomes is the method of terrain generation. Point cloud data, mainly available at the banks, are interpolated to create a terrain layer in HEC-RAS. The use of a detailed bathymetry map is recommended for future studies, since local terrain height, discontinuities, locally (flat) slopes and elements such as weir structures and large riverine rocks are significantly underrepresented in the model.

As a sidenote regarding hydraulic structure modelling in HEC-RAS, the weir flow coefficient in HEC-RAS may have a relatively large impact on simulation results, since multiple submerged weirs are present at Juurikoski. The physical meaning of the weir flow coefficient is related to the shape of the weir and its crest and the introduced flow resistance. In HEC-RAS, this value is derived from experimental data or manufacturer specifications, after which hydraulic principles, including the energy equation, and numerical methods like the Finite Difference Method, are applied to solve for the flow rates (USACE Hydrologic Engineering Center, 2023). However, the input value of this weir flow coefficient could impact the calculation of velocities for flow regions above such weirs, in this case the rapids, drastically. Consequently, values in rapid regions could be significantly lower than they are in observed ADCP-data.

5.2.2. Potential LSPIV and ADCP to calibrate and validate the hydrodynamical model – Juurikoski
Currently, state-of-the-art methods to calibrate, and ultimately validate the model, concern a few challenges in practical terms. Firstly, HEC-RAS oversimplifies rapid areas, especially when dealing with extremely low or high values. Secondly, a variation between high and low velocity values does not occur naturally in x- and y-direction. Concluding, HEC-RAS is limited in reproducing rapidly changing velocities. There can be multiple causes for this, such as the flow stabilization during warm-up conditions, where results are being ‘over-polished’.

ADCP instruments provide high-frequency velocity data with relatively high accuracy along its path and along a certain depth. This makes ADCP relatively time intensive, but highly applicable to create detailed visualizations of flow such as velocity-depth profiles. Another aspect related to ADCP is that velocity profiles seem to have a rather natural profile, with varying velocity-values along the z-axis. On HEC-RAS profile lines, these variations are absent by software definition. A 3D model may provide a better comparison between state-of-the-art methods. Another possibility is to provide a dense and therefore more complete bathymetry point cloud along the banks and river bed in HEC-RAS to improve modelled velocity-values.

Although ADCP has previously mentioned advantage, LSPIV is typically more cost- and time-effective, making the method more accessible for smaller-scale research projects. LSPIV relies on video or imagery data, so human effort is limited. If a drone is applied for example, there is a wide area coverage in only a few minutes time. While drone based LSPIV-data of surface velocities is qualitatively valuable, it is not quantitatively rich. This makes calibration and validation based on this type of data scientifically challenging. Quality of data is also dependent on the area investigated. Flow area near banks and heavily vegetated areas are captured rather poorly, making LSPIV unfit for calibration if these type of areas are significant for the model. As is the case for Juurikoski. However, on rapid areas, where variation between velocities is rather clearly visible, LSPIV proves effective in the approximation of real velocity-values. Therefore, LSPIV-data proves useful for an indication of flow behaviour.

The research objective largely dictates the state-of-the-art methods applied. High-accuracy measurements by ADCP and the corresponding in-depth flow analysis gives overall better representation for a realistic flow situation. However, the area spanning Juurikoski is overall too big to do by ADCP-data alone. Therefore, visual LSPIV-data for a qualitative analysis may be useful for flow areas left undefined by ADCP.

5.2.3. Recommendations modelling approach implementation

A denser point cloud to generate terrain or bathymetric images from an echosounder would benefit the modelling approach greatly. Nonetheless, the implementation of an echosounder is expensive. In the case of Juurikoski, more logger locations along a cross-section could prove more beneficial. Generally, loggers are located at one specific point, but during calibration and validation the assumption is that the logger depicts general flow conditions for a cross-section. An inspection of logger conditions 3, related to the initial water level during calibration, a large relocation of logger 6 and an additional logger placement on the southern branch is recommended. Calibration based on ADCP could benefit from a 3D-modelling approach. Calibration related to LSPIV-data, could prove beneficial for a less complex reach (less vegetation and riverine boulders) and a relatively steady flow (which does not include hydropeaking impacts).

6. Conclusions

6.1. Answers to the research questions

Hydropeaking is a widely applied management practice in the generation of hydropower. When the demand in electricity is high, the operator of a hydropower plant rapidly increases released discharges to meet this demand. Vice versa, when the demand is low, no or less water is released. However, while river regulation practices offer valuable resources, they can also inflict adverse environmental consequences on downstream river segments. More specifically, hydropeaking introduces high sub-daily variance in downstream reaches of the hydropower plant. This large sub-daily variance is harmful to the river regime and ecosystems. In Finland, hydropeaking has the highest negative environmental impact of all river regulation practices. The most prominent, known negative impacts due to high flow variations are a direct impact on aquatic biota, such as trout, and a compromised recreational use of the river corridor. The main objective of the thesis research is to investigate the impact of hydropeaking on rapids in a complex riverine system. More precisely, a system that includes multiple subsequent weirs, vegetation, large riverine boulders, a rather flat topography and a small-scale anabranch. The main research question is:

How does the sub-daily variance introduced by upstream hydropeaking practices affect a complex rapid system situated near weirs downstream of a hydropower plant and how can these impacts be mitigated?

The formulation of operational and morphological mitigation measures to counter impacts is the secondary objective. Additionally, the potential of state-of-the-art modelling approaches based on LSPIV- and ADCP-data are also discussed. A case study for the downstream region of Hamari Hydropower Plant at Ylivieska (Finland), the site Juurikoski, provides insight on the different aspects related to these queries. During a series of simulation runs, including the original situation and three hypothetical mitigation scenarios, the impact of hydropeaking is quantified and studied. Results include post-processed water level, velocity and shear stress data. The main research question is answered by use of a series of sub questions **1**, **2**, **3**, **4**, **5**, **6** and **7**:

1. What defines a good modelling approach with the aim to improve reliability of the model to define appropriate mitigation measures?

A ‘good’ modelling approach considers the focus on rapids in the case study. A grid cell size of 3 m x 3 m accords with the scale of the rapids. A time step of 20 seconds agrees with the speed of the travelling flood wave and captures sub-hourly discharge variations in an output hydrograph with an interval of 5 minutes. Additionally, the report assesses the potential of calibration and validation for a 2D hydrodynamical model by state-of-the-art methods like a hot spot analysis comparison based on LSPIV-data (Method 2) and velocity profile comparisons based on ADCP-data (Method 3). This could improve the reliability of the model in localized refinement areas. This also enables a proposition of tailored and more reliable mitigation measures. Bullet points **2**, **3** and **4** dive deeper into the relevant queries.

2. Are ADCP measurements accurate enough to relatively measure very low and high flows?

The ADCP-measurements are accurate enough to measure relatively low and high flows. The precision lies in the order of $1e^{-3}$ and is therefore suitable to quantify hydropeaking impacts. ADCP-data from the 24th of June 2020 around the time interval 13:00-14:00 encompasses significant hydropeaking practices.

3. Can the model be calibrated by LSPIV drone-based surface velocities and is this calibration method beneficial?

The calibration of the 2D HEC-RAS model by ‘Method 1’ is described by coefficients of determination. From upstream to downstream, these coefficients are 0.83, 0.56 and 0.41 based on logger data. A second method relies on LSPIV drone-based surface velocities. The hot spot analysis comparison (see Method 2) shows that approximately more than 50% of raster area compared has a similarity value higher than 0.6, leaving room for improvement. Ideally, to increase both area percentage and similarity value, both LSPIV-analysis and HEC-RAS would have to be able to reproduce a clear distinction between relatively small differences in velocity-values.

4. Is ADCP-data relevant for calibration of the model and is it beneficial to locally alter the roughness of the channel bed based on a comparison analysis between measured and modelled value during this process?

ADCP can contribute to the calibration of the model (see Method 3), in a practical sense to benefit the reliability of regions of interest. In the case study, regions of interest refer to the rapids. These refinement regions can be fine-tuned on Manning’s values, according to a comparison analysis between measured and modelled section velocities.

5. In a hydrodynamical context, how is hydropeaking at the HHP influencing the main rapids of the Juurikoski site?

For CS1, a cross section with a pronounced rapid that is 3 meters wide, shows that at high discharge rates resulting from these hydropeaking practices, all measured mean velocities in the rapid are in the range of ≥ 0.2 m/s and ≤ 0.9 m/s. Measured ADCP defined depths in the rapid are above 2 m. Additionally, other velocities along the track typically stay well below 0.2 m/s and defined depths are relatively shallow. For a cross-section without pronounced rapids, velocities remain below the threshold of ≤ 0.6 m/s. ADCP defined depths lie in range of ≥ 0 m and ≤ 2 m. In conclusion, hydropeaking results in relatively deep water levels and a distinct fast-flowing pattern in a rapid region, despite the presence of vegetation and large riverine boulders.

6. & 7. How do the model outcomes differ when considering modified river hydrology or morphology compared to the original riverine system? What are the characteristics of efficient mitigation measures to counter environmental impacts?

The report provides a modelling approach to tailor mitigation measures according to riverine lay-out, even if the terrain definition is difficult due to limited bathymetry data and increased riverine complexity because of hydraulic structures. At regional level of the case study, four simulations were run in a 2D hydrodynamical model; one for maximizing economic gain, which is the current situation at Juurikoski, one solely for benefiting environmental standards by limiting ramping rates and lastly two experimental simulations with morphological adjustments to achieve a compromise to satisfy both ends. Firstly, operational measures seem to be effective. In comparison to the original case, the fluctuation extent of water levels is increased by 0.16 m for the lower limit and decreased 0.18 m for the upper limit. The ‘morphological change 2’-scenario shows a lot of potential. The scenario is a variation on the original

situation at Juurikoski and includes lowering of weirs to create less resistance than in the original case, besides the random spatial distribution of stones and vegetation along the stream. Moreover, the southside was branch was surrounded by large riverine rocks to induce a fast flowing stream on the northside and more varying stream on the southside. Consequently, the maximum water level is 0.17 m below the original reference case and velocities are gradually changing along the streamwise direction, described by a mean of 0.04 m/s and standard deviation of 0.03. These characteristics are much more preferable than occasional bottle necks and large variation between the sequential areas in streamwise direction along the river. Contrarily, ‘morphological change 1’-scenario introduces closure of the southern branch and drastically alters the original flow-situation at Juurikoski. It further induces extensive unpredictable water level fluctuations, and therefore possibly risk of flooding. Concluding, this scenario can be excluded from a practical point of view.

Concluding, hydropeaking practices introduce high variability and increased rapid flows in localized weir openings. In high sub-daily flow conditions, the restoration of naturally occurring rapids is challenging. However, operational mitigation and morphological mitigation measures have the potential to mitigate these impacts.

6.2. Regional and global recommendations

For a regional management point of view, the thesis makes a strong case for concrete change in operation policies of hydropower plants. Additionally, it can serve as input for future practical hydropeaking practice mitigation strategies. The findings of the 2D model can provide a solid basis to predict and specify fish habitat and stranding regions more accurately, as previously investigated by Addo (2019). It also suggest morphological changes to improve the environmental state of the river reach, while maintaining maximal profit at the plant. Knowledge institutes, such as ELY, could benefit from the insights for practical applications for Juurikoski, in terms of which mitigation measures to exclude and which ones have potential. On a local scale, ‘Morphological Change 2’ is suggested and ‘Morphological Change 1’ excluded from a practical point of view.

From a more global perspective, the report provides a modelling approach to tailor mitigation measures according to riverine lay-out, despite limited bathymetry data and increased riverine complexity. The results exhibit valuable information to further improve 2D hydrodynamical models, in terms of model conditions and calibration methods, and to proceed with fish habitat modelling, recreational or other studies. Additionally, to further open the discussion on aspects of creativity, effectiveness and practical implications related to hydropeaking mitigation measures.

Bibliography

- Addo, L. (2019). *The effects of short-term regulation on habitat conditions of brown trout, Salmo trutta in the lowermost part of River*. (Master's thesis, L. Addo).
- Ali, S. (2013). *Flow over weir-like obstacles*.
- Anindito, Y., Haas, J., Olivares, M., Nowak, W., & Kern, J. (2019). *A new solution to mitigate hydropeaking? Batteries versus re-regulation reservoirs*. *Journal of Cleaner Production*, 210, 477-489.
<https://doi.org/10.1016/j.jclepro.2018.11.040>
- Aronsoo, K., & Wennman, K. (2012). *Vesirakentamisen ja säännöstelyn sekä niihin liittyvien kompensatiotoimenpiteiden vaikutukset Kalajoen kala, nahkiais ja rapukantoihin*. Elikeino-, liikenne- ja ympäristökeskus [ELY].
<https://www.elykeskus.fi/julkaisut>
- Ashraf, F., Haghghi, A.T., Riml, J. et al. (2018). *Changes in short term river flow regulation and hydropeaking in Nordic rivers*. *Sci Rep* 8, 17232.
<https://doi.org/10.1038/s41598-018-35406-3>
- Barbosa, A. E., Alves, E., Cortes, R. M. V., Silva-Santos, P. M., Aguiar, F., & Ferreira, M. T. (2006). *Evaluation of environmental impacts resulting from river regulation works. A case study from Portugal*. *Proceedings and Monographs in Engineering*. R. Ferreira, E. Alves, J. Leal, A. Cardoso (eds.). Water and Earth Sciences. river Flow, 1-2.
- Batalla, R. J., Gibbins, C. N., Alcázar, J., Brasington, J., Buendia, C., Garcia, C., ... & Vericat, D. (2021). *Hydropeaked rivers need attention*. *Environmental Research Letters*, 16(2), 021001.
<https://doi.org/10.1088/1748-9326/abce26>
- Bengtson, H. (2017). *The Manning Equation for Open Channel Flow Calculations*.
- Bomers, A., Schielen, R. M. J., & Hulscher, S. J. (2019). *The influence of grid shape and grid size on hydraulic river modelling performance*. *Environmental fluid mechanics*, 19, 1273-1294.
<https://doi.org/10.1007/s10652-019-09670-4>
- Bunn, S. E., & Arthington, A. H. (2002). *Basic principles and ecological consequences of altered flow regimes for aquatic biodiversity*. *Environmental management*, 30, 492-507.
<https://doi.org/10.1007/s00267-002-2737-0>
- Carolli, M., Vanzo, D., Siviglia, A., Zolezzi, G., Bruno, M. C., & Alfredsen, K. (2015). *A simple procedure for the assessment of hydropeaking flow alterations applied to several European streams*. *Aquatic sciences*, 77, 639-653.
<https://doi.org/10.1007/s00027-015-0408-5>
- Charmasson, J., & Zinke, P. (2011). *Mitigation measures against hydropeaking effects*. *SINTEF Energy Research*, 1, 51.

- Chicco, D., Warrens, M. J., & Jurman, G. (2021). *The coefficient of determination R-squared is more informative than SMAPE, MAE, MAPE, MSE and RMSE in regression analysis evaluation*. PeerJ Computer Science, 7, e623.
<https://doi.org/10.7717/peerj-cs.623>
- Coarer, Y. L. (2007). *Hydraulic signatures for ecological modelling at different scales*. Aquatic Ecology, 41, 451-459.
<https://doi.org/10.1007/s10452-005-9005-3>
- Costabile, P., Costanzo, C., Ferraro, D., Macchione, F., & Petaccia, G. (2020). *Performances of the new HEC-RAS version 5 for 2-D hydrodynamic-based rainfall-runoff simulations at basin scale: Comparison with a state-of-the art model*. Water, 12(9), 2326.
<https://doi.org/10.3390/w12092326>
- Dawson, C., & Mirabito, C. M. (2008). *The shallow water equations*.
https://users.oden.utexas.edu/~arbogast/cam397/dawson_v2.pdf
- Déry, S. J., Hernández-Henríquez, M. A., Stadnyk, T. A., & Troy, T. J. (2021). *Vanishing weekly hydropeaking cycles in American and Canadian rivers*. Nature Communications, 12(1), 7154.
<https://doi.org/10.1038/s41467-021-27465-4>
- Dieterle, F. J. (2003). *Multianalyte quantifications by means of integration of artificial neural networks, genetic algorithms and chemometrics for time-resolved analytical data* (Doctoral dissertation, Universität Tübingen).
<http://hdl.handle.net/10900/48496>
- European Commission [EC]. (n.d.). *Hydropower*. Research and innovation - Energy.
https://research-and-innovation.ec.europa.eu/research-area/energy/hydropower_en
- FCG Finnish Consulting Group Oy. (2011). *Ylivieskan Kaupunki: Keskustan Osayleiskaava 2030*.
- Figueiredo, J. S. M. D., Fantin-Cruz, I., Silva, G. M. S., Beregula, R. L., Girard, P., Zeilhofer, P., ... & Hamilton, S. K. (2021). *Hydropeaking by small hydropower facilities affects flow regimes on tributaries to the Pantanal wetland of Brazil*. Frontiers in Environmental Science, 9, 577286.
<https://doi.org/10.3389/fenvs.2021.577286>
- Fortum. (n.d.). *Hydropower – Renewable and Clean Energy*.
<https://www.fortum.com/energy-production/hydropower>
- Fokkens, B. (2007). *The Dutch strategy for safety and river flood prevention*. In Extreme hydrological events: new concepts for security (pp. 337-352). Dordrecht: Springer Netherlands.
- Greimel, F., Schülting, L., Graf, W., Bondar-Kunze, E., Auer, A., Zeiringer, B., & Hauer, C. (2018). *Hydropeaking Impacts and Mitigation*. Aquatic Ecology Series, vol 8. Springer, Cham.
- Google. (2023). Google Maps. <https://www.google.com/maps>

- Guerrero, M., Di Federico, V., & Lamberti, A. (2013). *Calibration of a 2-D morphodynamic model using water–sediment flux maps derived from an ADCP recording*. *Journal of Hydroinformatics*, 15(3), 813-828.
<https://doi.org/10.2166/hydro.2012.126>
- Guillén, N. F., Patalano, A., García, C. M., & Bertoni, J. C. (2017). *Use of LSPIV in assessing urban flash flood vulnerability*. *Natural Hazards*, 87, 383-394.
<https://doi.org/10.1007/s11069-017-2768-8>
- Harms, J. (2021). *Physical modelling of submerged groynes*. TU Delft Repositories.
<https://repository.tudelft.nl/islandora/object/uuid%3Ac042a0e1-2ff7-492a-a0fb-8c017a6b145e>
- Hauer, C., Siviglia, A., & Zolezzi, G. (2017). *Hydropeaking in regulated rivers: from process understanding to design of mitigation measures*. *Science of the Total Environment*, 579, 22-26.
- Hayes, D. S., Schülting, L., Carolli, M., Greimel, F., Batalla, R. J., & Casas-Mulet, R. (2022). *Hydropeaking: Processes, effects, and mitigation*.
<https://doi.org/10.1016/B978-0-12-819166-8.00171-7>.
- International Energy Agency [IEA]. (n.d.). *Hydroelectricity*.
<https://www.iea.org/energy-system/renewables/hydroelectricity>
- Jelovica, B., Marttila, H., Ashraf, F. B., Kløve, B., & Torabi Haghighi, A. (2023). *A probability-based model to quantify the impact of hydropeaking on habitat suitability in rivers*. *River Research and Applications*, 39(3), 490-500.
<https://doi.org/10.1002/rra.4050>
- Kolkman, P.A. (1989). *Models for Study of the Dynamic Behaviour of Structures in Flow and Waves*. In: *Martins, R. (eds) Recent Advances in Hydraulic Physical Modelling*. NATO ASI Series, vol 165. Springer, Dordrecht.
https://doi.org/10.1007/978-94-009-2344-7_3
- Kuhanestani, P. K., Bomers, A., Booij, M. J., Warmink, J. J., & Hulscher, S. J. (2022). Calibration approaches for hydraulic river models for high and low flows: A review. In 39th IAHR World Congress 2022: From snow to sea. IAHR.
- Le Coarer, Y., Testi, B., & Beguin, J. (2017). *Ecohydraulic quantification of hydropeaking alterations by the use of hydrosignatures: a two scale approach*. *La Houille Blanche*, (2), 15-19.
<https://doi.org/10.1051/lhb/2017012>
- Mario, J. F. & Valero, D. & Liu, X. (2022). *Treatise on Geomorphology (Second Edition) –Volume 6.1*. Academic Press.
<https://doi.org/10.1016/B978-0-12-818234-5.00135-8>
- Meile, T., Boillat, J. L., & Schleiss, A. J. (2011). *Hydropeaking indicators for characterization of the Upper-Rhone River in Switzerland*. *Aquatic Sciences*, 73, 171-182.
<https://doi.org/10.1007/s0027-10-0154-7>

- Metsa. (n.d.). *Ekoenergy Hydropower Criteria Review: Background study*.
<https://www.ekoenergy.org/lets-talk-about-hydropower>
- Moreira, M., Hayes, D. S., Boavida, I., Schletterer, M., Schmutz, S., & Pinheiro, A. (2019). *Ecologically-based criteria for hydropowering mitigation: A review*. *Science of The Total Environment*, 657, 1508-1522.
<https://doi.org/10.1016/j.scitotenv.2018.12.107>
- Moreira, M., Schletterer, M., Quaresma, A., Boavida, I., & Pinheiro, A. (2020). *New insights into hydropowering mitigation assessment from a diversion hydropower plant: The GKI project (Tyrol, Austria)*. *Ecological Engineering*, 158, 106035.
<https://doi.org/10.1016/j.ecoleng.2020.106035>
- Mosselman, E. (2020). *Studies on river training*. *Water*, 12(11), 3100.
<https://doi.org/10.3390/w12113100>
- Nordic Investment Bank [NIB]. (n.d.). Nib finances hydropower plant upgrades and small-scale plant in Finland. <https://www.nib.int/releases/nib-finances-hydropower-plant-upgrades-and-small-scale-plant-in-finland>
- Paikkatietoikkuna. (n.d.).
<https://kartta.paikkatietoikkuna.fi/?lang=en>
- Paituli. (n.d.).
<https://paituli.csc.fi>
- Parsapour-Moghaddam, P., & Rennie, C. D. (2018). Calibration of a 3D hydrodynamic meandering river model using fully spatially distributed 3D ADCP velocity data. *Journal of hydraulic engineering*, 144(4), 04018010.
[https://doi.org/10.1061/\(ASCE\)HY.1943-7900.0001424](https://doi.org/10.1061/(ASCE)HY.1943-7900.0001424)
- Person, E. (2013). *Impact of hydropowering on fish and their habitat*. EPFL-LCH.
- Refaeilzadeh, P., Tang, L., & Liu, H. (2009). *Cross-validation*. *Encyclopedia of database systems*, 532-538.
- Roney, T. (2021). *Wet-season dam operations hit Mekong Ecology and Communities*. *Eco-Business*.
<https://www.eco-business.com/news/wet-season-dam-operations-hit-mekong-ecology-and-communities/>
- Salmaso, F., Servanzi, L., Crosa, G., Quadroni, S., & Espa, P. (2021). *Assessing the impacts of hydropowering on river benthic macroinvertebrates: A state-of-the-art methodological overview*. *Environments*, 8(7), 67.
<https://doi.org/10.3390/environments8070067>
- Saltveit, S. J., Halleraker, J. H., Arnekleiv, J. V., & Harby, A. (2001). *Field experiments on stranding in juvenile atlantic salmon (Salmo salar) and brown trout (Salmo trutta) during rapid flow decreases caused by hydropowering*. *Regulated Rivers*, 17(4-5), 609-622.
<https://doi.org/10.1002/rrr.652>

- Ali, S. (2013). *Flow over weir-like obstacles*.
<http://dx.doi.org/10.4233/uuid:b9c67923-a84a-47b0-8c0f-6d873ffd1d85>
- Shinn, L. (2018). *Renewable energy: the clean facts*. NRDC: New York, NY, USA, 1-2.
<https://www.nrdc.org/stories/renewable-energy-clean-facts#sec-what-is>
- Shrestha, A., Bhattacharjee, L., Baral, S., Thakur, B., Joshi, N., Kalra, A., & Gupta, R. (2020, May). *Understanding suitability of MIKE 21 and HEC-RAS for 2D floodplain modeling*. In World Environmental and Water Resources Congress 2020 (pp. 237-253). Reston, VA: American Society of Civil Engineers.
<https://doi.org/10.1061/9780784482971.024>
- Shustikova, I., Domeneghetti, A., Neal, J., Bates, P. D., & Castellarin, A. (2019). *Comparing 2D capabilities of HEC-RAS and LISFLOOD-FP on complex topography*. *Hydrological Sciences Journal-journal Des Sciences Hydrologiques*, 64(14), 1769–1782. <https://doi.org/10.1080/02626667.2019.1671982>
- Suomen ympäristökeskus (SYKE). (n.d.). *Assessing and valuing ecosystem services for managing hydropower constructed river systems (ECORIVER)*.
<https://www.syke.fi/projects/ecoriver>
- Suomen ympäristökeskus (SYKE). (n.d.). *Corine maanpeite 2018*. Corine maanpeite 2018 - Aineistot - SYKEN metatietopalvelu.
<https://ckan.ymparisto.fi/dataset/%7B0B4B2FAC-ADF1-43A1-A829-70F02BF0C0E5%7D>
- Tonolla, D., Bruder, A., & Schweizer, S. (2017). *Evaluation of mitigation measures to reduce hydropeaking impacts on river ecosystems—a case study from the Swiss Alps*. *Science of the Total Environment*, 574, 594-604.
<https://doi.org/10.1016/j.scitotenv.2016.09.101>
- Ruokamo, E., Juutinen, A., Ashraf, F. B., Haghghi, A. T., Hellsten, S., Huuki, H., ... & Vermaat J. E. (2023). *Estimating the economic value of hydropeaking externalities in regulated rivers*. *Applied Energy*, 353 (Part A), 122055.
<https://doi.org/10.1016/j.apenergy.2023.122055>
- USACE Hydrologic Engineering Center. (2023). *HEC-RAS 2D User's Manual*.
<https://www.hec.usace.army.mil/confluence/rasdocs/r2dum/latest>
- Valentin, S., Lauters, F., Sabaton, C., & Souchon, Y. (1996). *Modelling temporal variation of physical habitat for brown trout (Salmo trutta) in hydropeaking conditions*. *Regulated Rivers: Research & Management*, 12(2-3), 317-330.
[https://doi.org/10.1002/\(SICI\)1099-1646\(199603\)12:2/33.3.CO;2-T](https://doi.org/10.1002/(SICI)1099-1646(199603)12:2/33.3.CO;2-T)
- Virk, Z. (2022). *A modelling approach for evaluating impacts of hydropeaking in a sub-arctic river*. (Master's thesis, Z. Virk).
<https://urn.fi/URN:NBN:fi:oulu-202210123485>
- Voorendt, M. Z. (2022). *Manual Hydraulic Structures (edition February 2022)*.

Wang, Q. G., Du, Y. H., Su, Y., & Chen, K. Q. (2012). Environmental impact post-assessment of dam and reservoir projects: a review. *Procedia Environmental Sciences*, 13, 1439-1443.
<https://doi.org/10.1016/j.proenv.2012.01.135>

YLE. (2012). *Flooding in North Ostrobothnia peaks*.
<https://yle.fi/a/3-6252516>

Zolezzi, G., Vallefucio, F., Casari, A., Larsen, S., Dallafior, V., & Bruno, M. C. (2023). *Assessing the eco-hydraulic effects of a hydropeaking mitigation measure with increased energy production in the Noce River (Italian Alps)*. In EGU General Assembly 2023, Vienna, Austria, 24-28 April 2023. European Geosciences Union.
<https://doi.org/10.5194/egusphere-egu23-14621>

Appendix A – Juurikoski ortography

Orthophotos (see Figure A.1), aerial photographs that have been geometrically corrected, show a clear evolution of the rapid systems at Juurikoski (Paikkatietoikkuna, n.d.). Rapids in 1998 are less distinct from each other in comparison to the current rapids. The most impactful events is the restoration of Juurikoski between 2004 and 2005. Around this time, the banks and submerged weirs were implemented. The previously relatively flat bottom slope became discontinuous due to the elevation of the weirs. Moreover, large riverine rocks were scattered among the site and inland islands were geometrically modified. This was necessary to counter ice problems and avoid dry lands, maintaining an overall permanent flow.



1947



1958



1993



1998



2004



2005



2010



2011



2015



2019

Figure A.1: Orthophotos Juurikoski 1947-2019 (Paikkatietoikkuna, n.d.)

In light of a masterplan for the city of Ylivieska to be accomplished by the year 2030, FCG Finnish Consulting Group Oy established a report in 2011. Figure A.2 shows the defined valuable areas in this report. On the map, A stands for the “Kirkko-Rohkoranta”-area and B for the “Kauppakatu-juurikoski”- area. Interventions in river lay-out are bounded by these predefined limits, since within these boundaries, the natural environment and aesthetics of the landscape can in principle not be modified. In practical terms, aesthetic value is of uttermost importance for the central Juurikoski site according to the Juurikoski City plants. Thus, visual impact has to be limited.

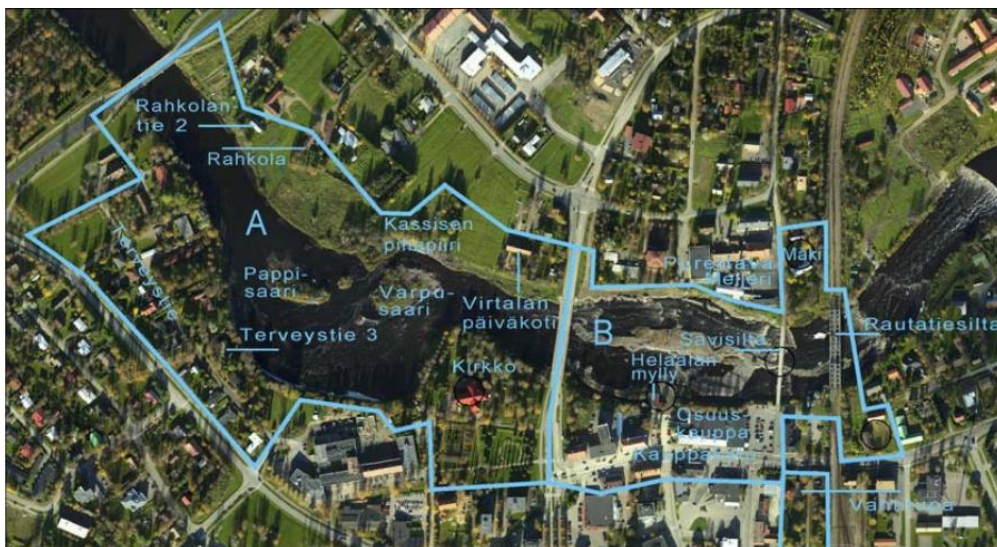


Figure A.2: City Plans Juurikoski - Vulnerable Areas. From *Ylivieskan Kaupunki Keskustan Osayleiskaava 2030* (p. 8), by FCG Finnish Consulting Group Oy, 2011. Copyright 2011 by FCG.

Appendix B – Discharge HHP

Table B.1: Released discharge HHP (*Hamari Virtaama* [m^3/s]), upstream water levels at HHP (*Hamari Ylävesi* [m]) and downstream water levels HHP (*Hamari Alavesi* [m]) - 24th of June 2020

Time	Hamari Ylävesi [m]	Hamari Alavesi [m]	Hamari Virtaama [m^3/s]
00:00	62.14	55.41	6.67
01:00	62.14	55.41	5.19
03:00	62.14	55.40	4.77
04:00	62.14	55.38	4.07
05:00	62.14	55.38	3.27
06:00	62.15	55.38	3.26
07:00	62.15	55.38	3.03
08:00	62.15	55.38	2.64
09:00	62.15	55.38	2.65
10:00	62.15	55.37	1.94
11:00	62.16	55.37	1.95
12:00	62.15	55.37	2.99
13:00	62.16	55.38	2.98
14:00	62.16	55.40	6.01
15:00	62.13	55.47	11.29
16:00	62.14	55.43	2.62
17:00	62.15	55.39	2.57
18:00	62.17	55.38	4.07
19:00	62.16	55.41	7.51
20:00	62.16	55.43	8.05
21:00	62.15	55.44	8.06
22:00	62.14	55.44	7.62
23:00	62.14	55.42	4.76

Appendix C – Weir equations, types and flow regimes

C.1. Submerged weirs

Figure C.1 schematizes the flow principles over a weir. Flow contracts when approaching a weir and expands downstream of the backward facing step. The principle of conservation of energy for flow contraction and conservation of momentum for flow expansion determines the head loss, denoted by ΔH in Figure C.1, over the weir (Ali, 2013).

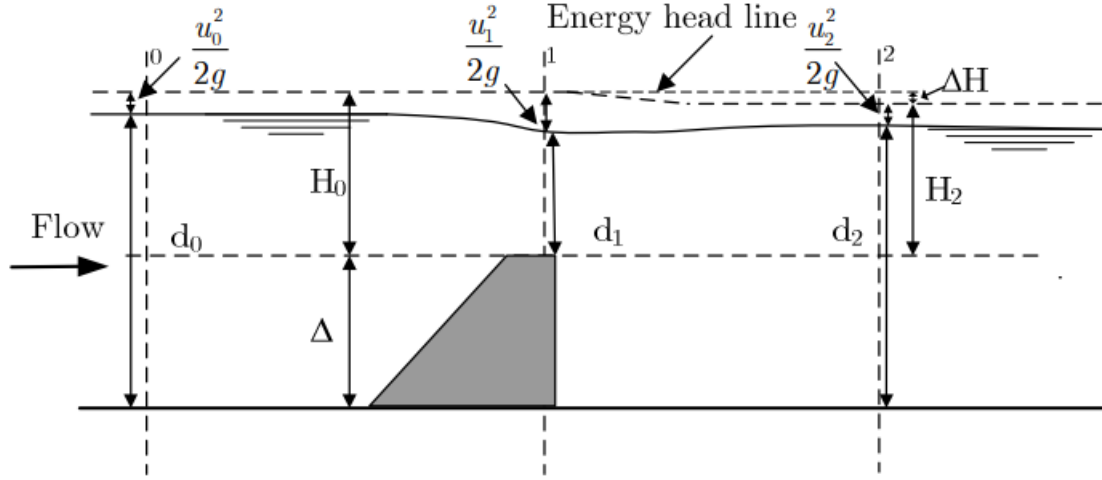


Figure C.1: Schematization of the flow over a weir. From *Flow over weir-like obstacles*, by S. Ali, 2013. Copyright 2013 by S. Ali.

The flow equations over a weir are part of the 1D shallow water equations. These equations only take into account streamwise flow to simplify the interpretation of flow over a weir. At the point of contraction, there is a loss of momentum. For the upstream part and on top of the weir, the water level can be estimated by the conservation of energy (see Formula C.1). Indices 0,1,2 are used to specify cross sectional cuts in Figure C.1.

$$d_0 + \alpha_0 \frac{u_0^2}{2g} = h_{weir} + d_1 + \alpha_1 \frac{u_1^2}{2g} \quad (C.1)$$

The loss of energy during expansion of the flow is determined by the conservation of momentum (see Formula C.2):

$$\frac{1}{2}g(d_1 + h_{weir})^2 + q_1 u_1 = \frac{1}{2}g d_2^2 + q_2 u_2 \quad (C.2)$$

The parameter α accounts for the concentration of energy in part of the flow. Based on Formula C.3, Carnot defines head loss downstream of the backwards facing step as:

$$\Delta H = \frac{\Delta H^2}{2g} \quad (C.3)$$

Furthermore, there are different types of flow regimes over weirs. These flow regimes heavily depend on the weir design. As a consequence, the type of weir in question needs to be classified by the following:

$$\frac{H_1}{L_c} < 0.1 \quad (\text{C.4})$$

$$0.07 < \frac{H_1}{L_c} < 0.35 \quad (\text{C.5})$$

$$0.35 < \frac{H_1}{L_c} < 1.5 \quad (\text{C.6})$$

$$1.5 < \frac{H_1}{L_c} \quad (\text{C.7})$$

Enumeration (C.4) stands for the long crested weir, (C.5) for the broad crested weir, (C.6) for the narrow crested weir and (C.7) indicates the sharp crested weir. For either long or broad crested weirs, there is little curvature in the streamlines of the flow and the water depth can be assumed to be hydrostatic. The flow has time to adapt to new depths when passing over the weir. However, for long weirs energy loss by friction cannot be neglected. For narrow and sharp crested weirs, the vertical velocities are significant and consequently curvature cannot be neglected. Especially for the sharp crested weir, where flow does not reattach. Note there is also vertical separation of the flow in the backward facing step, usually more present for steep profiles. A large part of the energy loss comes from the highly turbulent vortices and reattachment of the flow (Harms, 2021). Note that the principles above are all described from a one-dimensionality perspective, while hydraulic models are often in a 2D- or 3D-plane.

C.2. Weirs types and flow regimes

There are two primary types of weirs: fixed weirs and weirs equipped with moveable gates. Furthermore, weirs can be further subdivided in submerged weirs and emerged weirs. Compound weirs, or flexible spillways, have the capacity to regulate the river discharge, commonly in the context of flood protection. Weirs positioned in river systems introduce resistance to the flow and elevate water levels for a considerable length upstream of the structure (Hydraulic Structures, 2022). At Juurikoski, submerged weirs were introduced to maintain a sufficient water depth to facilitate fish migration and habitat (Aronsoo & Wennman, 2012). Simultaneously, they provide flood protection downstream for the Juurikoski area.

Kolkman (1989) delineates distinct flow regimes over weirs (see Figure C.2); A *free flow regime*, a *submerged flow regime* and a *transitional flow regime*. For the free flow regime, flow remains independent of the downstream water depth and a hydraulic jump is present on the backward face of the weir. The submerged flow regime is characterized by an almost horizontal water surface and formation of a recirculation zone behind the weir. The transitional flow regime depicts an undulating water surface on the backward face, accompanied by the presence of a circulation zone (Ali, 2013).

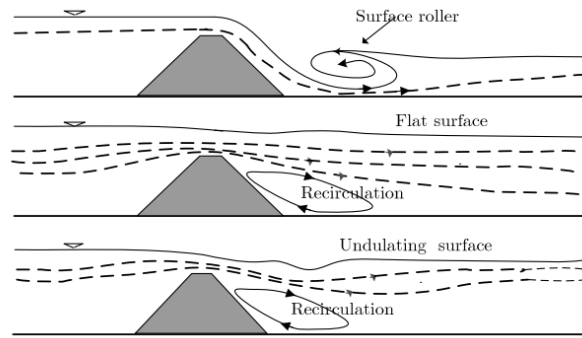
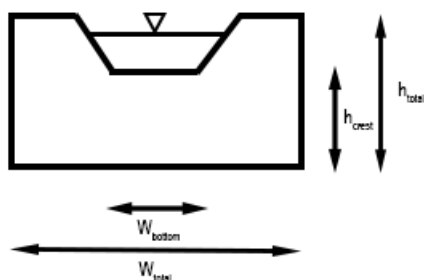


Figure C.2: Type of flows on top of weir. From *Flow over weir-like obstacles*, by S. Ali, 2013. Copyright 2013 by S. Ali.

The weirs at Juurikoski are most likely associated with either the second or the third flow regime, since water level fluctuations both on top and behind the weirs are minimal regarding field observations and measurements. Additionally, visual observations give undulating surfaces behind some of the weirs. The previously mentioned assumption simplifies the interpretation of flow characteristics near rapids, since relatively straight stream lines indicate hydrostatic pressure and minimal head losses.

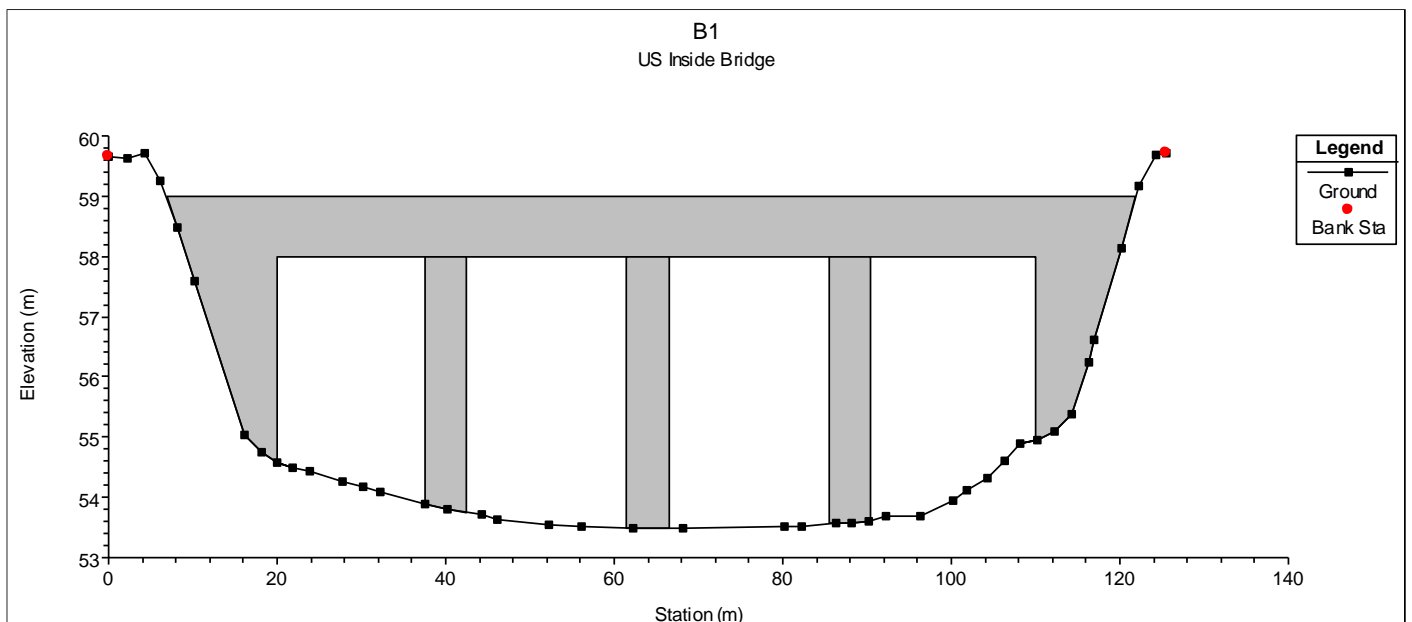
Appendix D – Juurikoski: Dimensions of hydraulic structures



h_{crest} = weir crest height
 h_{total} = weir total height
 W_{bottom} = weir bottom width
 W_{total} = weir total width

Structure Name	Dimensions [m]
Weir 1	$h_{crest} = 0.2$ $h_{weir} = 0.5$ $W_{bottom} = 5$ $W_{total} = 68$ $L = \text{weir length} = 5$ Weir gaps at centrelines: 39.5 and 60.5
Weir 2	$h_{crest} = 0.1$ $h_{weir} = 0.2$ $W_{bottom} = 5$ $W_{total} = 73$ $L = 5$ Weir gaps at centrelines: 20.5 and 45.5
Weir 3	$h_{crest} = 0.25$ $h_{weir} = 0.4$ $W_{bottom} = 5$ $W_{total} = 94$ $L = 35$ Weir gaps at centrelines: 61 and 91
Weir 4A	$h_{crest} = 0.6$ $h_{weir} = 0.9$ $W_{bottom} = 5$ $W_{total} = 28$ $L = 35$ Weir gaps at centrelines: 23
Weir 4B	$h_{crest} = 0.3$ $h_{weir} = 0.6$ $W_{bottom} = 5$ $W_{total} = 33$

	$L = \text{weir length} =$ Weir gaps at centrelines: 25
Weir 5	$h_{crest} = 0.3$ $h_{weir} = 0.6$ $W_{bottom} = 5$ $W_{total} = 75$ $L = \text{weir length} = 25$ Weir gaps at centrelines: 61 and 81
Weir 6	$h_{crest} = 0.6$ $h_{weir} = 0.9$ $W_{bottom} = 5$ $W_{total} = 75$ $L = \text{weir length} = 30$ Weir gaps at centrelines: 41 and 71
Bridge 1 (B1)	Deck width: 14 Span: 112 Pier diameter: 5 Pier centrelines: 40, 63 and 88
Bridge 2 (B2)	Deck width: 14 Span: 96 Pier diameter: 5 Pier centrelines: 36 and 60



Appendix E – LSPIV: Graphical representation of surface velocities near rapids

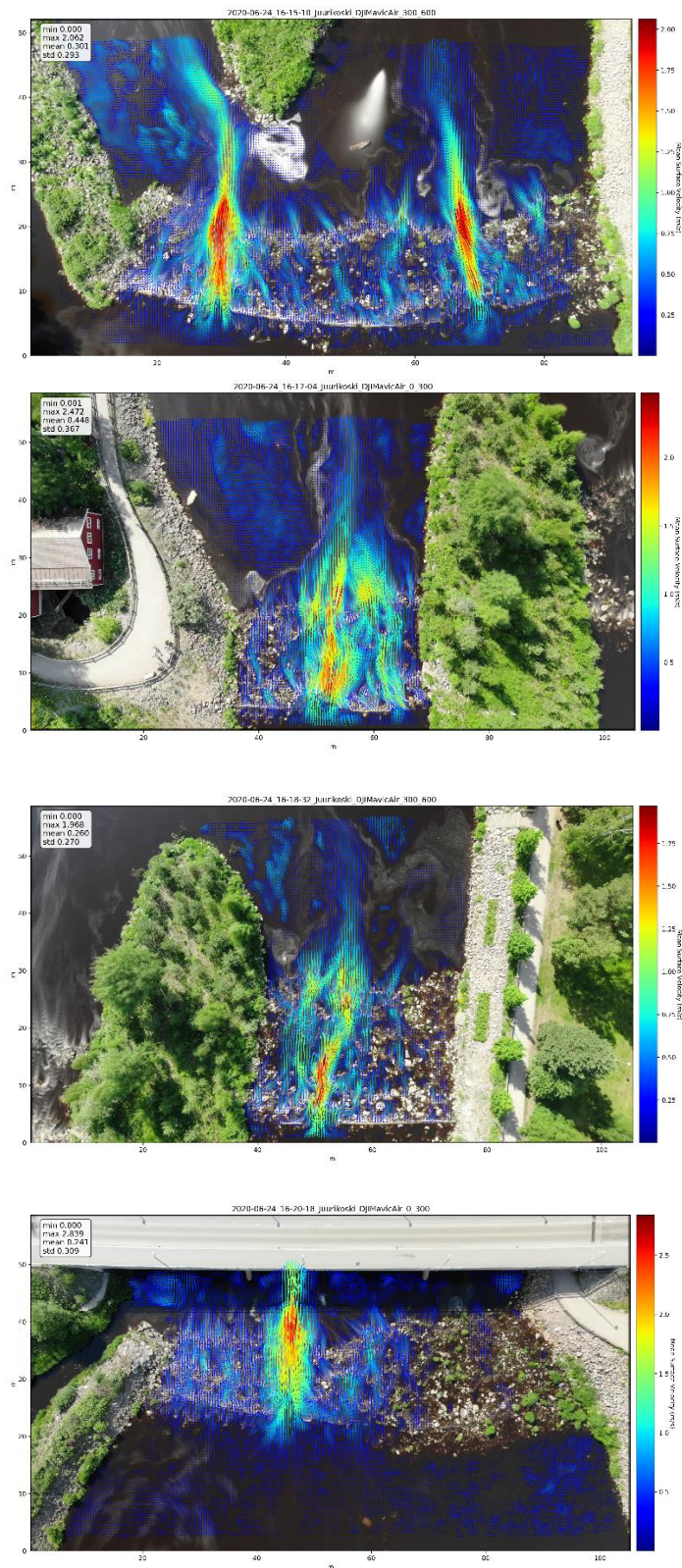


Figure E.1: Plotted LSPIV-data for rapid 3, 4A, 4B and 5 (from top to bottom) and the flow area behind the second bridge - 24th of June 2020

Appendix F – ADCP: Velocity profiles for multiple cross sections near rapids

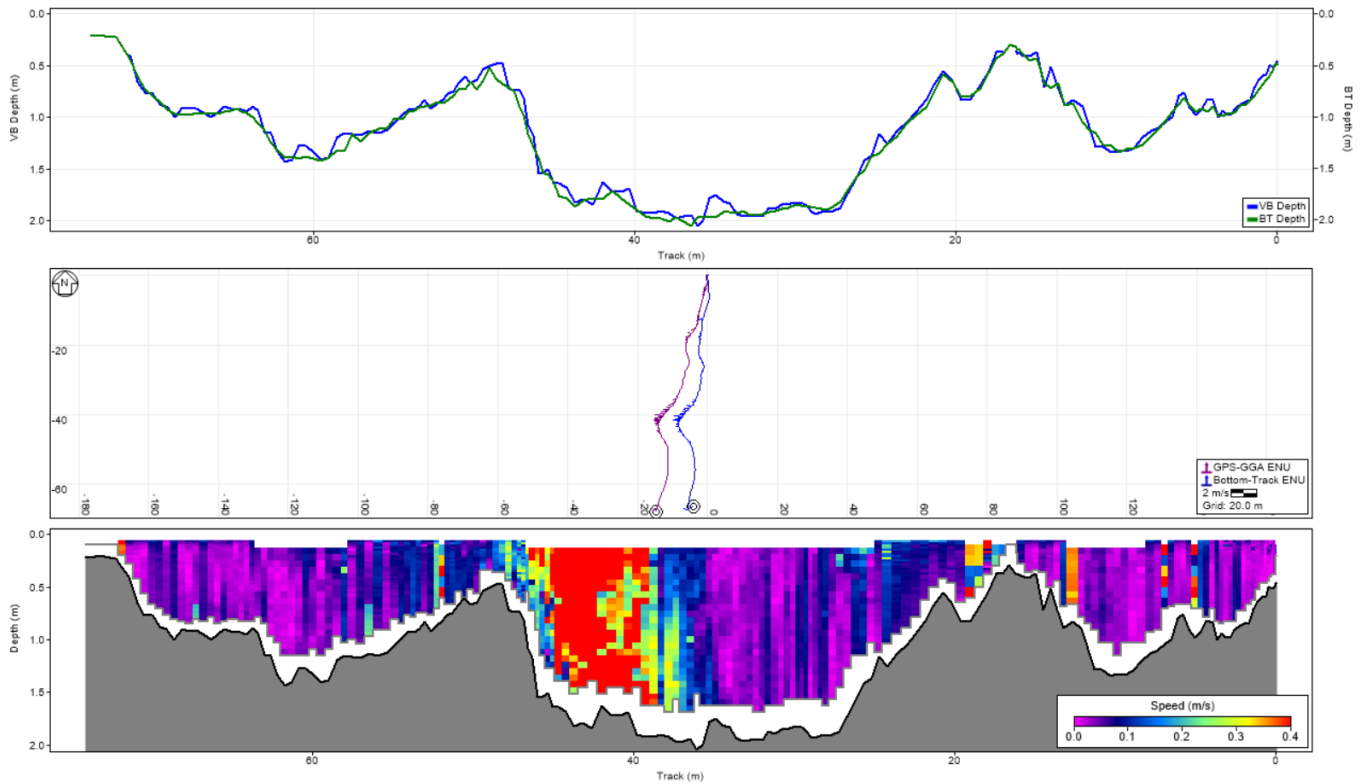


Figure F.1: Plotted ADCP-data for cross-section '14500' - 24th of June 2020, recording starting time 12:19:20 AM

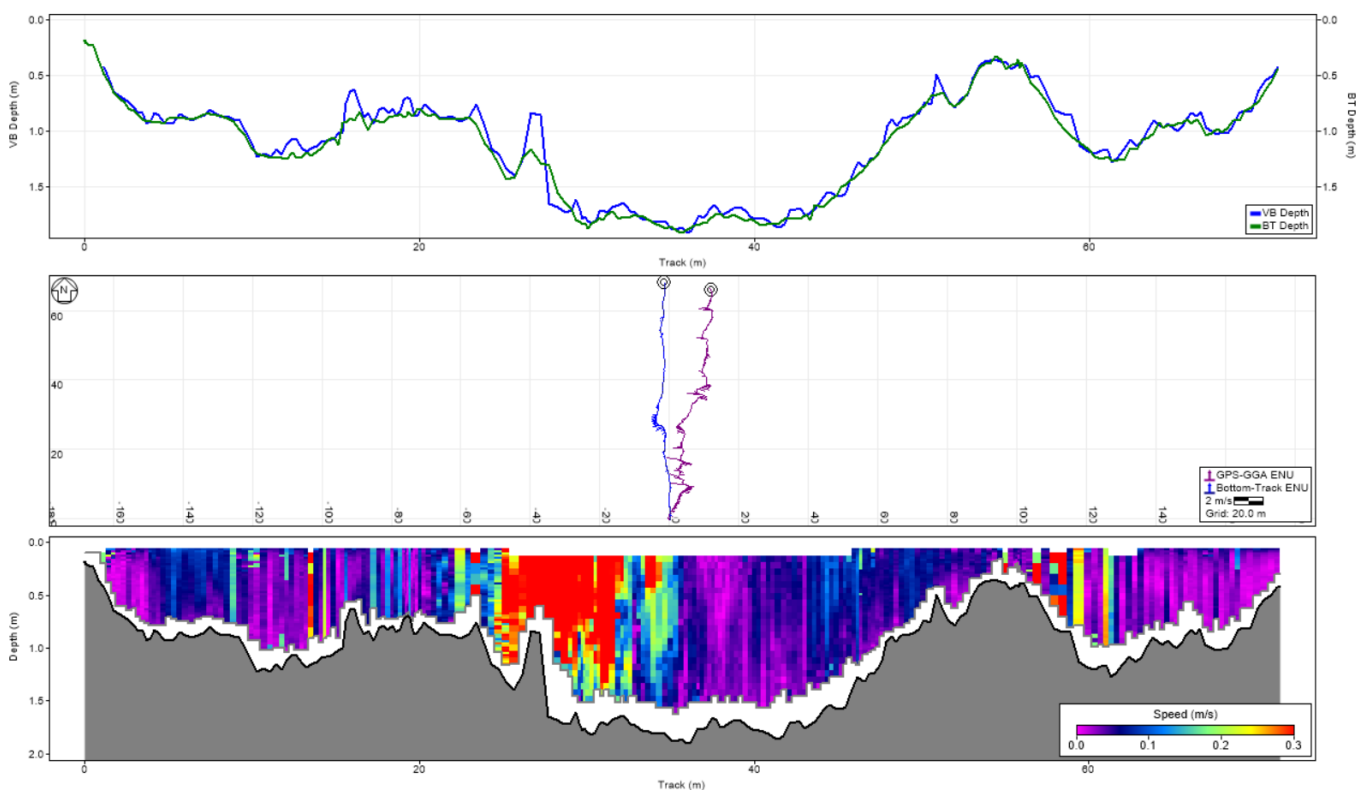


Figure F.2: Plotted ADCP-data for cross-section '122200' - 24th of June 2020, recording starting time 12:24:17 AM

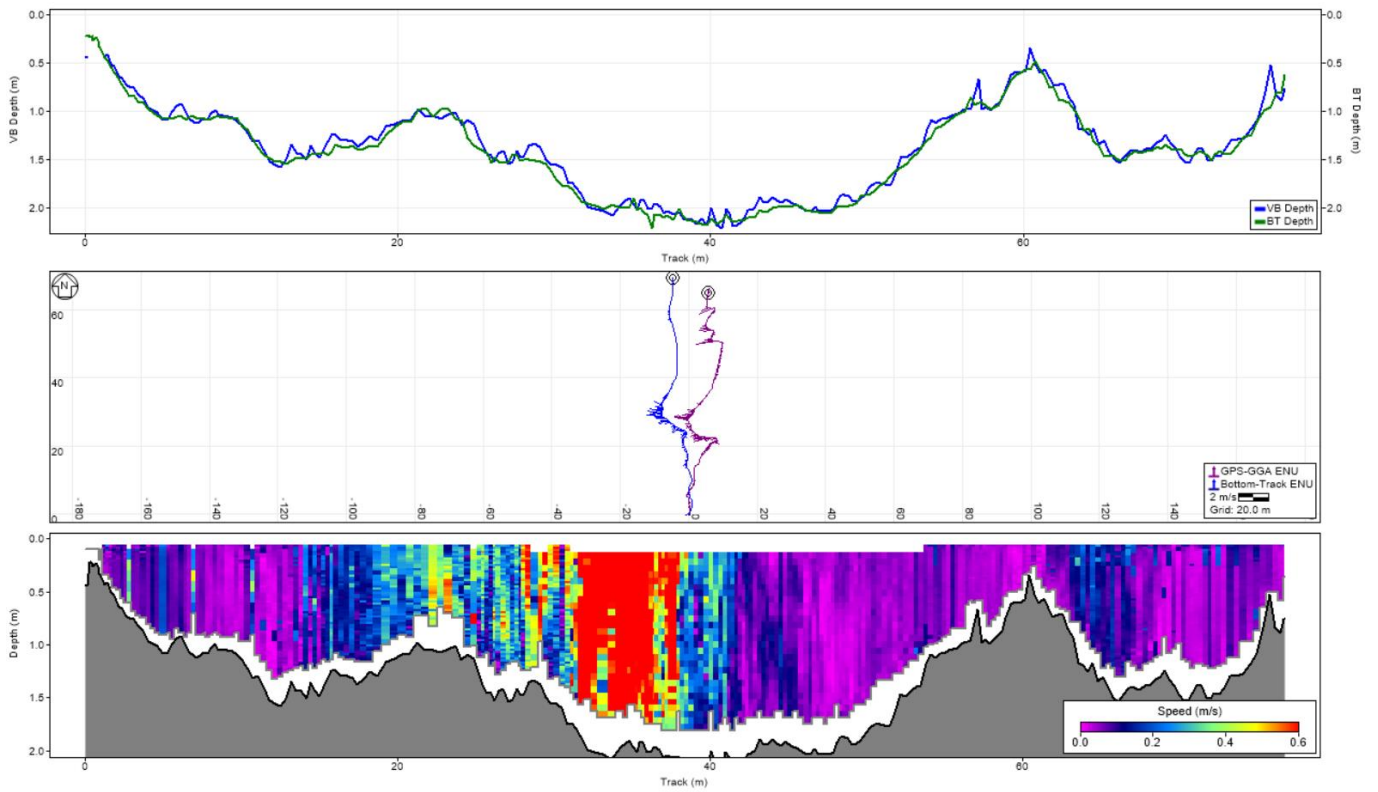


Figure F.3: Plotted ADCP-data for cross-section '155100' - 24th of June 2020, recording starting time 01:20:24 PM (referred to as CS1)

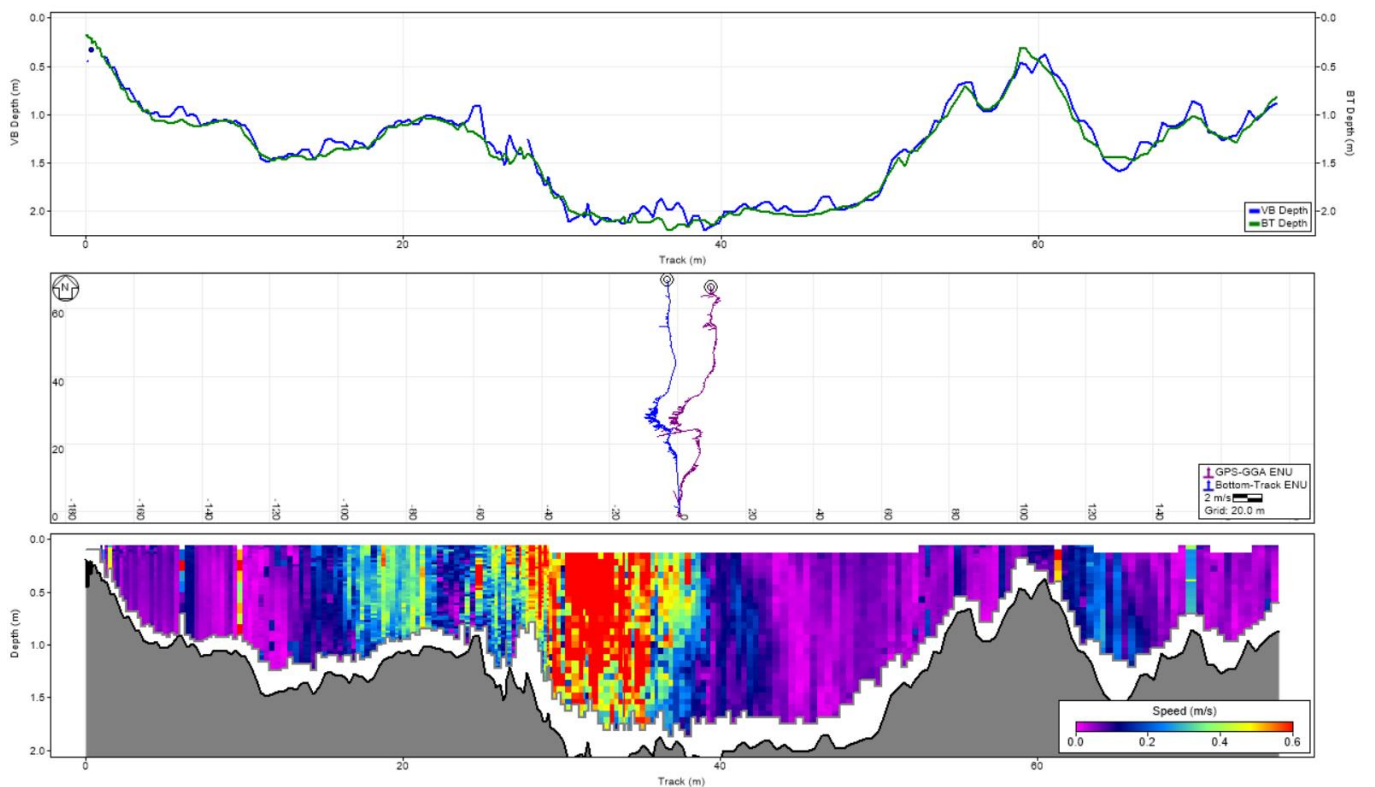


Figure F.4: Plotted ADCP-data for cross-section '160100' - 24th of June 2020, recording starting time 01:29:54 PM

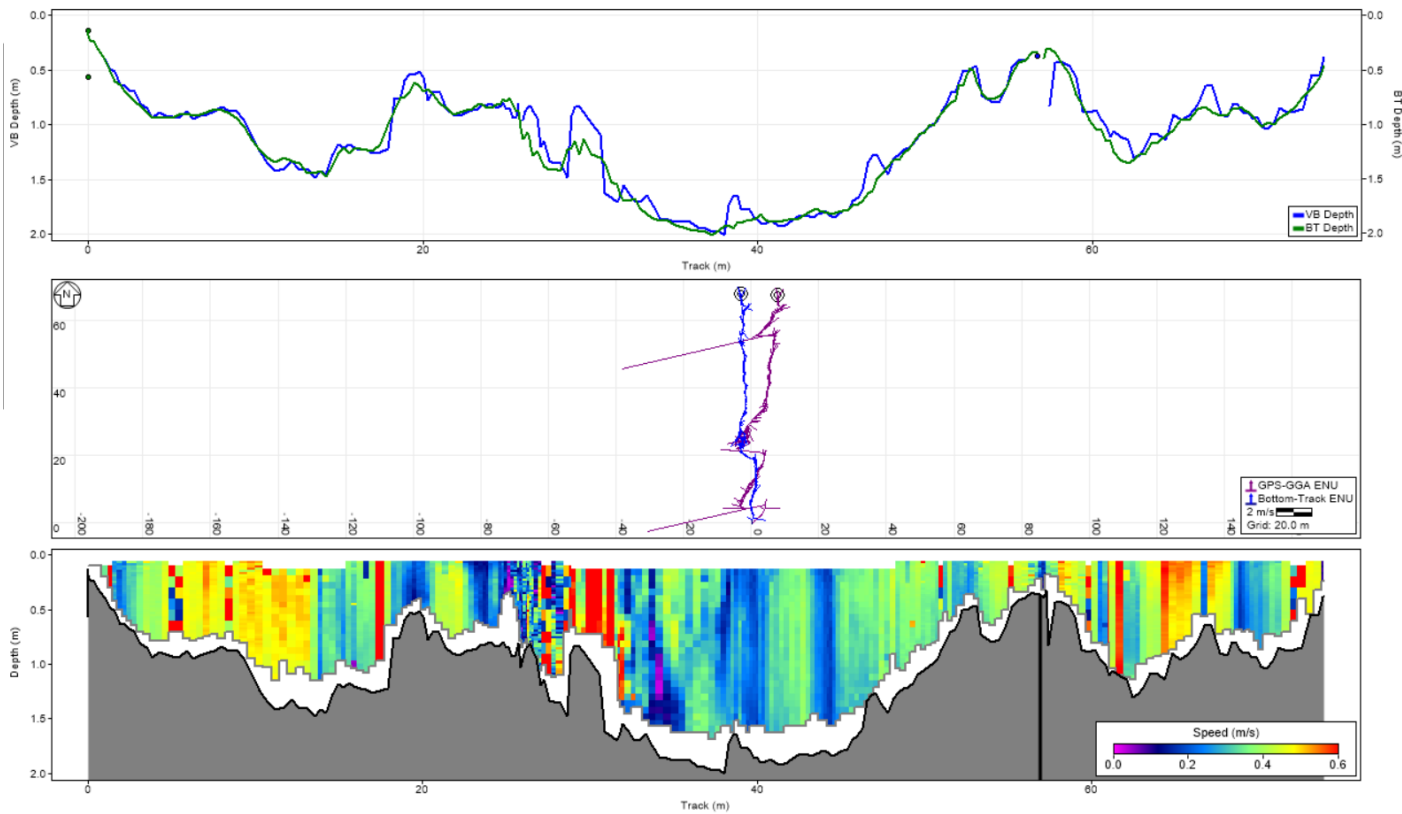


Figure F.5: Plotted ADCP-data for cross-section '133800' - 24th of June 2020, recording starting time 01:39:26 PM

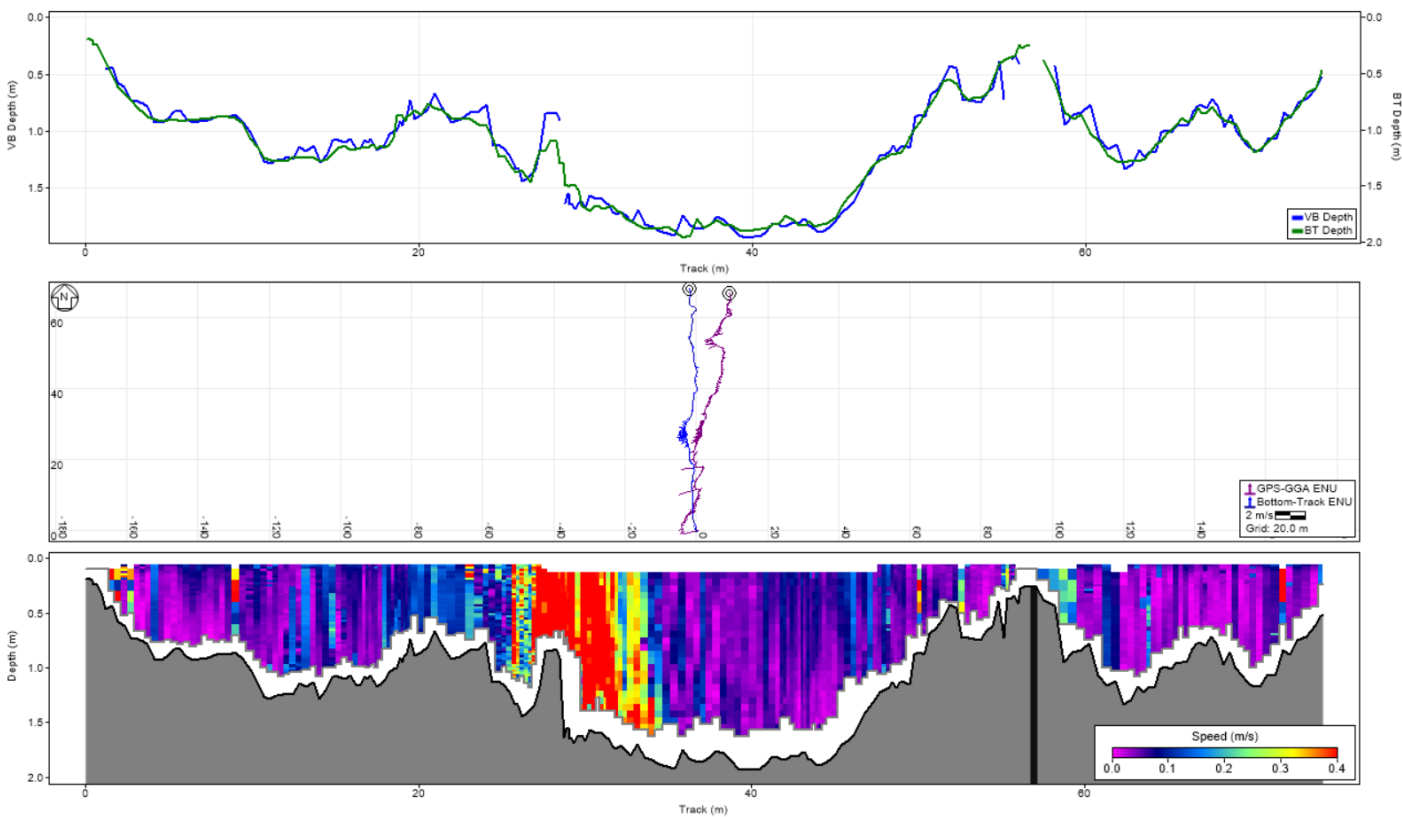


Figure F.6: Plotted ADCP-data for cross-section '135100' - 24th of June 2020, recording starting time 01:51:19 PM (referred to as CS2)

Table F.1: Velocity profiles (in E-, N-, U- and D- direction) corresponding to ADCP cross-sections 14500, 122200 155100, 160100, 133800 and 135100 (ltr.)

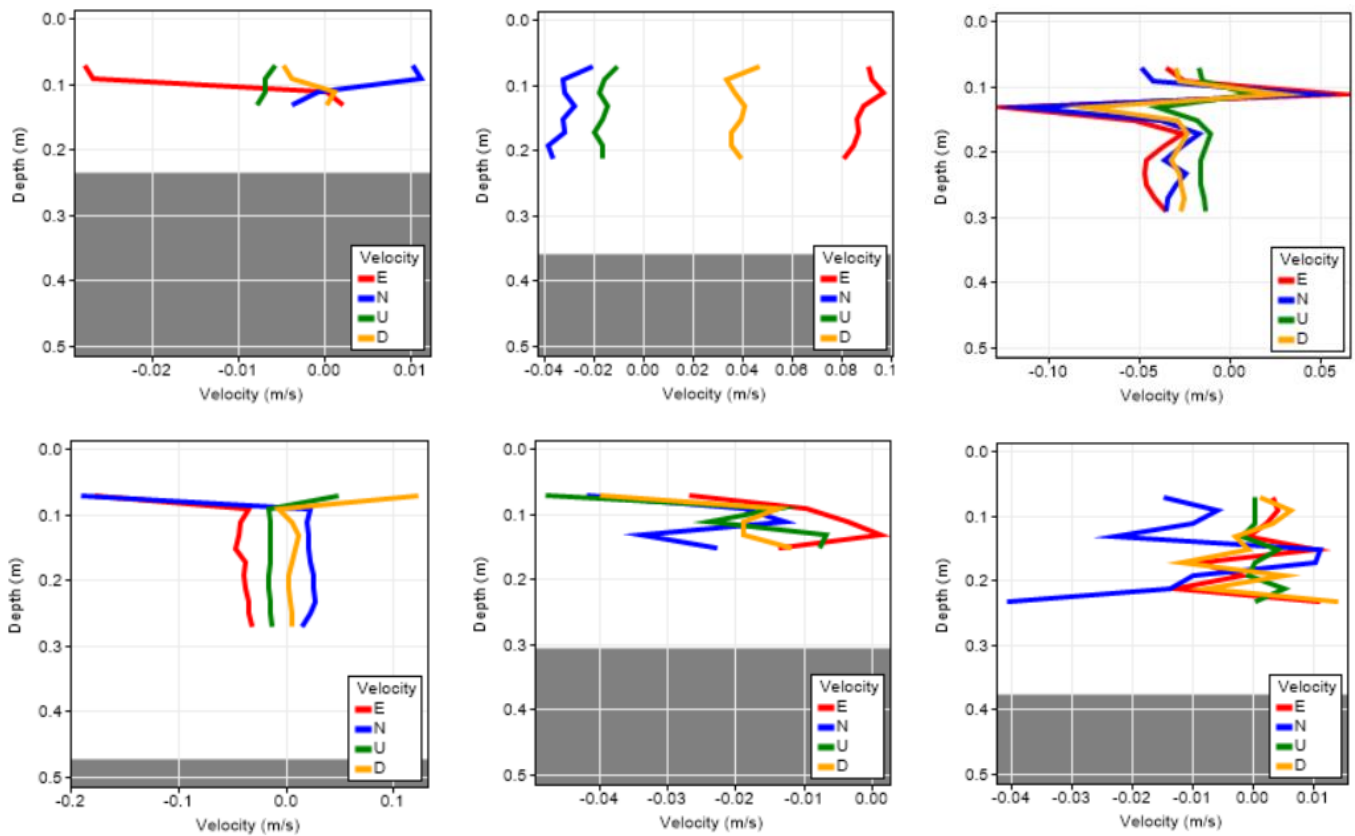


Table F.1 illustrates four velocity component versus depth for various cross-sections, based on the ADCP-data at the downstream end of the second bridge at Juurikoski; in eastward direction (E), in northward direction (N), in upward direction (U) and in downward direction (D). ‘E’ and ‘N’ represent horizontal components, while ‘U’ and ‘D’ the vertical components, to achieve a three-dimensional description of the velocity of a water body.

Appendix G – Model results: Water levels

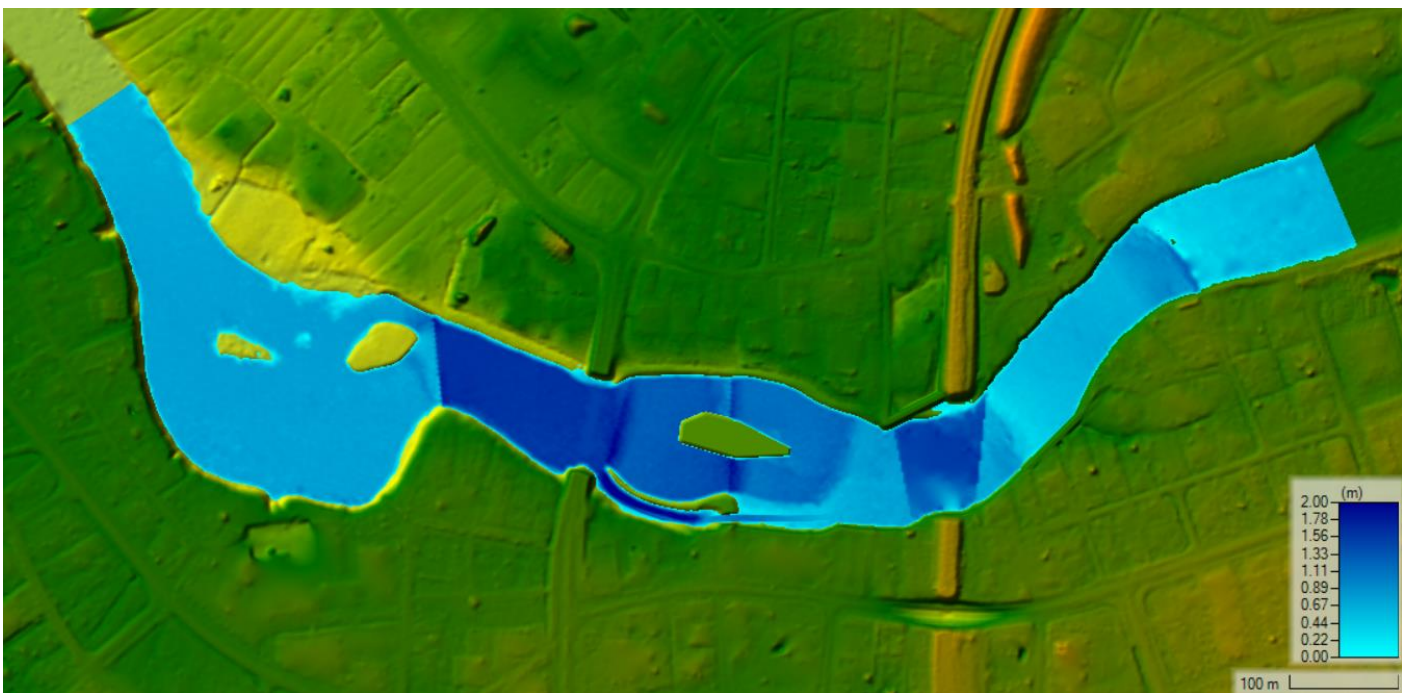
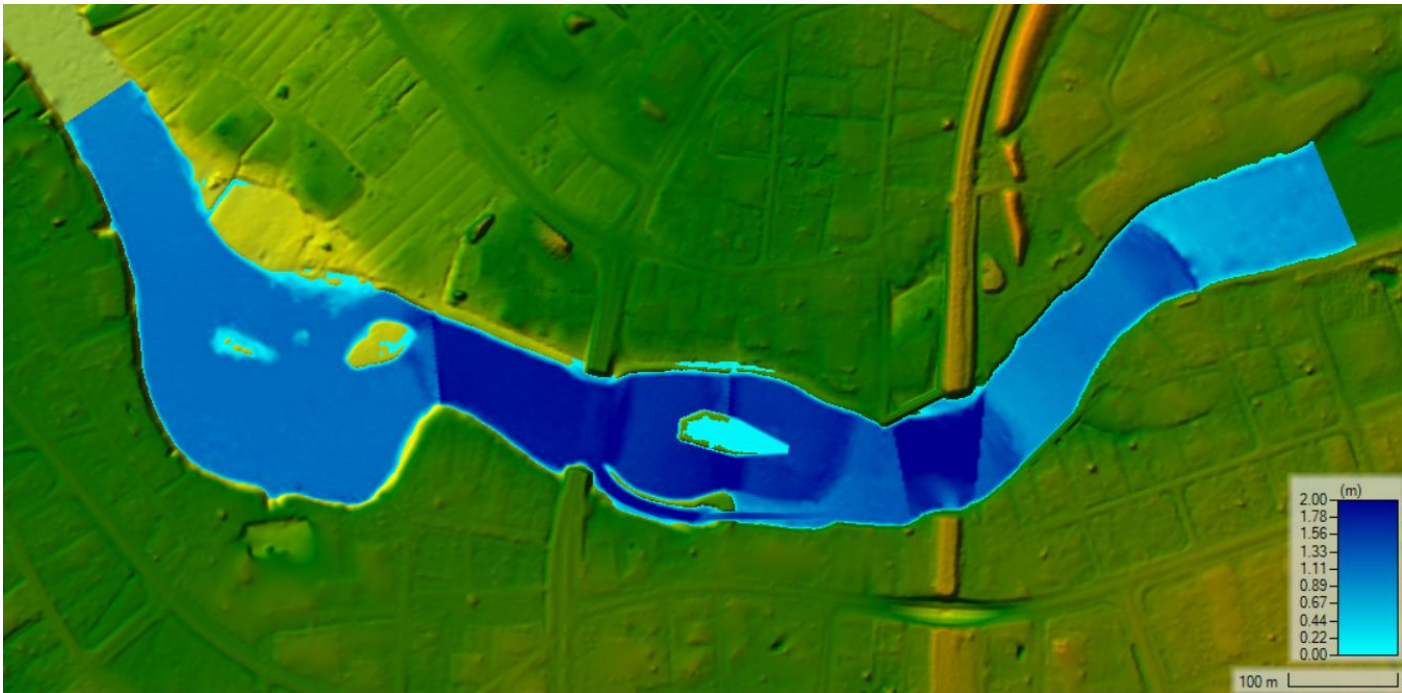
Table G.1 Statistical water level results per scenario

	Logger 2	Logger 3	Logger 4	Logger 5	Logger 6
count	71	67	66	67	66
mean	1.73856	1.54558	1.42921	1.65231	1.13532
std	0.277598	0.224407	0.174737	0.110019	0.209986
min	1.444	1.289	1.254	1.553	0.903
25%	1.48	1.33	1.2655	1.5595	0.924
50%	1.615	1.477	1.3455	1.589	1.0725
75%	2.004	1.77	1.60875	1.773	1.3515
max	2.207	1.89	1.712	1.841	1.438

	Logger 2	Logger 3	Logger 4	Logger 5	Logger 6
count	71	67	66	67	66
mean	1.71493	1.55528	1.39932	1.697	1.2318
std	0.190474	0.153387	0.119446	0.0737685	0.150401
min	1.519	1.384	1.278	1.629	1.063
25%	1.5395	1.4085	1.2875	1.632	1.0805
50%	1.624	1.51	1.345	1.654	1.201
75%	1.9	1.707	1.519	1.777	1.38475
max	2.029	1.791	1.589	1.82	1.45

	Logger 2	Logger 3	Logger 4	Logger 5	Logger 6
count	71	67	66	67	66
mean	1.43197	0.877925	1.20277	1.15348	1.44391
std	0.087484	0.30109	0.308035	0.233527	0.1469
min	1.303	0.561	0.878	0.945	1.308
25%	1.3665	0.5915	0.9085	0.965	1.32125
50%	1.426	0.748	1.0715	1.006	1.3625
75%	1.5015	1.1825	1.5215	1.419	1.60225
max	1.584	1.359	1.685	1.549	1.686

	Logger 2	Logger 3	Logger 4	Logger 5	Logger 6
count	71	67	66	67	66
mean	1.599	1.33472	1.28086	1.66481	1.1017
std	0.25073	0.20816	0.153331	0.124707	0.188972
min	1.338	1.091	1.133	1.552	0.911
25%	1.365	1.131	1.142	1.5605	0.923
50%	1.487	1.287	1.1965	1.591	1.011
75%	1.825	1.535	1.429	1.7975	1.319
max	2.039	1.655	1.541	1.881	1.366



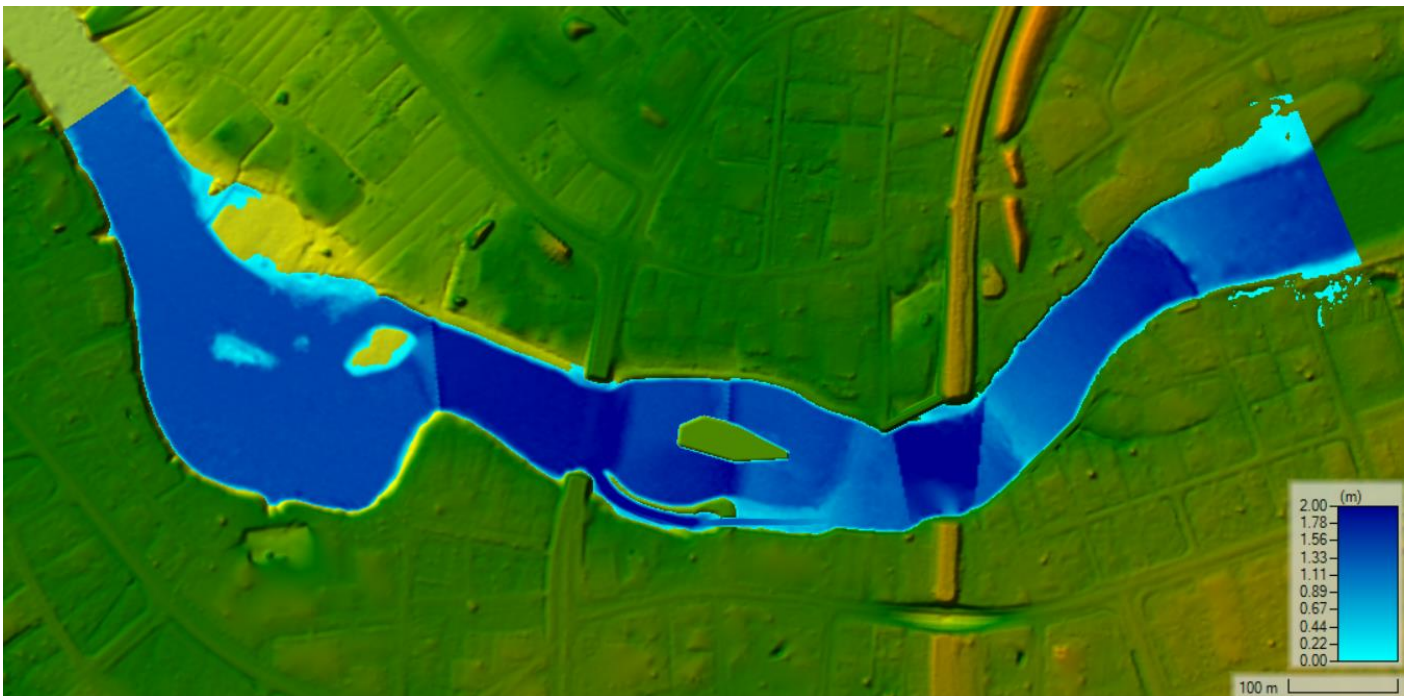
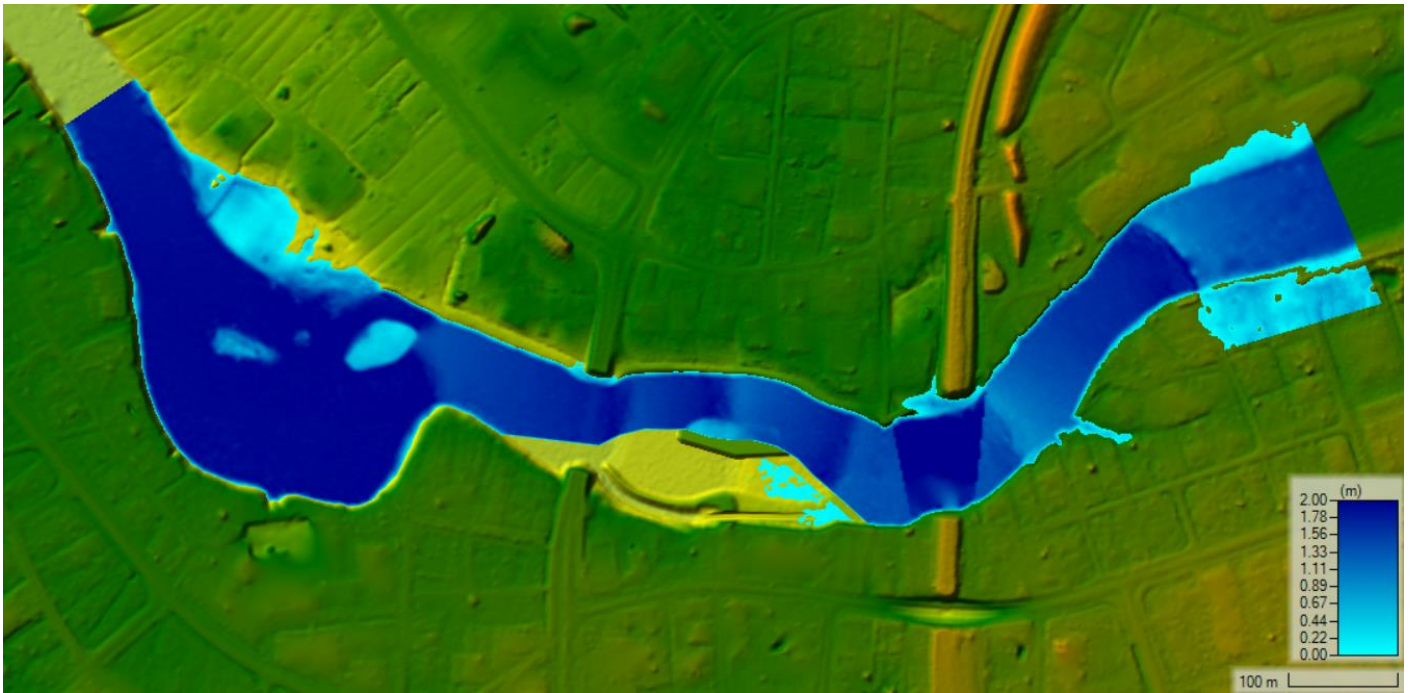


Figure G.1: Maximal water level results for 'Original', 'OL', 'M1' and 'M2' simulation scenarios (ttb.) - Simulation Date: 24th of June 2020

Appendix H – Uncertainty and sensitivity analysis data sources

H.1. Uncertainty quantification

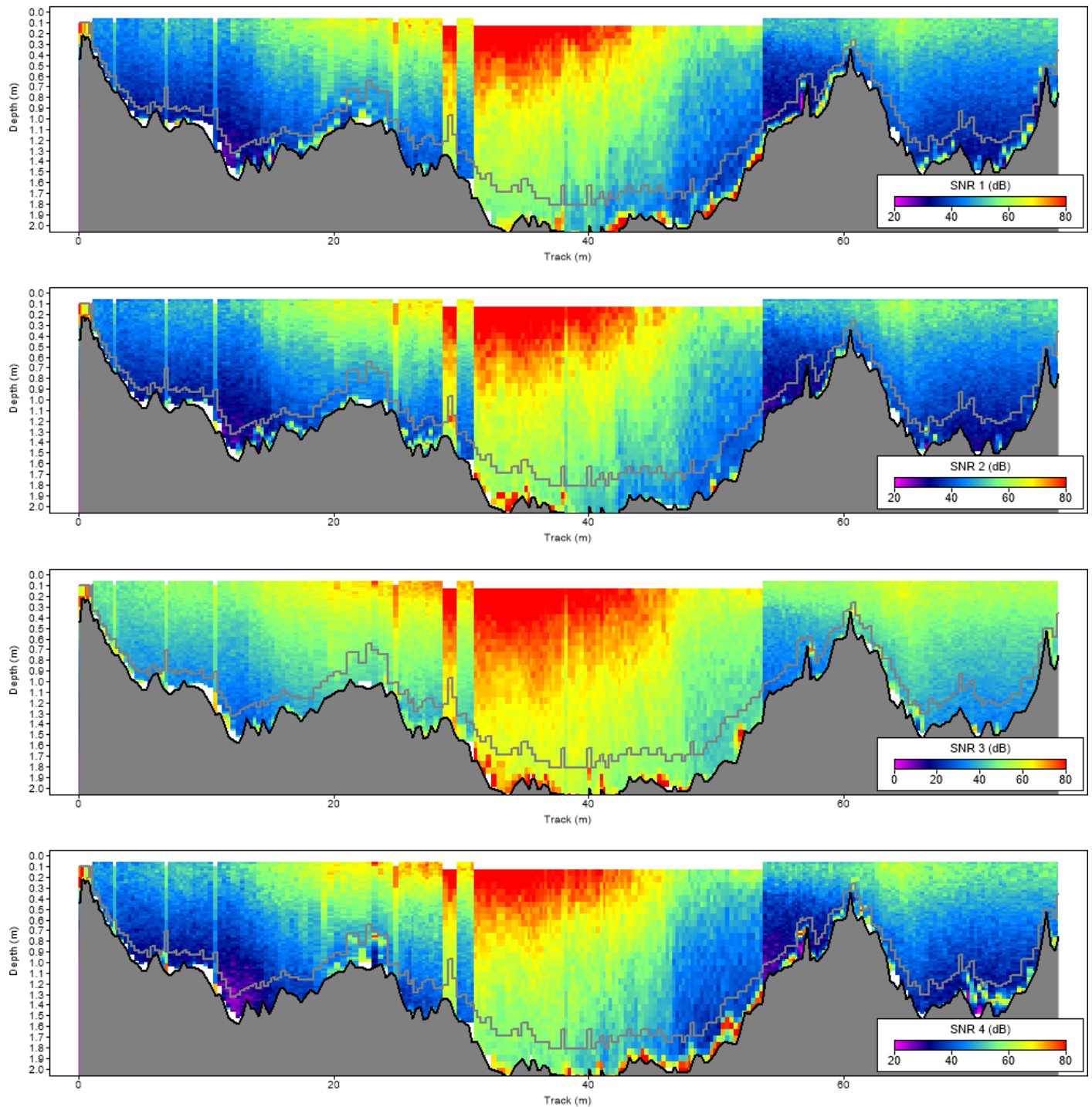


Figure H.1: Cross-sectional SNR-values at 1, 2, 3 and 4 dB (ADCP-file CS1)

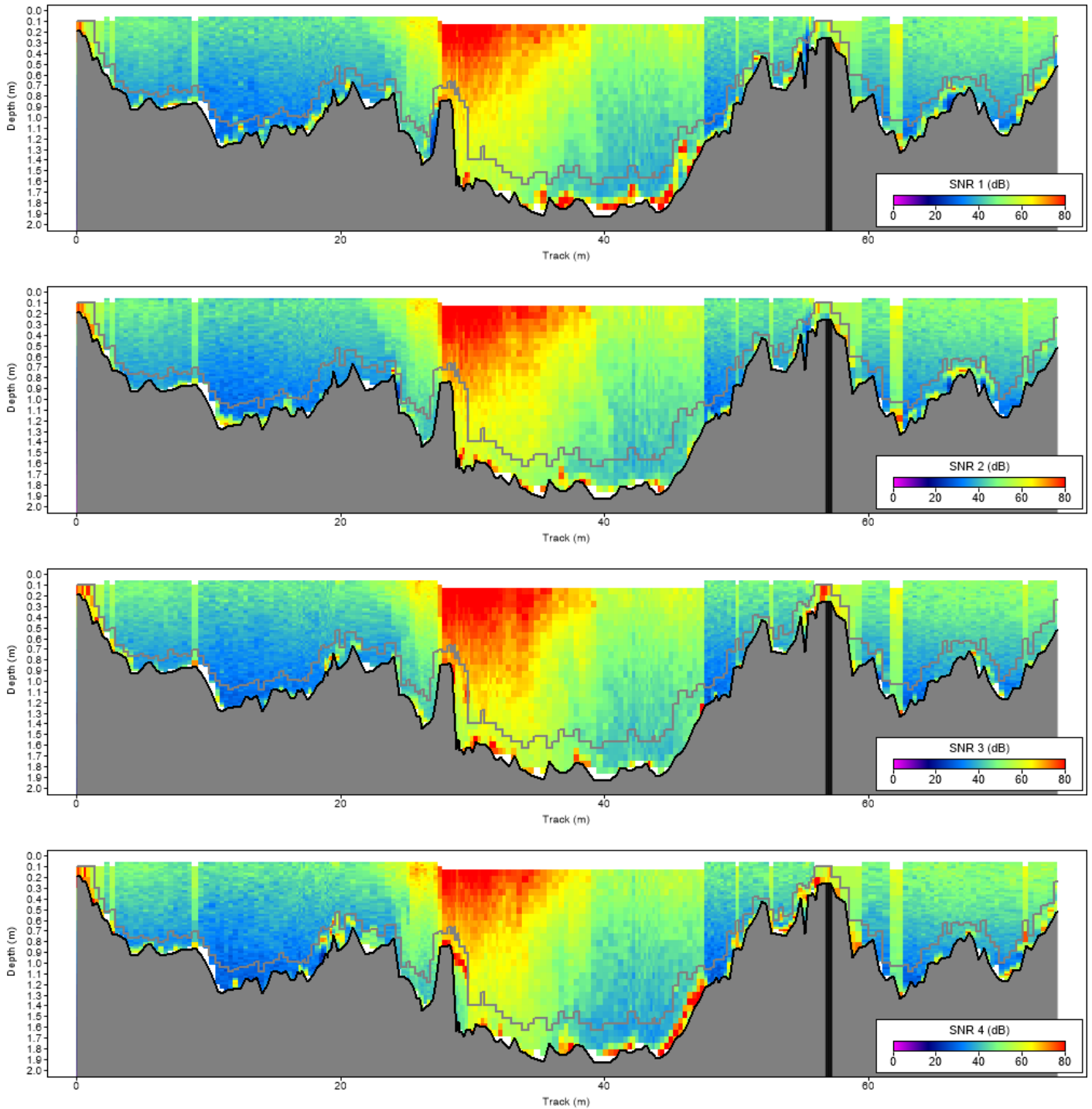


Figure H.2: Cross-sectional SNR-values at 1, 2, 3 and 4 dB (ADCP-file CS2)

Table H.1 Uncertainty quantification: statistical measures for ADCP- and LSPIV-files

	Mean [m/s]	Standard Deviation	95% Confidence Interval	Coefficient of Variation
CS1	0.12	0.18	[0, 0.68]	1.52
CS2	0.09	0.13	[0, 0.52]	1.50
R5_1	0.24	0.31	[0, 1.20]	1.28
R5_2	0.19	0.24	[0, 0.70]	1.27

Note: R5_1 and R5_2 refer to time stamps 13:24:02 and 16:23:26 on the 24th of June 2020 for the location of rapid 5. CS1 and CS2 had already been defined in Chapter 3.

H.2. Sensitivity analysis data

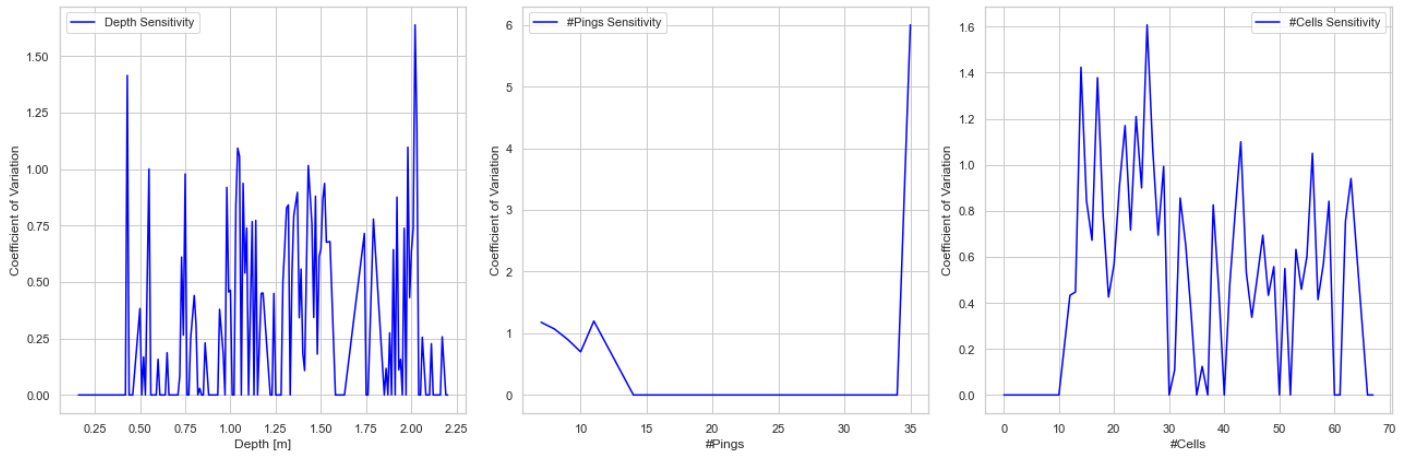


Figure H.3: Sensitivity analysis velocities based on depth, number of pings and number of cells (ADCP-file CS1)

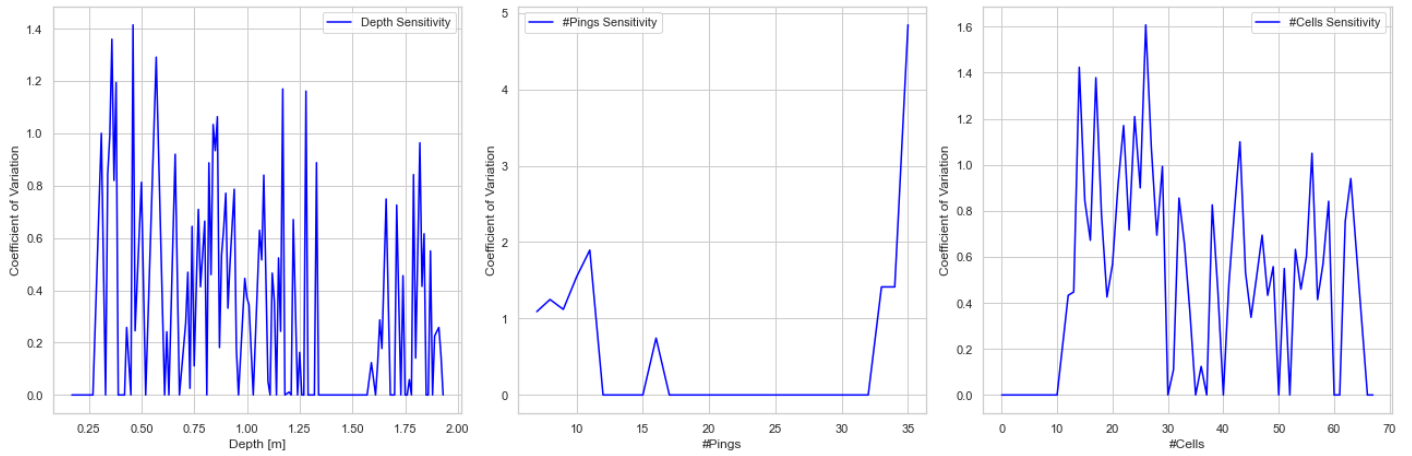


Figure H.4: Sensitivity analysis velocities based on depth, number of pings and number of cells (ADCP-file CS2)

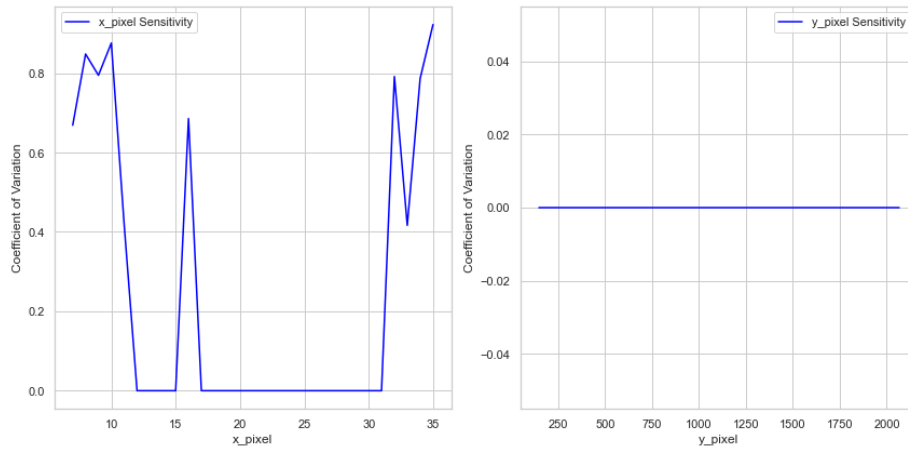


Figure H.5: Sensitivity analysis velocities based on x- and y-pixels (LSPIV-file R5_1)

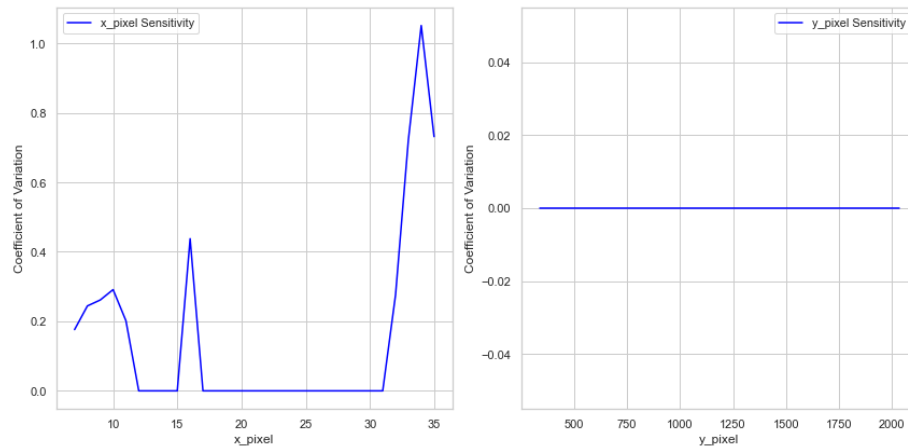


Figure H.6: Sensitivity analysis velocities based on x- and y-pixels (LSPIV-file R5_2)

Related to ADCP-measurements, ‘Depth’ refers to the depth measured for the last profile processed in meters, ‘#Cells’ to the number of cells used in the last vertical profile and ‘#Pings’ to the number of pings related to processing techniques. Depth impacts the velocity profiles, the number of pings affects the temporal resolution and number of cells the spatial resolution of the measurements. The pixel values in the x- and y-direction, ‘x_pixel’ and ‘y-pixel’, influence the spatial resolution of the LSPIV-measurements. These parameters control the size and orientation of the observation window.